

Structure-Property Relationship of
Polyurethane Flexible Foam Made from Natural Oil Polyols

A DISSERTATION
SUBMITTED TO THE FACULTY OF THE GRADUATE SCHOOL
OF THE UNIVERSITY OF MINNESOTA
BY

LING ZHANG

IN PARTIAL FULFILLMENT OF THE REQUIREMENTS
FOR THE DEGREE OF
DOCTOR OF PHILOSOPHY in CHEMICAL ENGINEERING & MATERIAL SCIENCE

Christopher Macosko, Advisor

Date: September, 2008

Minneapolis, Minnesota

© Ling Zhang 2008

Acknowledgements

The last five years I spent in graduate school has been a blessing! So many terrific people I met that I never would have crossed paths with if I had not chosen to pursue a higher degree and come to the University of Minnesota.

First and foremost, my advisor, Chris W. Macosko, deserves a great deal of credit for his knowledge, advice, patience, and trust. The many meetings and discussions we had not only moved the project along quite nicely, more importantly, taught me the essence of research. During my five-year graduate school, Chris provided me with more than research opportunities, but opportunities for personal development as well. It was Chris who encouraged me to try my hand in teaching senior design class, and gave me the opportunity to lead rheology short course labs.

The initiation and development of my research would not have been possible without the generous financial support from Cargill Inc. and Dow Chemical Co. Fellowship. Over the years, Jeff Malsam, Tim Abraham, Wei Zhang and nearly the entire Cargill BiOH Foam Lab, have provided me with technical data and materials. This collaboration turned out to be quite an exciting learning experience. In addition, I have met and worked with some amazing consultants. Ron Herrington, among all, inspires me with his passion for science and constant strives for learning. I treasure the short period of time I had working with Ron and his “infectious” enthusiasm. John McNeil, who taught me the

difference between cold curing and hot curing, has been a great resource and a helpful friend. Dave Henton, whom I have been working with for the longest, has been a major contributor to this research. I am grateful for Dave's knowledge and his many questions and suggestions during our meetings.

Professor Tom Hoye and his research group at Department of Chemistry at the University of Minnesota has been a great resource. Although I am not one of Prof. Hoye students, he still generously shares his knowledge and helps with chemistry related questions. Dr. Hyun K. Jeon, postdoctor-ed in my group, is another great resource and to whom I am indebted. Although Hyun and I only had little over one-year working together, her diligence and dedication to science taught me just what it takes to be a good researcher. Needless to mention Hyun also helped me jump-start the project and gave many advices and suggestions. Dr. David Giles has lent me a great deal of his help with rheometers. I enjoyed all the designs and redesigns of the rheometers tools with David and all the discussions we had on measuring foams. Dr. Shengxiang Ji, one of Prof. Hoye's graduate students, offered his expertise with NMR reaction studies. Thanks to Shengxiang's patience and experience, we worked out procedures to take reaction data in-situ. Dr. Greg Haugstad at the Characterization Facility at the UMN was a great help on Atomic Force Microscopy studies. Greg has always been patient with my many questions about the instrument as well as data interpretations. One of the chapters in this thesis explores the reaction kinetics during foaming using FTIR coupled with optical fibers. This study would not have been completed without the generous help from both Dr. Mark Listemann and Dr. Gary Johnson at Air Products and Chemicals. It was a delightful 2-day experiment, where I learnt a great deal from Dr. Gary Johnson from fiber preparation to data acquisition.

A fraction of my graduate study is to provide teaching assistance. To my surprise, I enjoyed, more than anything, teaching classes. I am grateful for the opportunities being in the same classrooms with some of the most passionate

professors I know and able to teach the senior design class under the guidance of Prof. Dan Frisbie, and the support of Prof. Frank Bates and my advisor Chris Macosko.

Everyone in the UMN polymer group has been a great companion, especially my group members. Mike Dolgovskij, Joel Bell, Mike Owens, Yutaka Mura, Hyunwoo Kim, Harikrishnan G, Carlos Lopez, Zhengxi Zhu, Jie Song, Patrick Lee, Dawud Tan, Luca Martinetti, and Suqin Tan have all been the source of great friendship and support. I am lucky to share my days with my officemates: Emilie Rexeisen, Alison Tisdale, Ashish Garg and Kamlesh Shroff. Many friends I met here, in particular, Lisa Lun, Katie and Aaron Walchin, and Erica Redline have made my days enjoyable and my graduate school experience so much richer. Kim Christianson, who I met just a few months ago, has been a great friend indeed. My hardworking undergraduate researchers, Scott Dixon, Ryan Seelbach, and Kari Tanaka have brought with them so much energy. I thank all my undergrads for being part of my graduate school experience and all the contributions they made.

Many staff members at the Department of Chemical Engineering and Material Science have also brightened my days. Mary Haverkost, and CJ Stone not only brought me laughter but sweets as well. Teresa Bredahl, Lisa Wissbaum and Julie Prince are the super ladies, who made my life so much easier by lending their helping hands whenever I needed. Mary Nissen, Rachel Surber, Jody Peper, Phil Engen and many others have also helped me throughout the years.

I can never be where I am today without my parents: Dr. Yunshu Zhang and Libin Wang. They are probably the best parents one can ever ask for. They have always placed my dreams and happiness ahead of their own. I thank my parents for letting me be the way I am and raising me so unconventionally. I am thankful that I have become every bit like them! My extended family members

have also been supportive. All those inquiries asking “When will you graduate?” have made me realize just how precious it is to actually graduate.

Lastly, I give my most sincere thanks to Dr. Rick B. Watson, my boyfriend of seven years. The thought of you makes me speechless. For a long time, I thought living my life free was what kept me happy but as it turned out what made me happy all these years was you. I had never imagined, even, in my wildest dreams that I could find someone like you. Thank you for all the butt-kicking Frisbee golf, the pre-air hockey trash talks, the “hands to your sides” kitchen moments, the telepathic powers, and so much more. Thank you my dear, for everything!

to my parents and Rick B. Watson

— without your unconditional love and support, I'd be forever lost

and

to myself

Abstract

Ling Zhang

Number of Words: 350

The versatility of polyurethane (PU) flexible foam has made it an indispensable material in furnishing, transportation, and packaging. To make PU flexible foam, petroleum-derived reactants, polyol and isocyanate, are used. As the price of crude oil has escalated and the cost of PU reactants doubled, researchers have turned to renewable natural oils for polyols. Recent developments have successfully derived polyols from natural oils and synthesized a range of PU products from them. However, making flexible foam from natural oil polyols is still proving challenging. The goal of this thesis is to understand the potentials and the limitations of natural oil polyols as an alternative to petroleum polyols.

An initial attempt to understand natural oil polyols showed that flexible foams could be synthesized from castor oil, a naturally occurring polyol, but not from soybean oil-derived polyol (SBOP), which produced a rigid foam. Characterization results indicated that both foams were phase-mixed and the glass transition temperature (T_g) was the predominant factor that determines the

rigidity of the foam. The high T_g of SBOP foam was attributed to the low number of covalent bond between crosslinkers.

As neither castor oil nor SBOP was suited as sole polyol component for flexible foams, we partially substituted petroleum polyol with these natural oil polyols in a flexible foam formulation. A 30-wt% replacement with SBOP more than doubled the foam compressive modulus and this increase was achieved by changing the hard domain morphology as well as creating a SBOP-rich second soft phase. Although foaming natural oil polyol-containing samples showed no signs of kinetic issues, an infrared spectroscopy (IR) study demonstrated that not only was urethane formation rate reduced but phase separation in foams was delayed as well.

To further explore the potentials of natural oil polyols as sole polyol component in flexible foam, the relationship between the T_g and the number of covalent bonds between crosslinks was investigated. It was found that with increasing number of covalent bonds between crosslinks, the T_g of PU can be systematically lowered and that the dangling chains present in natural oil polyols act as a plasticizer to help lowering the T_g further.

Chris W. Macosko

Table of Contents

Acknowledgements	i
Dedication	v
Abstract	vi
Table of Content	viii
List of Tables	xii
List of Figures	xiv
Chapter 1 Introduction	1
1.1 Background	1
1.2 Polyurethane Chemistry and Morphology	3
1.2.1 Chemistry	3
1.2.2 Morphology	9
1.3 Natural Oil Polyols	12
1.4 Natural Oil Polyol-based Polyurethanes	16
1.5 Organization of Thesis	19
Chapter 2 Polyurethane Foams made with Single-polyol Component	21
2.1 Chapter Overview	22

2.2 Introduction	22
2.3 Experimental	23
2.3.1 Materials	23
2.3.2 Foam Synthesis	26
2.3.3 Characterization	28
2.4 Results and Discussion	31
2.4.1 Foam Kinetics	31
2.4.2 Thermal-mechanical Properties	36
2.4.3 Small Angle X-ray Scattering	43
2.4.4 Fourier Transform Infrared Spectroscopy	45
2.5 Conclusion and Outlook	49
Chapter 3 Partially-substituted Polyurethane Flexible Foams	51
3.1 Chapter Overview	52
3.2 Introduction	52
3.3 Experimental	54
3.3.1 Materials	54
3.3.2 Foam Synthesis	57
3.3.3 Characterization	60
3.4 Results and Discussion	63

	3.4.1 Solvent Extraction	63
	3.4.2 Foam Cellular Structures	64
	3.4.3 Polymer Phase Characterization	66
	3.5 Conclusion	86
Chapter 4	Reaction Kinetics	88
	4.1 Chapter Overview	89
	4.2 Introduction	89
	4.3 Experimental	92
	4.3.1 Materials	92
	4.3.2 Procedures and Characterizations	94
	4.4 Results and Discussion	99
	4.4.1 Hydroxyl-isocyanate Reaction	99
	4.4.2 Polyol-TDI Reaction	106
	4.4.3 Foaming Kinetics	110
	4.5 Conclusion	126
Chapter 5	Effects of Molecular Weight and Molecular Weight Distribution	129
	5.1 Chapter Overview	129
	5.2 Introduction	129
	5.2.1 Theoretical Models	130

5.3 Experimental	134
5.3.1 Materials	134
5.3.2 Synthesis	135
5.3.3 Characterization	144
5.4 Results and Discussion	147
5.4.1 The Effect of Molecular Weight	147
5.4.2 The Effect of Molecular Weight Distribution	165
5.5 Conclusion	173
Chapter 6 Conclusion and Future Work	175
6.1 Conclusion	175
6.2 Future Work	178
Appendix A: Polyol Structure Effect on PU	181
Appendix B: Model Polyols Viscosity	189
References	192

List of Tables

Table 1.1	Initiators commonly used for polyether polyol synthesis	8
Table 1.2	Compositions of some common natural oils	13
Table 2.1	Properties of polyols used	23
Table 2.2	Foam formulations of single-polyol systems	26
Table 2.3	IR band assignments in carbonyl region	31
Table 2.4	Normalized peak areas under the IR bands	47
Table 3.1	Foam formulations used in sample synthesis, all	58
	formulations are based on 100 parts by weight of polyol	
Table 3.2	Measured foam properties	63
Table 3.3	IR band assignment in C=O region and peak area under ...	83
	the bands	
Table 4.1	Alcohols used in hydroxyl reactivity study	93
Table 4.2	Formulations used for hydroxyl reactivity study	95
Table 4.3	Formulations used for polyol-TDI reaction study	96
Table 4.4	Sample formulations for foam kinetics study	97
Table 4.5	Reaction constants for hydroxyl-isocyanate reactions in	104
	DMF	
Table 4.6	Reaction constants for polyol reactions with TDI	109
Table 4.7	Extrapolated relative reactivity data in the unit of intensity ..	121

Table 5.1 A	Reactant details and polyol properties	138
Table 5.1 B	Properties of additional polyols: castor oil and Arcol [®] F3022	139
Table 5.2	Collapsed foam formulations for single polyol systems	143
Table 5.3	Collapsed foam formulation for molecular weight	144
	distribution study	
Table 5.4	The number of covalent bonds (n, in Equation 5.5) between	149
	two neighboring hydroxyls	
Table 5.5	Tensile / elongation properties of collapsed foams	164
Table A-1	Formulations used for sample synthesis	183
Table A-2	Transition temperatures of polyols and their corresponding	186
	PUs	
Table B-1	Viscosity of polyols at 25 °C	190
Table B-2	Temperature-viscosity relationship equations	191

List of Figures

Figure 1.1	Polyurethane flexible foam applications	2
Figure 1.2	Processes for making slabstock and molded foams	3
Figure 1.3	Gelling and blowing reactions	4
Figure 1.4	Diisocyanates commonly used in foaming	5
Figure 1.5	Polyether polyols made from ethylene oxide and propylene oxide	6
Figure 1.6	Morphology of flexible foam at different length scales	10
Figure 1.7	Phase separated morphology of PU flexible foams	11
Figure 1.8	Conversion of a triglyceride molecule to an alcohol via hydroformylation followed by hydrogenation method	14
Figure 1.9	Methods for converting natural oil to polyol: (II) epoxidation and oxirane ring-opening with methanol, (III) ozonolysis, (IV) microbial conversion, and (V) halogen addition and nucleophilic substitution.	16
Figure 2.1	Idealized structure of castor oil and SBOP	25
Figure 2.2	The adiabatic temperature rise during foam formation	32
Figure 2.3	The isocyanate conversions calculated from temperature rises during foaming	34
Figure 2.4	DSC traces of foams	37

Figure 2.5	DMA curves showing G' and G'' as functions of temperature	40
Figure 2.6	DMA curves showing $\tan(\delta)$ as a function of temperature	42
Figure 2.7	SAXS profiles of foam samples	43
Figure 2.8	FTIR-ATR spectra of foams and the spectra after the ester linkage band has been subtracted	46
Figure 2.9	An example of peak deconvolution showing the Gaussian fit for the absorbance bands in Hyperlite [®] E-848.	48
Figure 3.1	GPC trace of SBOP used in this study	56
Figure 3.2	SEM images of the foam samples	65
Figure 3.3	Average cell diameter and standard deviation for foams	66
Figure 3.4	DMA results of partially substituted foams (I) showing G' as a function of temperature	68
Figure 3.5	DMA results of partially substituted foams (I) showing $\tan(\delta)$ as a function of temperature	69
Figure 3.6	DMA results of partially substituted foams (II) showing G' as a function of temperature	70
Figure 3.7	DMA results of partially substituted foams (II) showing $\tan(\delta)$ as a function of temperature	71
Figure 3.8	DSC traces of partially substituted foams	72
Figure 3.9	DSC results showing T_g and the breadth of glass transition.	73

Figure 3.10	Scattering profiles of foams obtained using SAXS	75
Figure 3.11	Tapping mode AFM images	79
Figure 3.12	FTIR-ATR spectra of the carbonyl region	82
Figure 3.13	Compression properties of foams. Column data show the pressure required to achieve 65% compression, and the line data show shear modulus, G' , measured at 25 °C	86
Figure 4.1	FTIR setup used for foaming kinetics study	98
Figure 4.2	^1H NMR spectra of diethylene glycol and the urethane derived thereof by reaction with phenyl isocyanate	100
Figure 4.3	^1H NMR Spectra of diethylene glycol-phenyl isocyanate ... reaction at different times	101
Figure 4.4	Second order kinetic plots used to calculate reaction constants	103
Figure 4.5	Isocyanate conversion (p) as a function of time during hydroxyl-isocyanate reaction at 25 °C by FTIR-ATR	106
Figure 4.6	Plots for obtaining reaction constants of polyol reaction ... with TDI. Dashed lines are linear fits to the experimental data	108
Figure 4.7	Chemical structures of a bidentate urea, a monodentate ... urea, and free ureas	111
Figure 4.8	Three-dimensional surface of the isocyanate absorbance band for control foam	112

Figure 4.9	Isocyanate conversion calculated from temperature rises (open symbols) and extrapolated from FTIR data (solid line)	113
Figure 4.10	Isocyanate conversion during foaming	114
Figure 4.11	Time resolved FTIR spectra of control foam. The three-dimensional plots shown only the carbonyl region and the dashed lines are indicative of the positions of free urethane and free urea absorbance bands	117
Figure 4.12	Free urethane absorbance change as a function of time (I)	118
Figure 4.13	Free urethane absorbance change as a function of time (II)	120
Figure 4.14	Free urea absorbance change as a function of time	122
Figure 4.15	Bidentate urea absorbance change as a function of time ..	123
Figure 4.16	Bidentate urea absorbance change as a function of	125
	isocyanate conversion	
Figure 5.1	Synthesis scheme for natural oil-based model polyols	140
Figure 5.2	GPC trace of model polyol synthesized and reactants	141
Figure 5.3	DSC curves of model polyols	150
Figure 5.4	DSC curves of collapsed foams	151
Figure 5.5	A line fit to the T_g data of samples forced through the origin of coordinates	152
Figure 5.6	Plots of T_g values for different crosslinked polymers	153
	showing the validity of Equation of 5.1	

Figure 5.7	DMA curves of collapsed foam samples	156
Figure 5.8	Tan (δ) curves of collapsed foam samples	157
Figure 5.9	DMA curves of both collapsed foam and foamed sample .. based on castor oil	158
Figure 5.10	Scattering profiles for collapsed foams	160
Figure 5.11	FTIR-ATR results on collapsed foam samples	162
Figure 5.12	Stress-strain curves of collapsed foams measured at 25 °C	165
Figure 5.13	DMA curves of collapsed foams showing G' and tan(δ) Traces	167
Figure 5.14	DSC curves of collapsed foams	169
Figure 5.15	DMA and tan(δ) curves of collapsed foams	171
Figure A-1	Chemical structures of polyols	182
Figure A-2	DSC traces of polyols	185
Figure A-3	DSC traces of collapsed foam samples	186
Figure A-4	Small angle X-ray scattering profiles of the samples	187
Figure B-1	Temperature dependence of polyol viscosity	190

Chapter 1

Introduction

Contents

1.1	Background	1
1.2	Polyurethane Chemistry and Morphology	3
	1.2.1 Chemistry	3
	1.2.2 Morphology	9
1.3	Natural Oil Polyols	12
1.4	Natural Oil Polyol-based Polyurethanes	16
1.5	Organization of Thesis	19

1.1 Background

Polyurethane (PU) is one of the most versatile polymeric materials with regard to both applications and processing methods. From anti-fogging coating, elastomeric shoe soles to rigid insulation foams, polyurethane can be found in almost all aspects of life. Among all PU products, flexible foam is the largest

product family by quantity, constituting more than 40% of all PUs and is the primary concern of this research work [1-3]. Major applications of PU flexible foam are illustrated in Figure 1.1.

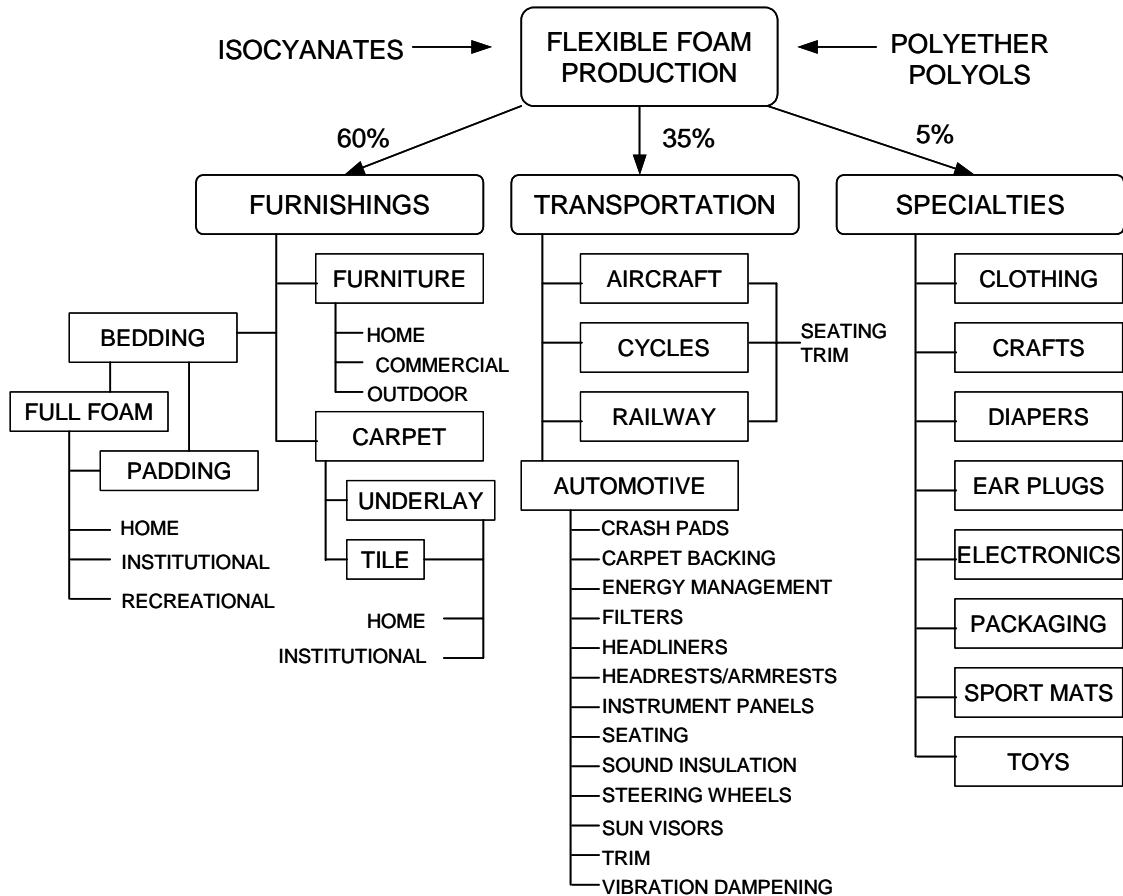


Figure 1.1: Polyurethane flexible foam applications [4].

PU flexible foams are made via two processes: molded and slabstock foaming. Molded foams are largely used in transportation applications, such as automotive seating. The process begins by mixing all the reactants together and transferring the foaming mixture to a mold. The foam is then risen to take on the

shape of the mold. Slabstock foams are largely used in furnishing industry, such as mattress and carpet backing. This process is performed in an open environment. Well-mixed reactants are spread onto a conveyor belt. As the conveyor belt moves forward, the foaming mixture expands and rises to shape. Figure 1.2 depicts the two processes side by side.

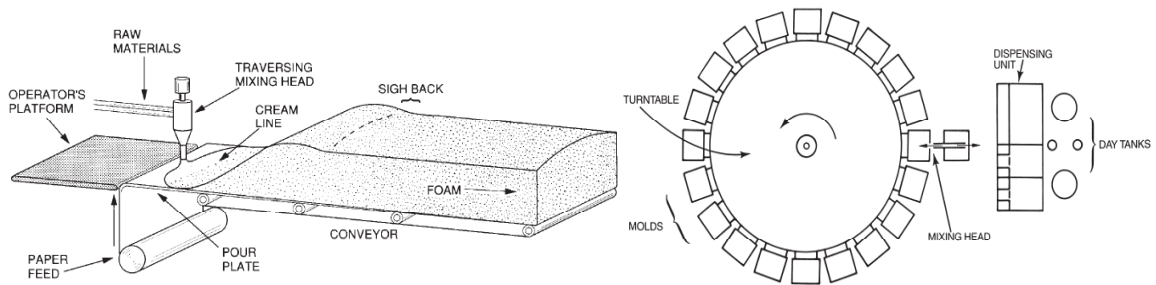


Figure 1.2: Processes for making slabstock (left) and molded (right) foams, taken from reference [4].

Clearly, molded foaming is a batch process while slabstock foaming is a continuous process. When a high productivity is desired, a batch process becomes seemingly less attractive. To compensate the slow turn-around in batch process, more reactive polyols can be used in formulations to speed up the reactions. Details on manipulating polyol reactivity through synthesis are discussed in the next section.

1.2 Polyurethane Flexible Foam Chemistry and Morphology

1.2.1 Chemistry

Polyurethane is named after the urethane bond formed via the reaction of isocyanate with hydroxyl. In flexible foam formation, the hydroxyl-isocyanate

reaction is also known as the gelling reaction. In addition to the gelling reaction, the blowing reaction that produces gas is also involved in flexible foam synthesis. The blowing reaction occurs between water and isocyanate. The reaction product, carbon dioxide, expands the polymer into the final foam form. In some formulations, a low boiling point blowing agent, such as hydrofluorocarbon, is also used to aid gas bubble formation. A schematic representation of both gelling and blowing reactions is shown in Figure 1.3. A multi-functional alcohol, called polyol, and a di-functional isocyanate are used to illustrate the gelling reaction.

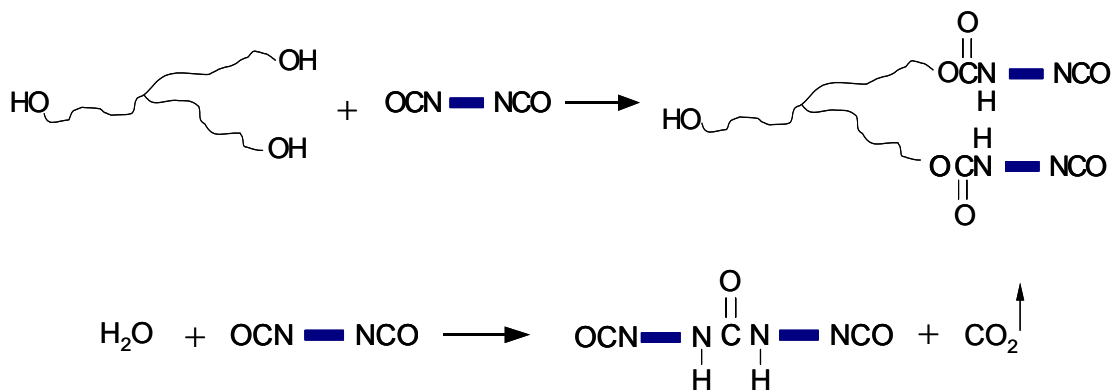


Figure 1.3: Gelling (top) and blowing (bottom) reactions.

The process to make flexible foam requires precise kinetic control over these two competing reactions. If the blowing reaction is much faster than the gelling reaction, a foam will likely to collapse early on. If the gelling reaction is faster than the blowing reaction, then a formed polymer network will likely entrap the gas and suppress bubble formation. Therefore, it is an intricate, and yet, critical step before manufacturing to find a kinetic balance point for the foaming

process. Industrially, catalysts have always been used to provide kinetic leverages [5-7].

The main reactants used in flexible foams, polyol and diisocyanate, deserve quite some attention because of the wide variety of these materials and their effects on foam properties. Diisocyanates, compared to polyol, has fewer options. Toluene diisocyanate (TDI) and methylene diphenyl diisocyanate (MDI) are the two types of diisocyanates used in flexible foam, among which TDI is the diisocyanate of choice. Chemical structure and structural variations of diisocyanates are shown in Figure 1.4.

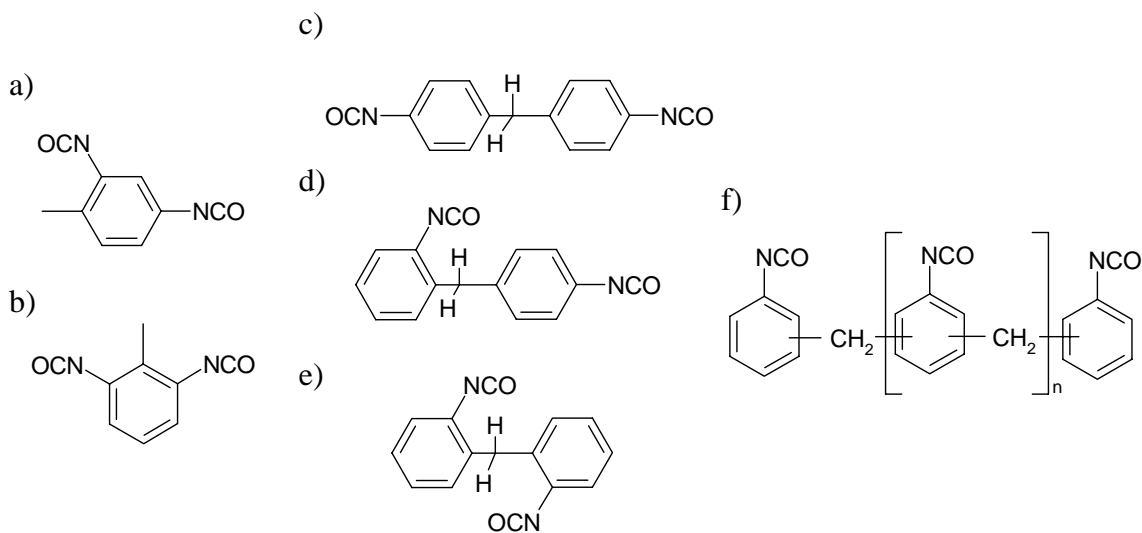


Figure 1.4: Diisocyanates commonly used in foaming: a) 2,4-toluene diisocyanate, b) 2,6-toluene diisocyanate, c) 4,4'-methylene diphenyl diisocyanate, d) 2,4'-methylene diphenyl diisocyanate, e) 2,2'-methylene diphenyl diisocyanate, and f) polymeric MDI

In contrast to diisocyanate, polyols come in a much wider range of varieties based on chemical structure, molecular weight, and functionality. The

type of polyol used in a formulation has a profound impact on foam's visco-elastic properties.

Because majority of the polyols used in flexible foam manufacturing are polyether polyols, we will focus on these polyols here [8]. A polyether polyol is made via polyaddition process. An initiator is first reacted with an alkylene oxide monomer by oxirane ring-opening reaction, and the polymerization process propagates as more monomers are added through the same reaction. To terminate, a proton exchange, by either adding water or acids, places a hydroxyl at the chain end. The most commonly used alkylene oxide monomers are ethylene oxide and propylene oxide. Due to its hydrophilic nature, ethylene oxide is seldom used as the sole monomer to make polyols, but is commonly copolymerized with propylene oxide [9]. Structures of polyols made with either ethylene or propylene oxides are illustrated in Figure 1.5. These molecules are intended to highlight the differences between polyols made with either monomer.

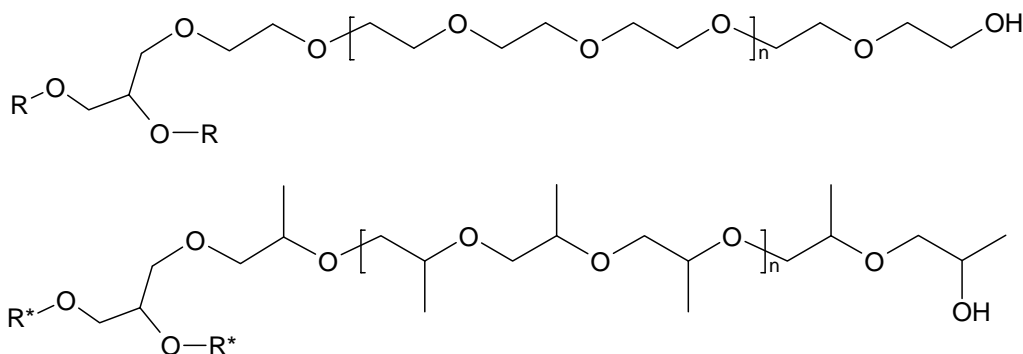


Figure 1.5: Polyether polyols made from ethylene oxide (top) and propylene oxide (bottom). The initiator used, for illustration purposes, is glycerol and R and R* represent the same structures as shown.

One apparent difference between the two molecules in Figure 1.5 is the order of hydroxyls. Ethylene oxide-based polyol has only primary hydroxyls,

whereas propylene oxide-based polyol has secondary hydroxyls. It has to be pointed out that propylene oxide-based polyol can also result in primary hydroxyls under cationic polymerization conditions. When selecting polyols for foaming, it is critical to understand how the order/position of hydroxyls may affect the process. In general, a high content of primary hydroxyls are preferred for molded foam process. This is because primary hydroxyl speeds up gelling reaction without increasing the catalyst loading and thus shortens turn-around time for manufacturing. For slabstock foaming, a range of polyols with different reactivity can be used based on application requirements and processing conditions. To make high primary hydroxyl content polyols, either polypropylene oxide or poly(propylene oxide-co-ethylene oxide) propagating chain is end-capped with ethylene oxides leaving a high content of primary hydroxyls at the chain ends.

Aside from chemical structural variations, polyols can also vary in molecular weight: from just a couple hundred up to slightly over six thousand grams per mole. For use in flexible foams, a polyol needs to have a molecular weight of 3000 g/mol or higher. Targeted molecular weight is achieved via a close monitoring of the monomer conversion and a tight control over the initiator-to-monomer ratio.

The third important variation between polyols is functionality. Functionality of a polyol simply implies the number of functional groups, in the case of polyol: hydroxyls, per molecule. Unlike molecular weight, functionality of a polyol cannot be controlled during polymerization but rather through initiator selection. The use of initiator to control functionality also helps to avoid allyl formation, which loses hydroxyls to form unsaturation sites. Because one propagating alkylene oxide chain results in one hydroxyl group, it is the number of active hydrogen on an initiator determines the number of propagating polymer chains, thus functionality

of the polyol. To meet the many needs of PU flexible foam applications, functionality of a polyol needs to be easily adjustable. Therefore, a range of initiators is available commercially. Table 1.1 lists the commonly used initiators and their functionalities.

Table 1.1: Initiators commonly used for polyether polyol synthesis [1].

Initiator	Functionality	Initiator	Functionality
<u>Carbohydrate Source</u>		<u>Amine Initiators</u>	
Sucrose	8	Alkanolamines	3
Sorbitol	6	Ethylene diamine	4
Methyl glucoside	4	Diethylene triamine	5
		Toluene diamine	4
<u>Aliphatic Initiators</u>		Diaminodiphenylmethane	4-5.5
Glycols	2	Mannich bases	3-7
Glycerol	3		
Trimethylolpropane	3		
Pentaerythritol	4		

One special family of polyols worth noting is grafted or copolymer polyol (CPP). These polyols are of great commercial significance ever since their debut in the 1950's [10]. Although CPP is referred to as a polyol, it is in fact a colloidal suspension of rigid particles sized 1 μm or smaller and does not necessarily contain reactive hydroxyls. Synthesis of CPP involves either chain or step growth polymerization in a nonaqueous media [11, 12]. In the case of a styrene-acrylonitrile copolymer polyol, styrene and acrylonitrile monomers are polymerized via chain growth polymerization reaction in the presence of unsaturated polyether polyol as a stabilizing precursor [13-15]. The polymerized

styrene-acrylonitrile copolymer polyol is comprised of stabilized particles and the polyol media.

The reason that CPP has received so much attention and been successful is its unique benefits. Incorporation of CPP allows harder flexible foams to be made without many modifications to existing formulations. In addition, CPP also adds processing benefit by promoting cell opening, which eliminates or reduces the post-crushing processes.

1.2.2 Morphology

The unique properties of flexible foams cannot be accounted for with a simple one-factor extrapolation. A combination of both the foam gas bubbles, or cells, and the polymer phase morphology contributes to the final properties.

The cellular structure, described as a collection of tetrakaidecahedral shaped cells, influences foam mechanical properties via a number of parameters [16]. Foremost, the foam modulus is most influenced by foam density, typically described by a power law relationship [17, 18]. At constant foam density, cell size and strut thickness are related to foam modulus through inverse quartic and quadratic relationships, respectively [19, 20].

At the microstructural level, polymer phase morphology varies at different length scales. Figure 1.6 depicts these variations.

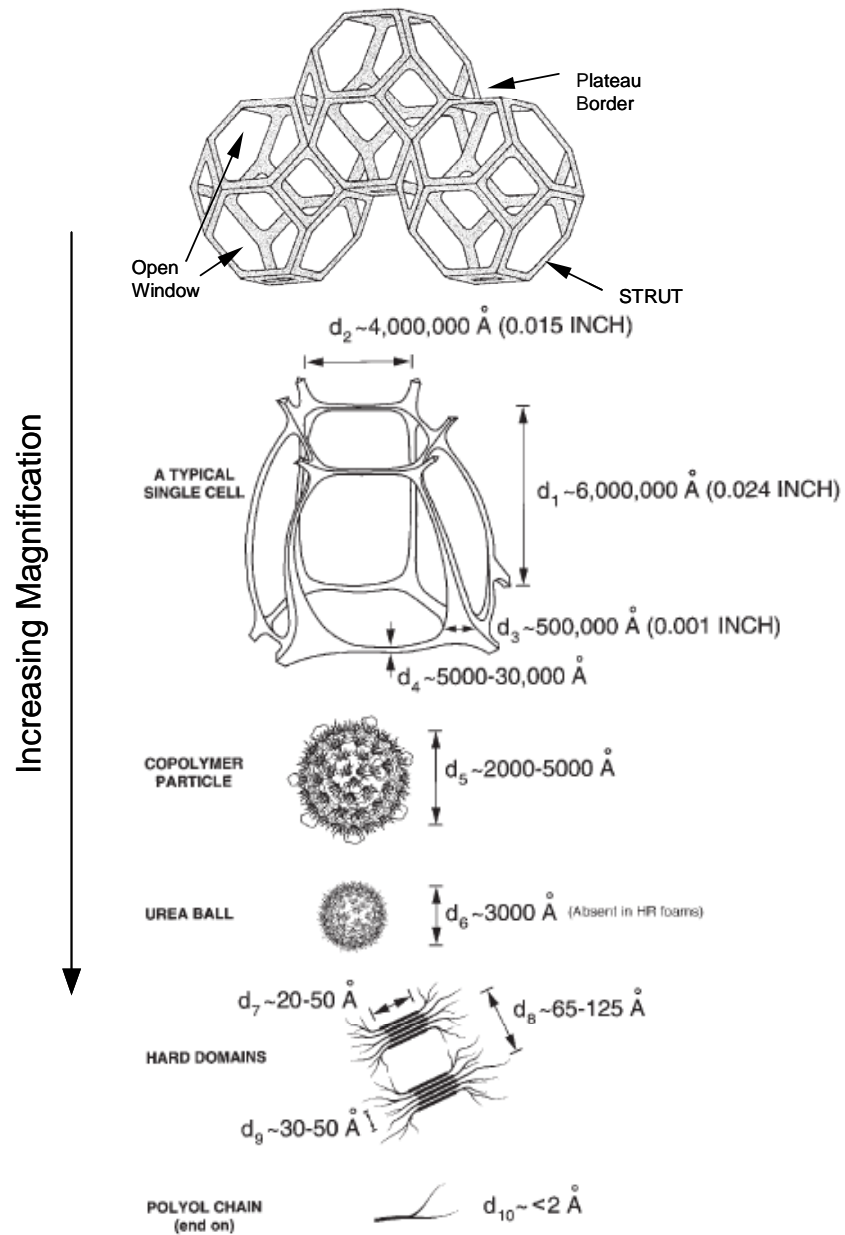


Figure 1.6: Morphology of flexible foam at different length scales [21].

To better understand polymer phase morphology in a flexible foam, we need to begin by examining the chemical reactions involved. Both blowing and

gelling reactions compete for isocyanates in the foaming mixture. The kinetically faster reaction, water-isocyanate reaction, quickly forms polyurea segments and releases CO_2 gas to expand the mixture [22]. The relatively slower reaction, hydroxyl-isocyanate reaction, gradually polymerizes isocyanates and polyols building up molecular weight. As either polyurea-based hard segment or polyol-based soft segment increases in the degree of polymerization, the interaction parameter (χ) between the two types of segments increases as well. At a critical conversion, the entire system crosses the thermodynamic boundary of a miscible system, and phase separation occurs [23-26]. The resulting polymer is a segmented block copolymer with domains that are rich in either polyurea segments or polyol segments [27]. Within a polyurea-rich hard domain, further association of the segments can also occur through hydrogen bonding [28-30]. A simple illustration of this phase-separated morphology is shown in Figure 1.7.

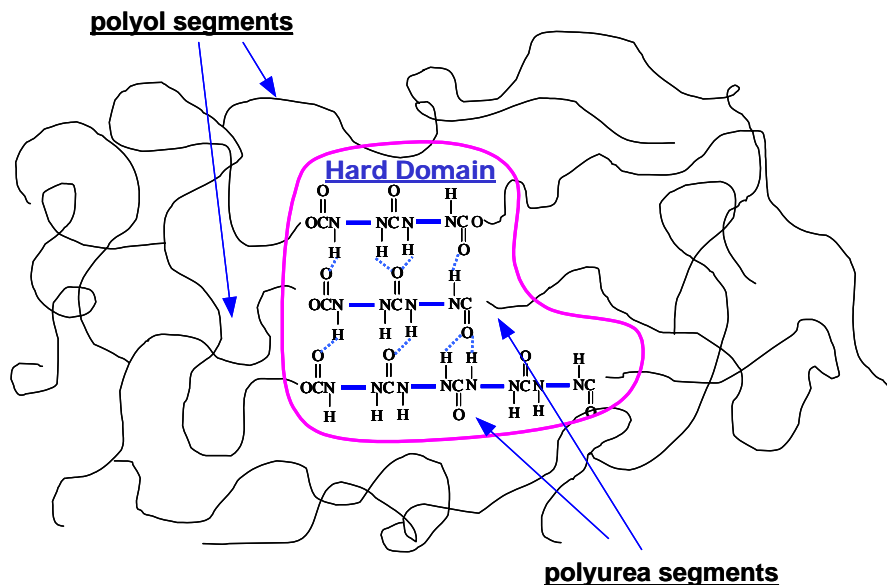


Figure 1.7: Phase separated morphology of PU flexible foams. Dashed lines indicate hydrogen bonding within a hard domain.

This phase-separated morphology gives flexible foam its unique properties. The polyol-rich domains, also called soft domains, have a low glass transition temperature (T_g) that can be anywhere from $-50\text{ }^\circ\text{C}$ to $-70\text{ }^\circ\text{C}$. The low T_g domains give PU flexible foam its visco-elastic properties and allow energy absorption and dissipation. The polyurea-rich domains, also called hard domains, have a much higher T_g , in comparison, generally above $200\text{ }^\circ\text{C}$. The high T_g hard domains provide PU flexible foam with its modulus and thermal stability.

Within the soft domains of a PU flexible foam, the polyol segments are covalently crosslinked as the polyols used in flexible foam synthesis have functionalities of 3 or higher. The entire polymer phase of a flexible foam is, therefore, comprised of both covalent crosslinks in the soft domains and physical crosslinks in the hard domains.

1.3 Natural Oil Polyols

Because of its unique properties, PU is an indispensable material in areas, such as construction, furnishing and transportation. Similar to most polymeric materials, PU relies on petroleum for feedstock. As the price of crude oil in US escalated from $\$11/\text{barrel}$ in 1998 to $\$110/\text{barrel}$ today, the cost of raw materials: polyol and isocyanate have risen steadily [31-36]. From both economic and environmental stand point, it is desirable to replace petroleum oil as a feedstock with a renewable resource.

As early as 1930's, Henry Ford envisioned that agricultural products, such as soybeans, would one day be the raw material sources for automobiles [37]. For PU raw materials, natural oils, such as soybean oil comprised of unsaturated triglycerides, can potentially lend themselves to polyol synthesis. Structurally, triglyceride is a branched molecule, similar to polyols. However, with the

exception of castor and lesquerella oils, natural oils do not contain hydroxyls inherently [38, 39]. Conversion steps are needed to add hydroxyls to natural oils. In Table 1.2, some of the natural oils can potentially be used for polyol synthesis are listed and their compositional variations are indicated.

Table 1.2: Composition of some common natural oils [38].

Natural Oil	Oleic (18:1) ^a	Linoleic (18:2)	Linolenic (18:3)	Ricinoleic (18:1) ^b	Stearic (18:0)	Palmitic (16:0)	Others
soybean oil	24	54.5	6.8	--	3.2	10.9	0.6
castor oil	6.0	1.0		89.5	1.0	2.0	0.5
safflower oil	13.1	77.7			2.4	6.5	0.3
palm oil	45.2	7.9			3.6	40.8	2.5

^a The numbers in the parenthesis indicates the total number of carbon bonds and number of unsaturation sites in the fatty acid residue.

^b Ricinoleic acid residue contains functional hydroxyl, see Figure 2.1 for details.

A number of methods adding hydroxyls at the unsaturation sites have been reported and Figure 1.8 and 1.9 show the five known processes. For illustration purposes, a single triglyceride molecule is used as the starting material.

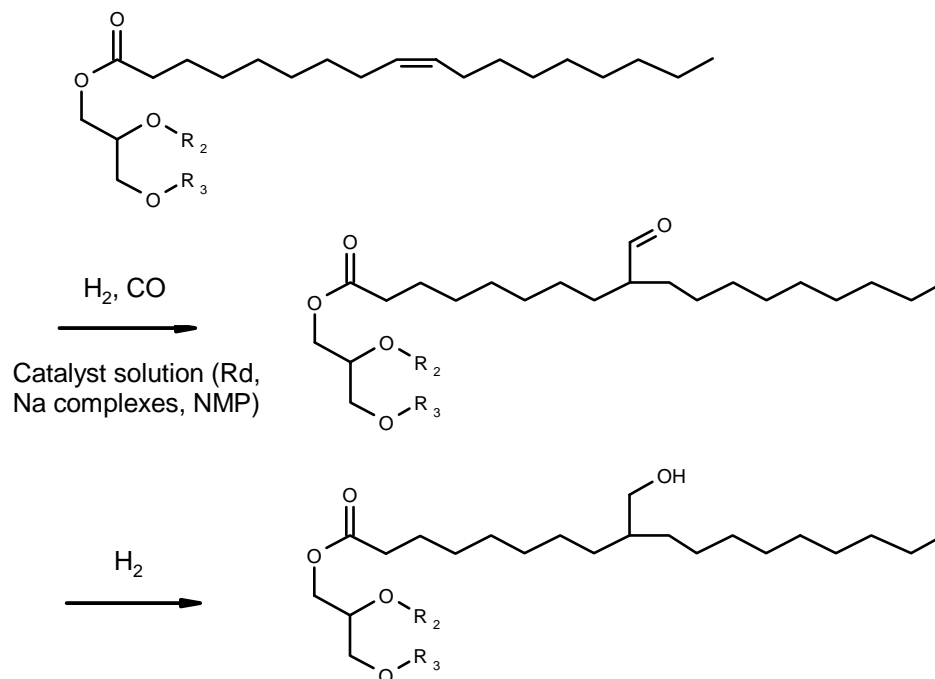
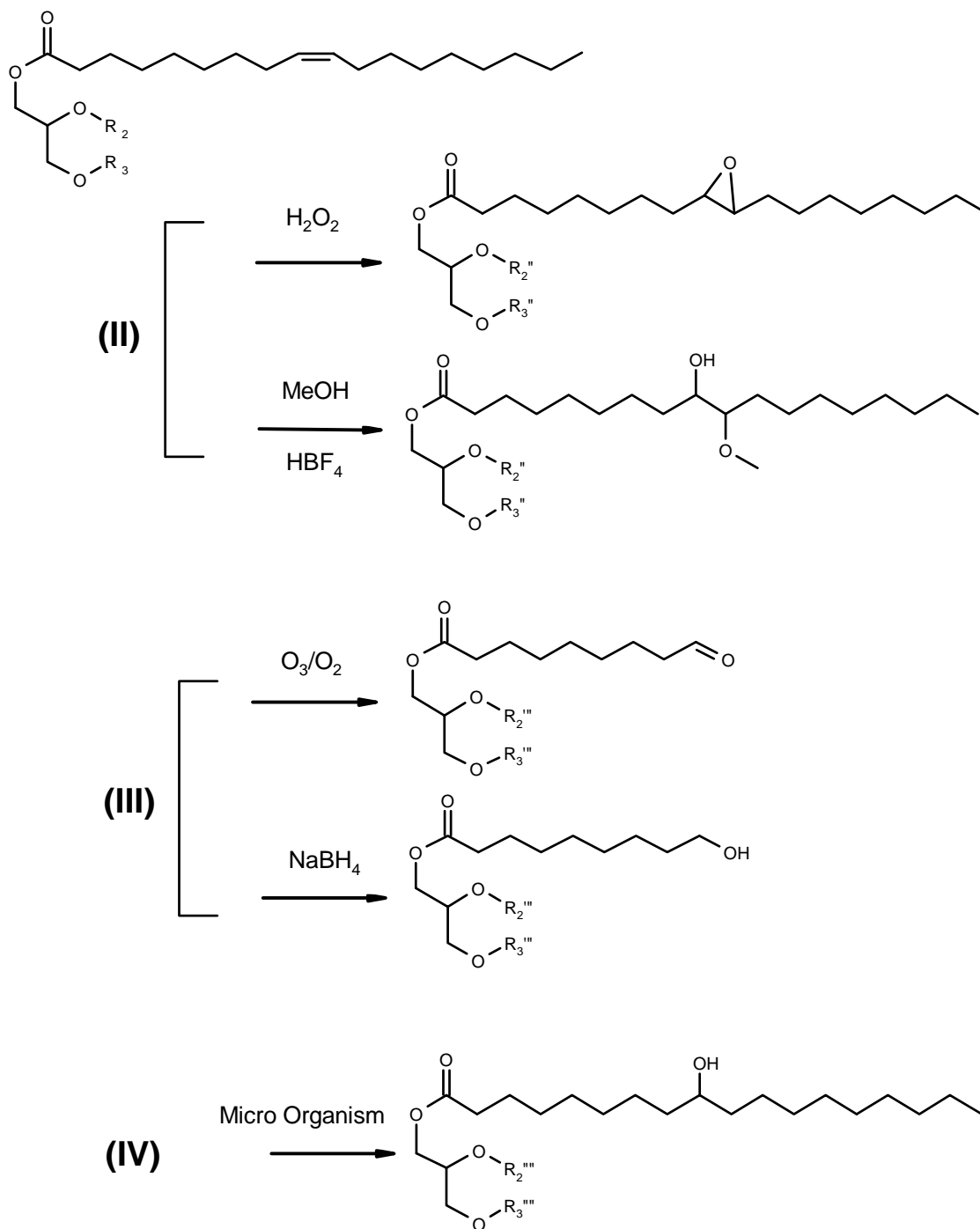


Figure 1.8: Conversion of a triglyceride molecule to an alcohol via hydroformylation followed by hydrogenation method, method (I) [40]. R₂ and R₃ are indicative of unsaturated fatty acid residues.

The hydroformylation followed by hydrogenation method is being used industrially to make polyols [40, 41]. Although in practice the reaction is different from illustrated as the starting material, instead of triglyceride, is fatty acid methyl esters. The triglyceride molecules first undergo a transesterification reaction with methanol to form methyl esters and are then subjected to the hydroformylation reaction outlined above. The hydroxyl-containing esters obtained at the end of reaction are further reacted with an initiator, could be a conventional initiator (Table 1.1) or a polyol, a polyamine, or other suitable molecules, to produce polyol with desired molecular weight [42]. This process allows easy molecular weight build up in addition to generating kinetically advantageous primary hydroxyls.



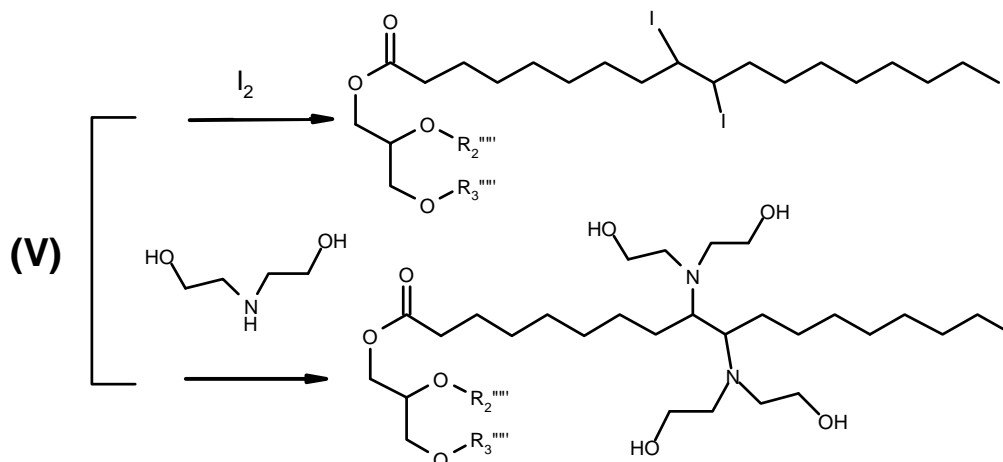


Figure 1.9: Methods for converting natural oil to polyol: (II) epoxidation and oxirane ring-open with methanol [43], (III) ozonolysis [44], (IV) microbial conversion [45], and (V) halogen addition and nucleophilic substitution [46]. R_2 and R_3 are indicative of unsaturated fatty acid residues and superscripted R_2 and R_3 are indicative of modified fatty acid residues.

Methods (II) through (V) can be directly applied to natural oils themselves as presented in Figure 1.9. Among these four methods, ozonolysis is a rather expensive process. Not only ozone generation is costly but also the process to separate the product from a significant amount of byproducts is economically undesirable. Method (IV), the microbial conversion method, is capable of generating high purity polyols at high yields. However, the low production rate makes this process impractical. Method (II) and method (V) are, thus, the most favorable routes for converting natural oils to polyols for industrial applications.

1.4 Natural Oil Polyol-based Polyurethanes

Natural oil polyols derived from different oil seeds, such as soybean, sunflower, canola, and rapeseed, have been successfully used in PU elastomer

synthesis [47-49]. Authors reported comparable hardness/modulus between elastomers synthesized from petroleum polyether polyols and natural oil polyols. Thermal degradation experiments indicated that natural oil polyols derived elastomers are superior to petroleum polyols derived samples in both thermal stability and oxidation resistance [47, 48]. Researchers believe that the thermal stability and oxidation resistance are attributable to a high content of hydrocarbons in natural oil polyols as oppose to the alkylene oxide in petroleum polyols. Other than processed natural oil polyols, unprocessed castor oil containing hydroxyls naturally, has also been experimented as a potential polyol for elastomer synthesis [50]. Unlike the processed polyols, the addition of castor oil was shown to lower the Young's modulus and improve elongation properties. Although both castor oil and processed oil polyols are considered as natural oil polyols, their resulting elastomers differ in mechanical properties. Some believe that the difference in heterogeneity between processed polyols and castor oil cause the differences in elastomer properties [51]. When functional hydroxyl groups are added to a triglyceride molecule, depending upon the location of unsaturation sites and process method used, the number of hydroxyls, or functionality, as well as the location of the hydroxyls vary significantly [43]. A naturally occurring polyol, such as castor oil, has less variations in its fatty acid residue structures, for castor oil ~ 90% of the fatty acid residues are ricinoleic acid [38, 52, 53]. Zlanatic et. al. surveyed a range of natural oil polyols and their elastomers and concluded mechanical properties are largely dependent upon the crosslinking density and functionality of the polyol, and less influenced by the position of the hydroxyls [51]. However when low functionality polyols are used, the heterogeneity of the polyols was shown to have an adverse effect on both young's modulus and elongation at break [54]. Authors further speculated that the loss in elongation properties, in particular, was due to the imperfections introduced through the heterogeneity of natural oil polyols [55].

Aside from elastomer applications, rigid foam, which is the second largest family of PU products, can also benefit from using natural oil polyols. Similar to the elastomer cases, rigid foams made from soybean oil-derived polyol showed superior thermal stability and oxidation resistance to the petroleum polyol foams [56]. Guo et. al. suggested that the absence of the ether linkage is the key to improved thermal and oxidation properties. Mechanical testing on rigid foams synthesized from a number of soybean oil-derived polyols showed that these rigid foams delivered similar compressive properties to the petroleum foams [57, 58]. Thermal conductivity of all foams tested showed no significant changes and was independent of polyol properties. Other than soybean oil polyols, rigid foam can also be made from rapeseed oil-derived polyols, however, the authors recommended that both polyol reactivity and long-term stability of the polyols should be further understood [59].

The most important family of PU products is flexible foams, however, making such foams from natural oil polyols has found limited success. John and coworkers synthesized flexible foam using entirely soybean oil polyol and concluded that soybean oil polyol can be potentially used [60]. However, the SEM images provided show large amounts of closed cells. Herrington et. al. and Babb et. al., instead of using entirely soybean oil polyols, replaced part of petroleum polyol with soybean oil-derived polyol and found improvements in foam loadbearing properties without sacrifices in the number of open cells [61, 62]. Zhang et. al. further studied flexible foams made with different substituent polyols including a soybean oil-derived polyol and concluded that both changes in hard domain morphology and the addition of a second soft domain with high glass transition temperature increased soybean polyol foam modulus [63]. There has been some success in using castor oil, however, samples made from this

natural polyol are limited to low resiliency foams, which means only partial recovery can be attained immediately after deformation [64].

The goal of this research is to understand the potentials and the limitations of natural oil polyols and ultimately synthesize flexible foams using entirely natural oil polyols.

1.5 Organization of Thesis

We focused our attention on flexible foam because replacing petroleum polyols using natural oil polyols in this application has the most profound impact on PU industry. In addition, no success has been reported, yet, on flexible foams synthesized *entirely* from natural oil polyols. To achieve our research goal of understanding natural oil polyols, we began by exploring an experimental soybean oil-derived polyol (SBOP), see details in Chapter 2, and expanded the study to natural oil-based model polyols.

Chapter 2 describes formulating foams with entirely natural oil polyols as we explore the potential of using either castor oil or SBOP as the sole polyol component in foams. Castor oil produced a low resiliency foam, while SBOP produced a rigid foam. Evidently, the two natural oil polyols are not the ideal candidates for flexible foam synthesis. Two approaches were taken thereon. In the first approach, SBOP was investigated as a substituent polyol in a flexible foam formulation. In the second approach, a series of natural oil-based model polyols was designed and investigated for their potentials as the sole polyol component in flexible foams.

Both Chapter 3 and 4 document the substituted polyol systems. In Chapter 3, we studied the morphology changes as natural oil polyols were used to replace a petroleum polyol. Comparative method was used to uncover the

role that a natural oil polyol played in changing foam mechanical properties. In Chapter 4, a different subject, reaction kinetics, was explored. Because of the structural differences between petroleum and natural oil polyols, the reactivity of the hydroxyls is expected to vary. In this chapter, we examined the reactivity of small molecule alcohols that are analogous to either petroleum or natural oil polyols and then followed foaming reactions of substituted polyol systems via Fourier transform infrared spectroscopy coupled with an optical fiber.

In Chapter 5, the focus shifted to design natural oil-based polyols that can be potential candidates as the sole polyol component in flexible foams. Based on results in Chapter 2, we hypothesized that the molecular weight between hydroxyls is the dominating factor in determining the thermal and mechanical properties of a foam. To substantiate this hypothesis, a series of polyols was synthesized using ricinoleic acid as repeating unit and polyurethane samples were made thereof. The experimental data indicate that high molecular weight natural oil-based polyols do result in foams of flexible nature. Included in this chapter also are the experimental results of molecular weight distribution (MWD) effects on polyurethane thermal-mechanical properties.

Chapter 6 provides a summary of the research and a brief overview of possible research directions in the future.

Chapter 2

Polyurethane Foams made with Single-polyol Component

Contents

2.1	Chapter Overview	22
2.2	Introduction	22
2.3	Experimental	23
2.3.1	Materials	23
2.3.2	Foam Synthesis	26
2.3.3	Characterization	28
2.4	Results and Discussion	31
2.4.1	Foam Kinetics	31
2.4.2	Thermal-mechanical Properties	36
2.4.3	Small Angle X-ray Scattering	43
2.4.4	Fourier Transform Infrared Spectroscopy	45
2.5	Conclusion and Outlook	49

2.1 Chapter Overview

In this chapter, four polyols, two petroleum and two natural oil polyols, were selected as the sole polyol components for polyurethane (PU) flexible foam synthesis. The goal is to examine whether natural oil polyols can be used as the sole polyol components for flexible foam synthesis and to understand the differences between petroleum and natural oil polyols. Foam samples obtained ranged quite widely in properties. One of the petroleum polyol produced a flexible foam, while the other petroleum polyol and castor oil produced semi-flexible foams. SBOP produced a rigid foam.

The thermal-mechanical study showed that the flexibility of a foam was closely associated with its glass transition temperature (T_g). Further examination of the data suggested that polyol molecular weight could have played a vital role in determining T_g . Although castor oil and SBOP are not the ideal sole polyol components for flexible foams, they provided us the first step toward understanding natural oil polyols.

2.2 Introduction

Flexible foam is the single largest product family in PU [65]. The unparalleled properties offered by PU, such as vibration damping, sound insulation, impact protection and consumer comfort, have made this material an indispensable component in furnishing, transportation and packaging industries [21].

In the recent years, the price of crude oil has escalated raising many concerns over the stability and the sustainability of petroleum resources [31]. The rising cost of crude oil also impacts the cost of PU products, because majority of the raw materials, such as polyols and isocyanates used in flexible

foams, are petroleum derivatives [34]. Finding an alternative feedstock for PU has become highly desirable for both economic and environmental reasons. Natural oils, such as soybean and safflower oils, have been shown to be a potential bio-renewable feedstock for PU [66-72].

Early research work has focused on synthesizing elastomers and rigid foams from entirely natural oil polyols and are proven to be successful, however, challenges remain in making flexible foams, the most significant PU product, using entirely natural oil polyols [47, 49, 59, 60]. Thus far, castor oil, a naturally occurring polyol, has been used as the sole polyol component for flexible foam synthesis [64]. The samples obtained, although are low resiliency flexible foams meaning slow recovery from deformation, are the first success case of entirely natural oil polyol-based flexible foams. On the other hand, polyols derived from natural oils using methods stated in Chapter 1.3, such as SBOP, have not been reported as a successful sole polyol component in flexible foam synthesis. In the open literatures, no mention has been made regarding the reason why these processed natural oil polyols are not used in flexible foams as the sole polyol components.

As the goal of this research is to understand the potentials and the limitations of natural oil polyols and ultimately synthesize flexible foams entirely from them, understanding both castor oil and SBOP is naturally the first step. Four polyols, two petroleum and two natural oil polyols, were selected and used in polyurethane foams synthesis.

2.3 Experimental

2.3.1 Materials

The four polyols selected for this study are: two petroleum polyols, a

naturally occurring polyol, and a processed natural oil polyol. Properties of the polyols used are shown in Table 2.1.

Table 2.1: Properties of polyols used.

Polyol	Hyperlite [®] E-848	Softcel [®] U- 1000	Castor oil	SBOP
OH # (mg KOH/g)	32	168	163	201
Molecular weight (g/mol)	6700	1000	930	1058
Manufacture /Source	Bayer Corporation	Bayer Corporation	Sigma- Aldrich	Experimental
T_g (°C)	68	65	64	35
ΔC_p (J/g/°C)	0.6	0.67	0.88	0.79

Hyperlite[®] E-848 is a propylene oxide-based, ethylene oxide-capped polyol commonly used in flexible foam formulations. Hyperlite[®] E-848 contains approximately 85% primary hydroxyls and has a functionality (f_n) of 3.8 [73]. Softcel[®] U-1000 is a propylene oxide-based, glycerol-initiated polyol with a f_n of 3.0 [73]. Castor oil is a triglyceride fatty acid and approximately 90 % of its fatty acid residues are ricinoleic acid and the rest 10 % varying mainly among oleic, linoleic, stearic and palmitic acids. The f_n of castor oil is 2.7 [38]. The SBOP used here is derived by epoxidizing soybean oil followed by an oxirane ring-opening reaction using a mixture of water and methanol [43]. SBOP has a f_n of 3.8, the same as Hyperlite[®] E-848. The idealized structure of both castor oil and SBOP are shown in Figure 2.1.

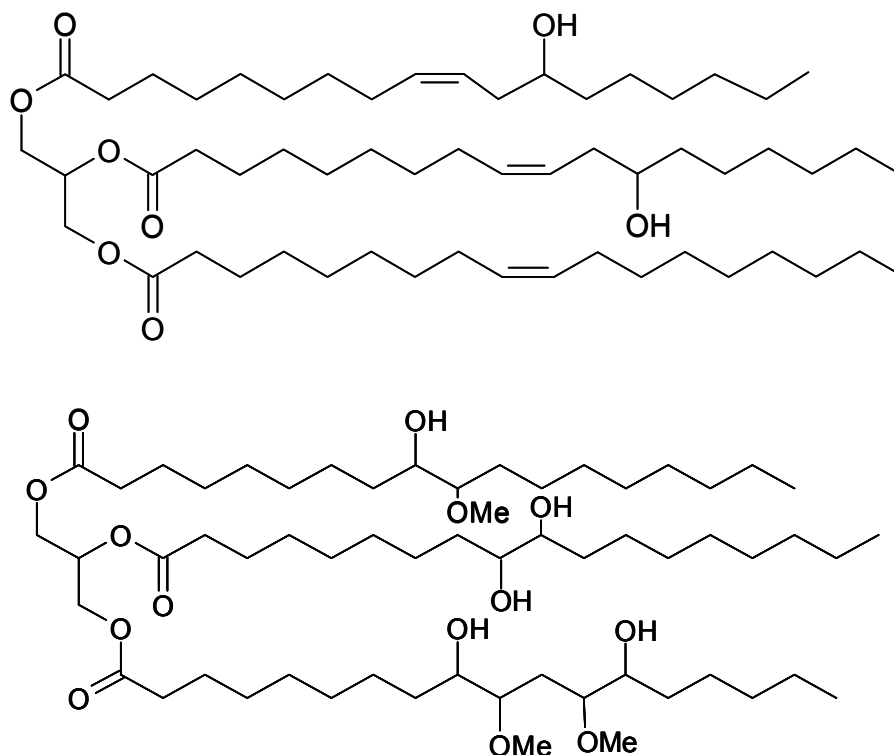


Figure 2.1: Idealized structures of castor oil (top) and SBOP (bottom). Castor oil shown above contains two units of ricinoleic acid and one unit of oleic acid residues.

Toluene diisocyanate (TDI) used is an 80:20 mixture of 2,4 and 2,6 isomers (Grade A Mondur[®] T-80, Bayer Corporation). Isocyanate in excess of that needed to react with the OH groups on the polyols reacts with distilled water to form CO₂, which acts as the only foam blowing agent. Gelling and blowing catalysts, Dabco[®] 33-LV, Dabco[®] T-12, and Dabco[®] BL-11, were obtained from Air Products and Chemicals and were used as received. Dabco[®] 33-LV and Dabco[®] T-12 are both gelling catalysts used to accelerate the reaction of NCO with OH. Dabco[®] 33-LV is a solution of 33 wt% triethylene diamine in dipropylene glycol and was used as the gelling catalyst in Hyperlite[®] E-848 foam only. Dabco[®] T-12 is a strong gelling reaction catalyst comprised of dibutyltin

dilaurate (DBTDL) and was used in foam formulations other than Hyperlite[®] E-848. Dabco[®] BL-11 is a blowing catalyst used to accelerate the reaction of NCO with water. Dabco[®] BL-11 is a solution of 70 wt% bis(2-dimethylaminoethyl)ether in dipropylene glycol.

Single surfactant was used in this study to stabilize the foam cellular structures: Niax L-3184 (Momentive Performance Materials, formerly GE Silicones, Huntersville, NC) is a silicone-based, molded foam surfactant.

2.3.2 Foam synthesis

Table 2.2 gives the details on foam formulations. All samples were made based upon a total mixture weight of 250 g. The amount of TDI used stoichiometrically balanced NCO to active hydrogen species, i.e. isocyanate index = 100. The amounts of water used were calculated to keep hard segment (HS) contents at ~28% between samples. For HS % calculation, see Equation 3.1 in Chapter 3 for details.

Table 2.2: Foam formulations of single-polyol systems.

Component	Hyperlite[®] E-848	U-1000	Castor oil	SBOP
Hyperlite [®] E-848	100	--	--	--
Softcel [®] U-1000	--	100	--	--
Castor oil	--	--	100	--
SBOP	--	--	--	100
Water, distilled	4.2	2.0	2.0	1.3
Niax [®] L-3184	1.0	1.0	0.6	0.6
Dabco [®] BL-11	0.08	0.08	0.08	0.08
Dabco [®] 33-LV	0.5	--	--	--
Dabco [®] T-12	--	1.0	2.0	2.0
TDI weight (g, index = 100)	75.7	74.5	74.7	74.1
Foam density (kg/m ³)	30.8	34.2	34.6	40.9
HS (%)	28.1	28.8	28.9	29.0

All ingredients except the TDI were weighed into a 500 mL polypropylene beaker cup and mixed using a 10-in shop drill (Delta ShopMaster, Model DP-200) equipped with a 3-inch diameter mixing blade (ConnBlade Brand, Model ITC, Conn & Co., Warren, PA) for 30 seconds at 1500 rpm. At the end of the mixing period, pre-measured TDI was added to the mixing cup and the mixing continued for another 6 seconds. The contents were quickly transferred into a 170 fl. oz paper bucket (International Paper Company, SFR-170, Memphis, TN). The foam was allowed to rise at room temperature for approximately 30 seconds

before it was transferred into a pre-heated curing oven controlled at 70 ± 1 °C. The foam was hand crushed after 8 minutes in the curing oven to open the cell windows and prevent foam shrinkage. For adiabatic temperature rise measurements during foaming, the samples were kept in the ambient and discarded after the experiments.

2.3.3 Characterization

Adiabatic Temperature Rise

Temperature profiles during foaming were taken using type J thermocouples made in-house. Two fine wires of Iron and constantan, 0.25 mm in diameter, were purchased from Omega Engineering Inc., Stamford, CT. The wires were first cut into 30 cm long pieces and the nylon jacket at one end was stripped. The exposed wires, one iron wire and one constantan wire, were brought to form a knot by twisting the exposed ends together by hand. A propane blowtorch was then brought to a quick contact with the twisted ends thus melting the two metals to form a welded tip. The thermocouple is accurate to 0.1 °C in measurements. The analogue temperature reading was recorded via an analogue connection on a rheometer (ARES II, TA instruments, New Castle, DE) at 1 Hz frequency. The conversion of the analogue signals to temperature reading was performed via a pre-measured calibration curve.

Differential scanning Calorimetry

Differential scanning calorimetry (DSC) (Q1000, TA Instruments, New Castle, DE) was used to determine the soft domain T_g . An amount of 3-7 mg of foam was loaded into an aluminum pan and sealed hermetically. The sample was first heated at 10 °C/min to 110 °C and equilibrated for 2 minutes before

cooling down to $-120\text{ }^{\circ}\text{C}$. The second temperature ramp heated the samples up to $300\text{ }^{\circ}\text{C}$ at $10\text{ }^{\circ}\text{C}/\text{min}$ and was used to determine the T_g and heat capacity change (ΔC_p).

The T_g of polyol was measured in the same instrument by loading approximately 5 mg of the polyol into an aluminum pan and sealed hermetically. The sample was first cooled down to $-100\text{ }^{\circ}\text{C}$ and equilibrated for 5 minutes, followed by heating up to $40\text{ }^{\circ}\text{C}$ at $10\text{ }^{\circ}\text{C}/\text{min}$. A cooling isotherm was also taken on the polyol samples when it was cooled to $-100\text{ }^{\circ}\text{C}$ at $10\text{ }^{\circ}\text{C}/\text{min}$. Both T_g and ΔC_p were determined.

Dynamic Mechanical Analysis

Dynamic mechanical analysis (DMA) was used to probe the mechanical properties of foams over a large temperature range. Foams were cut using a hot wire into 25 mm diameter and 10 mm thick disks and tested under sinusoidal oscillation mode between two 25 mm diameter serrated parallel plates (ARES II, TA Instruments, New Castle, DE). Contact between the sample and plates was ensured by first gluing the foam sample onto the serrated plates using Cyanoacrylate adhesives (KrazyGlue[®], Elmer's Products, Inc., Columbus, OH) and maintaining a constant normal force of 50 g throughout the experiment. Storage modulus (G') was recorded at a frequency of 1 Hz over the temperature range from -100 to $200\text{ }^{\circ}\text{C}$. The temperature ramp rate was controlled at $3\text{ }^{\circ}\text{C}/\text{min}$ and strain applied was 0.2 % for temperature above $25\text{ }^{\circ}\text{C}$ and 0.1 % for temperature below. Both strains are within linear viscoelastic region of the foam in the corresponding temperature range.

Small Angle X-ray Scattering

To examine the characteristics of internal structures in foams especially the phase-separated morphology, small angle X-ray scattering (SAXS) technique was employed. Approximately 10 mg of the foam sample was compressed into a copper sample holder to a thickness of 2mm and placed in a SAXS apparatus. The experimental setup is comprised of a Rigaku rotation anode, Cu source and a Siemens Hi-Star multi-wire area detector. The X-ray generator operates at 12 kW and 40 mA. The attainable scattering angle ($\theta/2$) ranges from 0.18° to 38° . The foam was exposed to X-rays for 5 minutes.

Fourier-transform Infrared Spectroscopy with Attenuated Total Reflectance

A Fourier-transform infrared spectroscopy (FTIR) (Nicolet Series II Magna-750, Thermo Fisher Scientific Inc., Waltham, MA) equipped with a single bounce attenuated total reflectance (ATR) attachment (ProfilirTM, SpectraTech, Oak Ridge, TN) and a mercury-cadmium-telluride detector was used to collect spectra at foam surfaces. Samples were cut using a razor blade to 2 x 2 x1 cm cubes from the center of the foam buns and a total of three samples were tested for each formulation. The foam was pressed against the ATR crystal to ensure complete contact. A total of 512 scans were taken on each sample over the wavelength range of 4000 to 400 cm^{-1} at a resolution of 4 cm^{-1} . The collected spectra were normalized with respect the absorbance of the aromatic C=C stretching in TDI at 1600 cm^{-1} . Deconvolution of each spectrum was performed in the carbonyl region (1800 - 1550 cm^{-1}) using Thermo Galactic's GRAMS/AI software. Each peak was fit to a Gaussian curve at a series of fixed wavelengths given in Table 2.3.

Table 2.3: IR band assignments in carbonyl region [74-76].

Chemical bond	Wavenumber (cm⁻¹)
Ester carbonyl	1745
Free urethane	1732
Free urea	1713
Hydrogen bonded urethane	1695
Monodentate urea	1676, 1662
Bidentate urea	1640-1645

2.4 Results and Discussion

2.4.1 Foam Kinetics

During foaming, both gelling and blowing reactions are exothermic reactions. As a foam takes on its shape, the cellular structures developed act as a layer of insulation around the center of a foam bun making it an adiabatic reactor. Figure 2.2 shows the adiabatic temperature rise profiles taken of the foam buns.

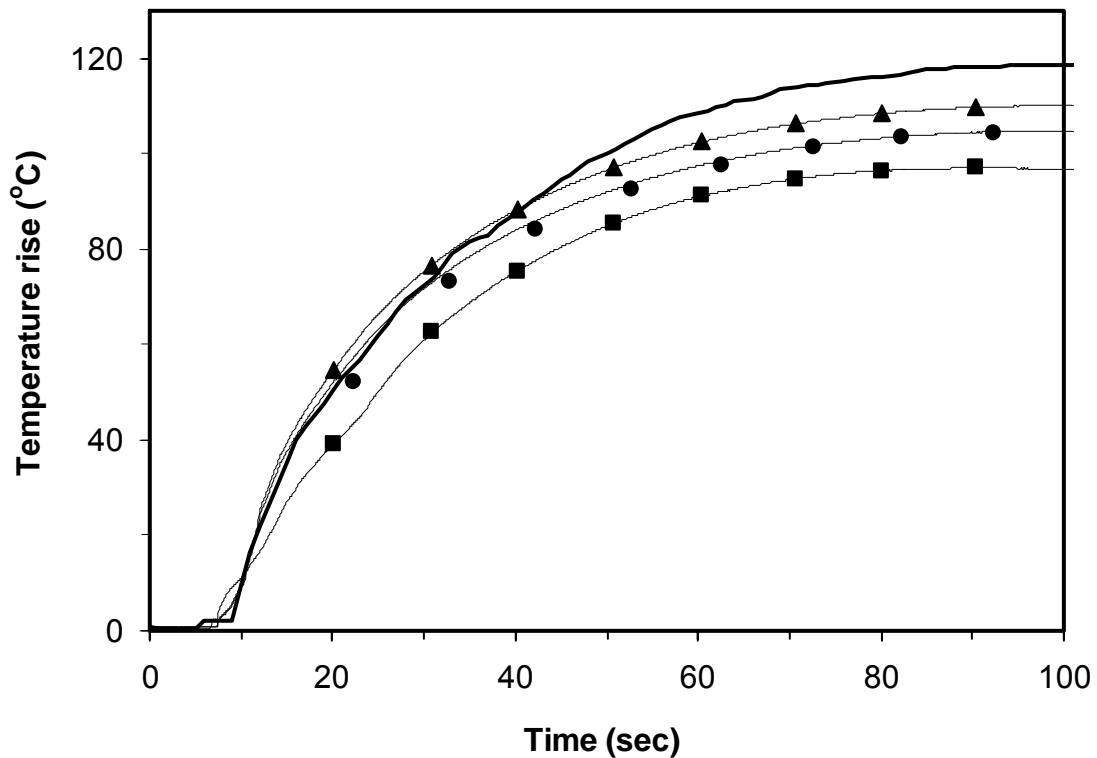


Figure 2.2: The adiabatic temperature rise during foam formation: Hyperlite® E-848 (solid line), U1000 (●), castor oil (▲), and SBOP (■). Timer started when TDI was added to the polyol mixture.

One of the characteristics of an adiabatic temperature rise is its direct relationship with reaction kinetics. In the case of PU foam formation, the temperature change is related to the consumption of a common reactant in both gelling and blowing reactions, isocyanate [24]. Equation 2.1 shows the relationship between the isocyanate conversion and the temperature rise. The calculated isocyanate conversions from the temperature rises are plotted in Figure 2.3.

$$p(NCO) = \frac{r\Delta T_m}{\Delta T_{rxn}} \quad (2.1)$$

$$\Delta T_{rxn} = \frac{Q}{C_p m_T} = \frac{\Delta H_{r,u} \frac{m_w}{M_w} + \Delta H_{r,r} \frac{m_{OH}}{M_{OH}} f_n}{C_p m_T}$$

where p is the isocyanate conversion, r is the stoichiometric ratio of functional groups, which is unity in this case, ΔT_m is the temperature rise during foaming measured via thermocouple, ΔT_{rxn} is the maximum temperature rise based on an adiabatic reactor, Q is the total amount of heat generated in the unit of J, ΔH_r is the heat of reaction in the unit of J/g, m is reactant mass, C_p is the specific heat capacity of foam, which is 1.81 J/g^oC, M is the molecular weight in the unit of g/mol, f_n is polyol functionality, and the subscripts, u,r, w, OH, and T indicate urea, urethane, water, polyol and total, respectively. The heat of reaction for urea and urethane formation were taken as -125.5 kJ/mol and -93.9 kJ/mol [77-79].

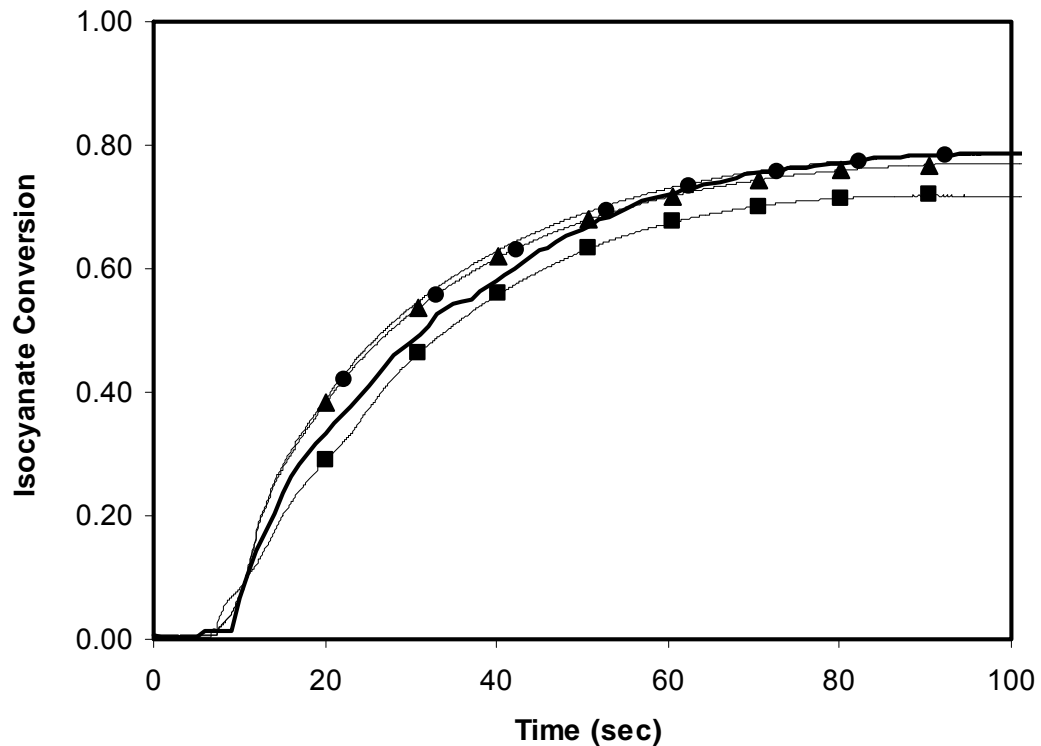


Figure 2.3: The isocyanate conversions calculated from temperature rises during foaming: Hyperlite® E-848 (solid line), U1000 (●), castor oil (▲), and SBOP (■). Timer started at the moment TDI was added.

The isocyanate conversion versus time curves in Figure 2.3 for all four foam samples are very similar. This similarity required changes in the gelling catalyst. In the Hyperlite® E-848 foam, a tertiary amine type of gelling catalyst, DABCO® 33-LV, was used and proven adequate. For the same catalyst, DABCO® 33-LV, when used in foam formulations containing natural oil polyols or Softcel® U-1000 at the same loading as in Hyperlite® E-848, no detectable string time¹ was found 10 minutes after the initial mixing. Furthermore, the foams collapsed during the curing step. The gelling reaction, when catalyzed by

¹ String time is defined as the amount of time between the initial mixing and the strings of viscous material can be pulled away from the surface, or gel time.

DABCO[®] 33-LV, is evidently too slow in foams containing natural oil polyols or Softcel[®] U-1000.

Test trials on the effect of gelling catalyst were performed at room temperature by reacting a polyol with TDI only and monitoring the reaction using a rheometer. Both castor oil and SBOP reaction with TDI showed gel times greater than one hour at 6 pph loading of DABCO[®] 33-LV. Compared to the polyol used in Hyperlite[®] E-848 foam, its reaction with TDI has a gel time of approximately 5 minutes at 0.4 pph loading of DABCO[®] 33-LV. Tertiary amine-type gelling catalyst is, therefore, not an effective catalyst for natural oil polyol-TDI reaction. The high content of primary hydroxyls in Hyperlite[®] E-848 polyol undoubtedly gives rise to the gel time differences as well as its less sterically hindered hydroxyls. Tin-based catalyst, on the other hand, is much more effective. At 4pph loading of DBTDL, the gel time for TDI-castor oil, TDI-SBOP, and TDI-Softcel[®] U-1000 reactions was reduced to approximately 8, 8.5, and 6.5 minutes, respectively. Further testing of the DBTDL catalyst in foam formulations indicated that at 2 pph loading the string time in either castor oil or SBOP foam was reduced to ~ 170 seconds, which is comparable to the string time in Hyperlite[®] E-848 foam. For Softcel[®] U-1000 sample, 1pph DBTDL was shown to be adequate giving a string time of ~ 160 seconds. The eventual 2pph, instead of 4pph, gelling catalyst loading in both natural oil polyol foams can be attributed to the autocatalytic effect of urethanes and the exothermic reactions, which increase reactivity through an increase in temperature.

The isocyanate conversion profiles in Figure 2.3 are nearly identical among Hyperlite[®] E-848, U-1000, and castor oil foams, whereas SBOP foam has a slightly lower isocyanate conversion. During the first 20 seconds of reaction, TDI was consumed at a 20 % slower rate in SBOP and nearly 10 % faster in castor oil and U-1000 foams than in the Hyperlite[®] E-848 sample. The difference

in TDI consumption could be attributed to the difference in urethane formation rates. If TDI conversion rate were dominated by water-isocyanate reaction, one would expect that Hyperlite[®] E-848 have the highest TDI conversion rate, as water concentration is the highest in this sample. The fact that both U-1000 and castor oil foams had higher TDI conversion rates during the first 20 seconds of foaming suggest urethane formation was a significant factor in TDI consumption. Nonetheless, the overall differences in isocyanate conversion remained small and at 100 seconds after the initial mixing, the isocyanate conversion difference is only 5 % between SBOP and the other three foams. Again, the overall foaming kinetics is similar among the foams.

The final conversions of isocyanate, based on the temperature profiles shown, are ~80% in all foams at $t = 100$ seconds. The reason isocyanate conversion did not reach the theoretical 100% conversion is likely due to vitrification of the hard segments, which makes the foaming mixture inhomogeneous. The isocyanate conversion during reaction will be further discussed in Chapter 4.

2.4.2 Thermal-mechanical properties

Differential Scanning Calorimetry (DSC)

Polymer phase morphology and thermal properties are the emphasis of this study and were carefully characterized. In Figure 2.4, the DSC curves of the foam samples are shown. Two distinct differences are noteworthy. First, the sample T_g varied significantly. In Hyperlite[®] E-848, the observed T_g is at -60 °C, whereas U-1000, castor oil and SBOP foams showed T_g 's at 3, 5, and 70 °C, respectively. SBOP, for having a T_g at 70 °C, will evidently be rigid at room temperature and is consistent with the observations. Second, the breadths of T_g

are quite different as well as the ΔC_p values. Hyperlite[®] E-848 has the sharpest transition with the shortest breadth, whereas the breadth of T_g is the largest in SBOP and the transition is the least pronounced. The measured ΔC_p values of Hyperlite[®] E-848, U-1000, castor oil and SBOP are: 0.33, 0.61, 0.23, and 0.14 J/g[°]C, respectively. Compared to the pure polyol ΔC_p at T_g , the U-1000 sample has the closest ΔC_p to its polyol followed by the Hyperlite[®] E-848, as in Table 2.1.

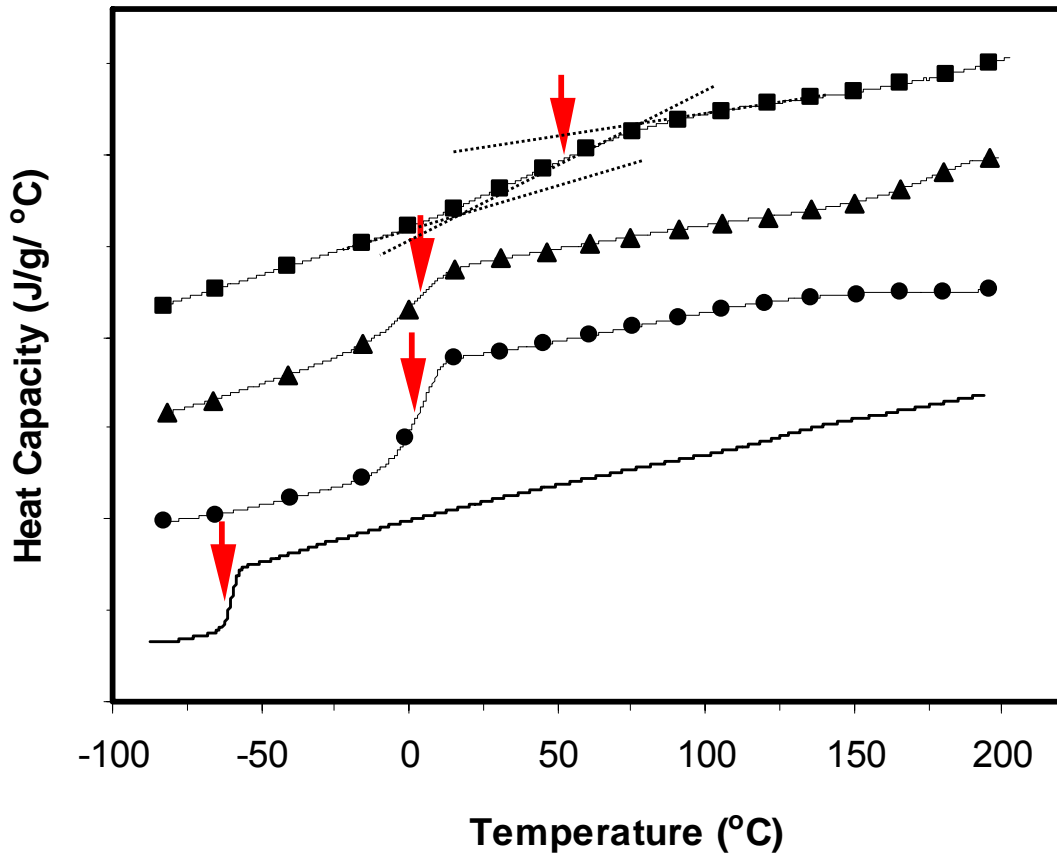


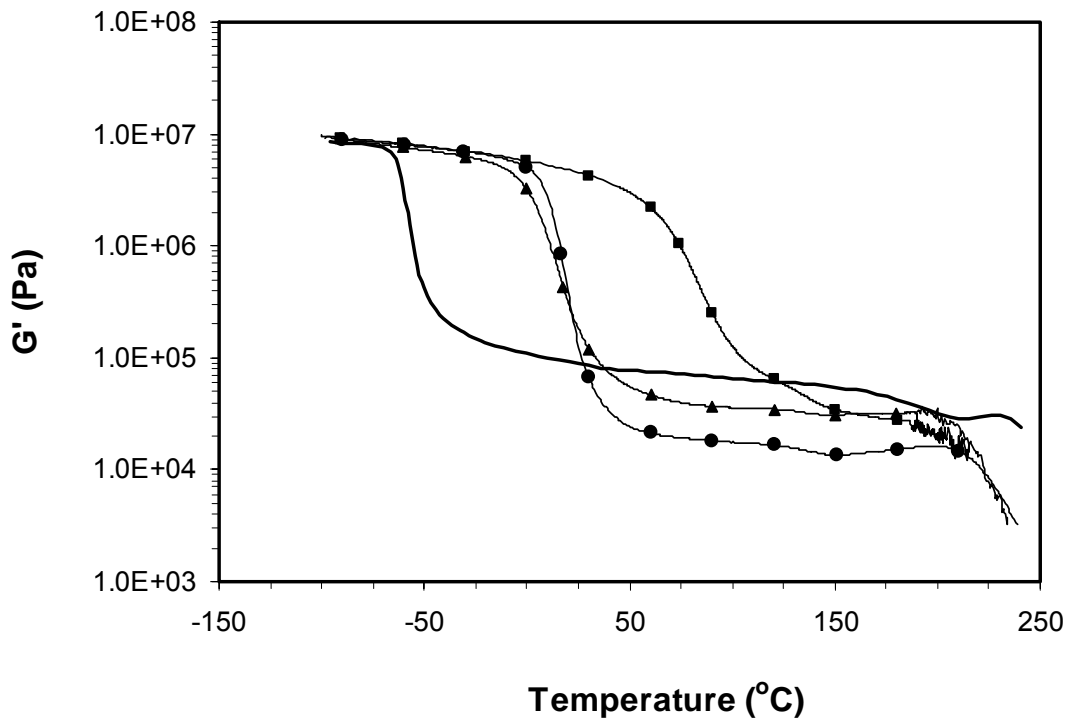
Figure 2.4: DSC results of foams. From bottom up: Hyperlite[®] E-848 (solid line), U1000 (●), castor oil (▲), and SBOP (■). The arrows indicate the T_g 's. These curves were shifted vertically to avoid overlapping. Dashed lines show the method for T_g and ΔC_p determinations.

In PU flexible foam, the polyurea hard segments are generally phase separated from the polyol soft segments forming soft domains that are rich in polyol and hard domains that are rich in ureas [9, 26, 80]. For well phase-separated foams, the soft domains share similar thermal properties as their polyols, which makes the T_g an indication of the degree of phase separation. The T_g 's of all polyols were measured and tabulated in Table 2.1. From the results of DSC, Figure 2.4, it is clear that Hyperlite[®] E-848 foam shares a similar T_g with its polyol, however, the rest of the foams do not. The U-1000, castor oil, and SBOP foams all showed significant shift of their foam T_g 's from the pure polyol T_g 's. In the case of SBOP, this shift is the most significant of 105 °C, while castor oil and U-1000 both showed a shift of 68-69 °C. The soft domains in foams other than the Hyperlite[®] E-848 clearly do not share similar thermal properties and is indicative of either structural or morphological changes in the PU network. Structurally, natural oil polyols as well as the U-1000 polyol have a low molecular weight between crosslinks, which could lead to high T_g of the soft domains [81, 82]. Morphologically, an increase in phase mixing could also result in high T_g 's and especially broader T_g .

Dynamic Mechanical Analysis (DMA)

To further probe the properties of PU flexible foams, the DMA technique was applied. DMA experiment measures the viscoelastic properties of both polyurea-based hard domains and polyol-based soft domains as temperature of the sample varies. In Figure 2.5, both the G' and G'' data are plotted for the sample foams. Hyperlite[®] E-848 sample, a standard flexible foam, shows a drop of G' at approximately – 60 °C, the soft domain T_g , and reaches a plateau region covering a range of temperatures up to 200 °C. The plateau region is characteristic to crosslinked polymers, such as PU flexible foams. The values of

the plateau G' are largely dependent upon two variables in a flexible foam: hard segment concentration and crosslinking density, where the former is the predominant factor [21, 83-86]. As the polyol component was changed to U-1000, castor oil and SBOP, the G' curve showed significant changes mainly in two areas: the drop off of G' shifted to higher temperatures and the plateau modulus varied as well. The drop off of G' curve indicates the transition of a foam sample from a glassy state to a rubbery state. Both U-1000 and castor oil foams show this transition at a similar temperature suggesting a similar T_g between these two foams. The G' curve of SBOP does not show a clear drop in G' value until a much higher temperature than the rest of the samples. Thus, the T_g of SBOP foam is the highest among all foams. The $\tan(\delta)$ curves in Figure 2.6 are used to determine the T_g 's of foams and will be discussed shortly.



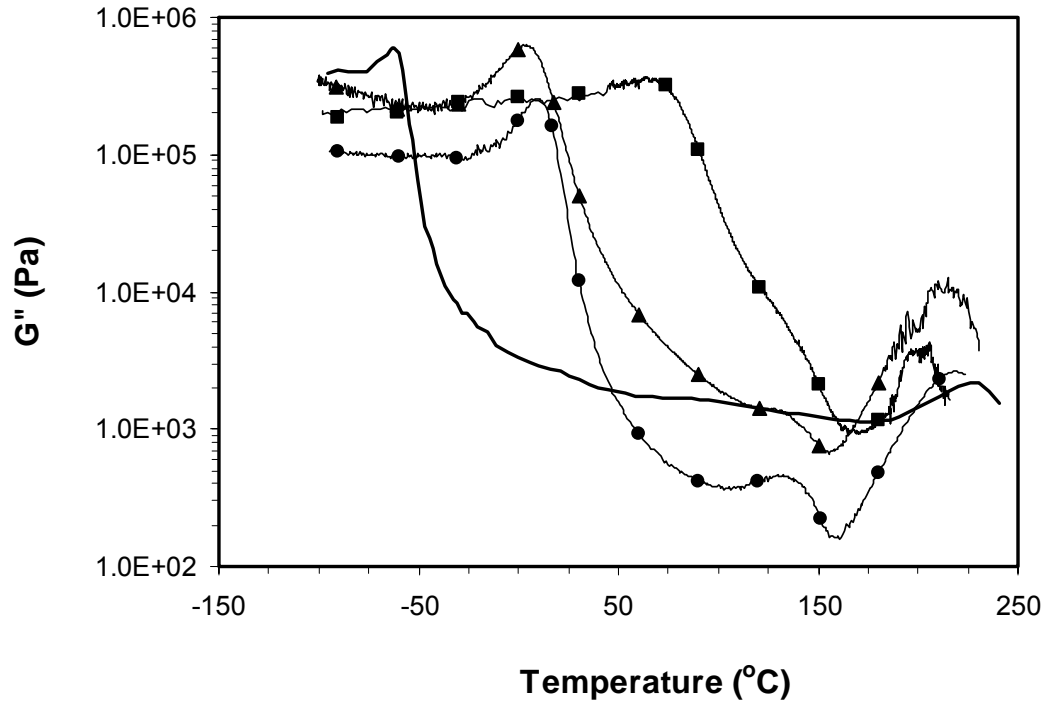


Figure 2.5: DMA curves showing G' (top) and G'' (bottom) as functions of temperature: Hyperlite® E-848 (solid line), U-1000 (●), castor oil (▲), and SBOP (■).

The plateau modulus G' of foams, in Figure 2.5, is the highest for the Hyperlite® E-848 foam valued at approximately 7×10^4 Pa at $T = 100$ °C followed by castor oil valued at 3.5×10^4 Pa, and U-1000 foam has the lowest G' plateau modulus valued at 1.5×10^4 Pa. Since all samples were formulated to have the same concentration of hard segments, the differences in plateau modulus are, thus, an indication of differences in the properties of hard domains, such as the effective volume fraction of hard domains or segmental length of the polyureas, or the crosslinking density of soft segments. For the Hyperlite® E-848 sample, the crosslinking density of its polyol soft segments is the lowest among all foams, and yet its plateau modulus is the highest. Indicatively, the hard segments are

well ordered in Hyperlite[®] E-848 foam with potentially higher effective volume fraction of hard domains than the rest of the samples, and thus showing a higher plateau modulus. This argument will be verified further in both SAXS and FTIR sections. Conversely, the lower plateau modulus in both U-1000 and castor oil samples are likely the result of a lower effective volume fraction of hard domains than in Hyperlite[®] E-848. Between U-1000 and castor oil foams, the plateau modulus of castor oil is approximately twice of the U-1000 implying, again, differences in the amount of effective hard domains as both sample share nearly the same soft segment crosslinking densities. Among all foams, SBOP foam is the only sample showing an absence of plateau region. The network in SBOP degrades shortly after the polymer reaches its rubbery state, and the degradation of the network is indicated by a second drop in G' values at approximately 200 °C.

All samples show similar degradation temperatures between 150 - 200 °C, as a second drop in G' values. The degradation temperatures seen from the DMA results are consistent with the values reported in literatures [87, 88].

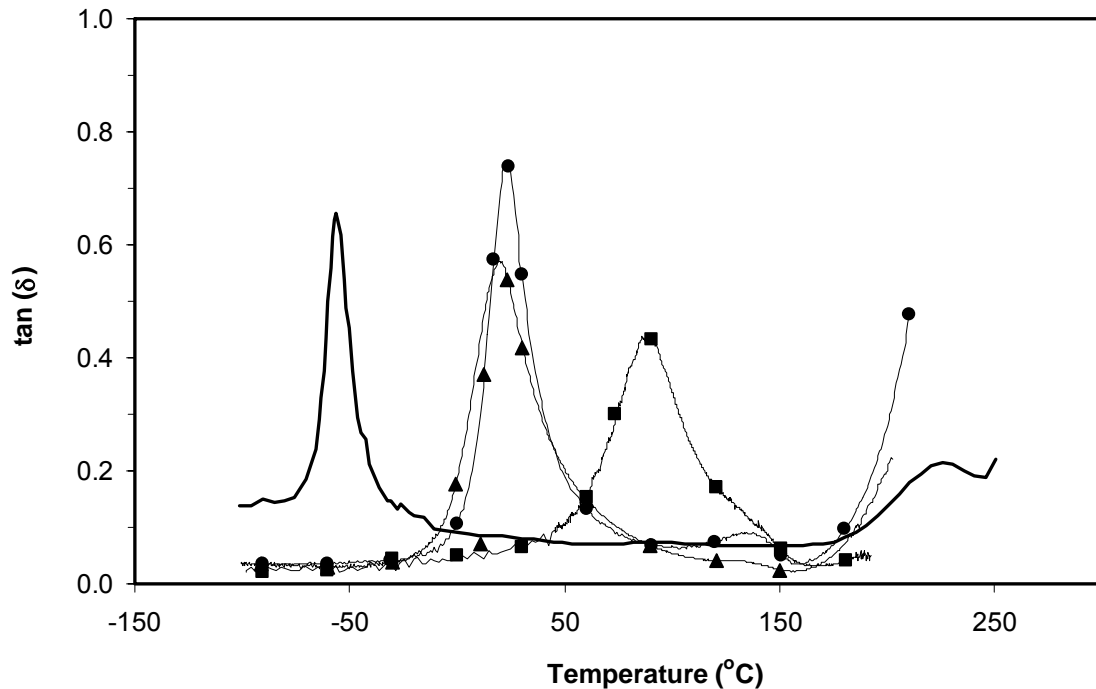


Figure 2.6: DMA curves showing $\tan(\delta)$ as a function of temperature for Hyperlite[®] E-848 (solid line), U-1000 (●), castor oil (▲), and SBOP (■).

A $\tan(\delta)$ curve shows the transition of a foam sample from its glassy state to rubbery state as a visible peak, such as those seen in Figure 2.6. The T_g 's determined from the $\tan(\delta)$ curves are: -56, 20, 19, and 84 °C for Hyperlite[®] E-848, U-1000, castor oil, and SBOP foam, respectively. These values are in a reasonable agreement with the DSC results, although are about 15 °C higher than the DSC results. Other than the peak position of the $\tan(\delta)$ curves, the distributions of the peaks also vary among the samples. Hyperlite[®] E-848 has the most pronounced peak with a narrow distribution while both U-1000 and castor oil foams show slightly broader peak distributions. SBOP, among all foams, has the broadest distribution and the lowest peak intensity. The distribution of the $\tan(\delta)$ curve is generally considered as an indication of network homogeneity and the

peak height is related to the relative elasticity of the sample. Hyperlite[®] E-848 having a sharp peak with high intensity implies uniform soft segments that are phase-separated from the hard domains. The other extreme, SBOP foam, having the broadest peak with low intensity suggests a lesser degree of uniformity in soft segments and is less likely phase-separated.

2.4.3 Small Angle X-ray Scattering (SAXS)

As we speculated from the DMA results that hard domain ordering might have played a significant role in determining foam mechanical properties, in this section a more detailed examination of morphology will be performed.

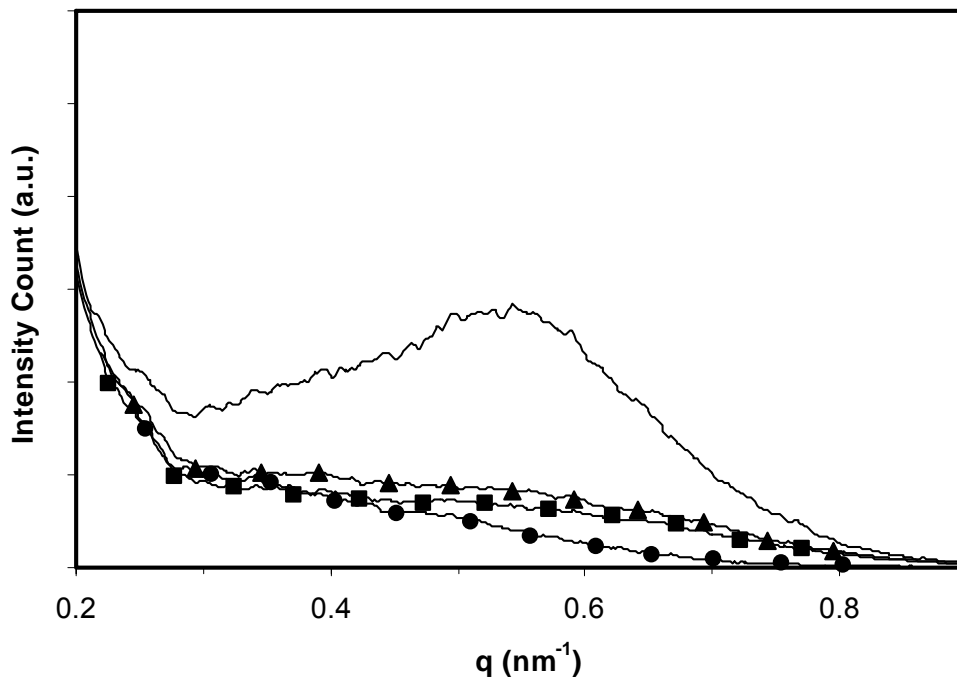


Figure 2.7: SAXS data for foams: Hyperlite[®] E-848 (solid line), U-1000 (●), castor oil (▲), and SBOP (■).

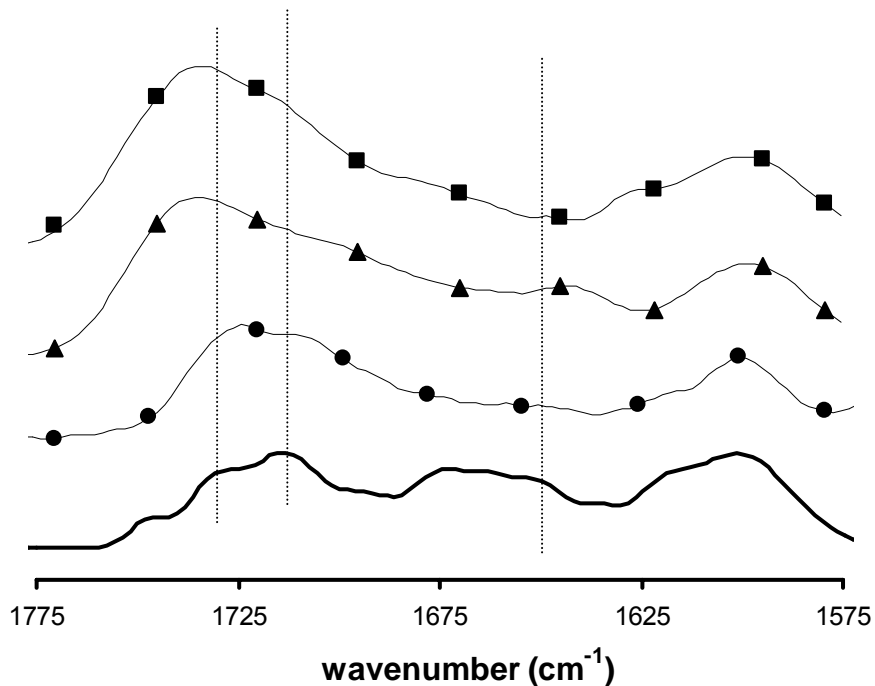
The scattering profiles of the foams are plotted in Figure 2.7. The Hyperlite[®] E-848 foam shows a broad peak characteristic to amorphous materials and the peak of the scattering profile corresponds to approximately 11 nm in spacing. Evidently, there is a distinguishable distribution of hard domain spacing in Hyperlite[®] E-848 foam. The SAXS profiles of U-1000, castor oil and SBOP foams are dramatically different from the Hyperlite[®] E-848 and differ only slightly between each other in scattering intensities, where castor oil has a higher intensity followed by SBOP and U-1000 has the lowest intensity. The fact that there is no distinguishable peak observed in U-1000, castor oil or SBOP suggests that all these samples are relatively homogenous. The X-ray scattering in PU flexible foams depends on two main factors: (1) the concentration of high electron density domains (hard domains), and (2) electron density contrast between the soft and hard domains. With all samples sharing a similar hard segment concentration, a change in either the degree of phase separation or inherent electron density contrast between hard and soft domains will result in changes of X-ray scattering intensity. Between Hyperlite[®] E-848 and U-1000 samples, the soft segments are all comprised primarily of polypropylene oxides. Thus, the electron density contrast between hard domains and the soft domains is expected to be similar in both Hyperlite[®] E-848 and U-1000 samples. The observed SAXS scattering intensity is dramatically lower in U-1000 than in Hyperlite[®] E-848 suggests that the hard segments are barely phase separated from the soft segments and a phase mixed morphology exists in U-1000.

The SAXS results, to a great extent, confirmed our speculation on the DMA data as plateau modulus differences were attributed to a difference in the volume fraction of hard domains or degree of phase separation. In the case of Hyperlite[®] E-848, the soft and hard segments are phase separated to domains resulting in distinguishable scattering peak in SAXS, and a highest plateau

modulus in DMA. Between U-1000 and castor oil foams, a slightly higher intensity is seen in the castor oil foam, although not by much but could be an indication of better phase separation in castor oil. The DMA plateau modulus is higher in castor oil than in U-1000, as seen in Figure 2.5.

The low intensity scattering profiles also raise the question whether the scattering angles used for experiments were adequate. Based on literature results, the range of hard domain spacing is from 6 up to 13 nm, or a corresponding scattering vector (q) range of 0.5-1.0 nm^{-1} [89]. The scattering angles used in SAXS experiments were adequate.

2.4.4 Fourier Transform Infrared Spectroscopy (FTIR)



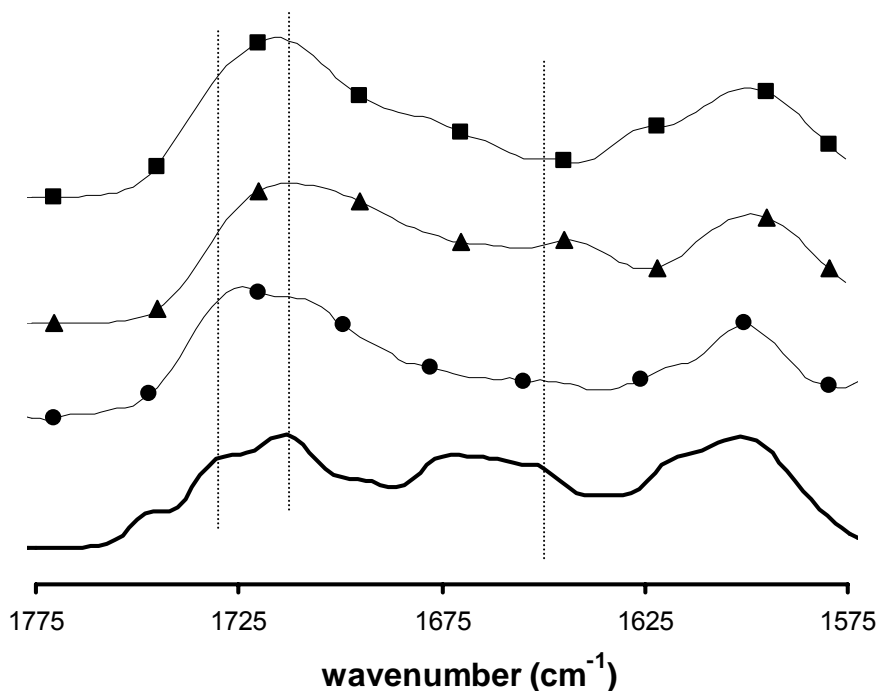


Figure 2.8: FTIR-ATR spectra of foams (top) and the spectra after the ester linkage band has been subtracted (bottom). Each plot shows from bottom up: Hyperlite[®] E-848 (solid line), U-1000 (●), castor oil (▲), and SBOP (■). The spectra were shifted vertically to avoid overlapping. Dashed lines (from left to right) are indicative of free urethane, free urea and bidentate urea peak positions.

In this section, the study is further extended to the molecular levels to examine microscopic differences between the foams and an FTIR-ATR technique was used. In Figure 2.8, both the as-is spectra and the spectra with ester linkage band subtracted are shown, and the detailed band assignments can be found in Table 2.3. In the free carbonyl region ($> 1700 \text{ cm}^{-1}$), which includes both free urethane and free urea, Hyperlite[®] E-848 shows a much less overall absorbance band than the other samples. This is partially because the hydroxyl concentration is lower in Hyperlite[®] E-848 than the rest of the samples, therefore, less urethane, and thus a smaller absorbance band, is expected in Hyperlite[®] E-

848. The free urea absorbance band is smaller in Hyperlite[®] E-848 despite a high amount of urea bonds. This likely implies that a significant fraction of the hard segments in Hyperlite[®] E-848 are participated in the formation of ordered hard domains. The ureas formed during foaming either remain free, not participated in the hard domain formation, or hydrogen bond to form hard domains, thus a lower absorbance band of free urea in Hyperlite[®] E-848 gives indication of a higher volume fraction of hard domains. For comparison, the areas under the absorbance bands of interest are tabulated in Table 2.3, and an example of the peak deconvolution is shown in Figure 2.9 for Hyperlite[®] E-848 sample.

Table 2.4: Normalized peak areas under the IR bands.

	Free urethane	H-bonded urethane	Free urea	Mono-dentate	Bi-dentate
Wavenumber (cm⁻¹)	1732	1695	1713	1776, 1662	1640-1645
Hyperlite[®] E-848	0.31	0.32	0.71	0.39, 0.26	0.33
U-1000	0.36	0.30	1.08	0.31, 0.15	0.11
Castor oil	0.32	0.30	0.89	0.49, 0.09	0.35
SBOP	0.34	0.29	1.06	0.32, 0.12	0.1

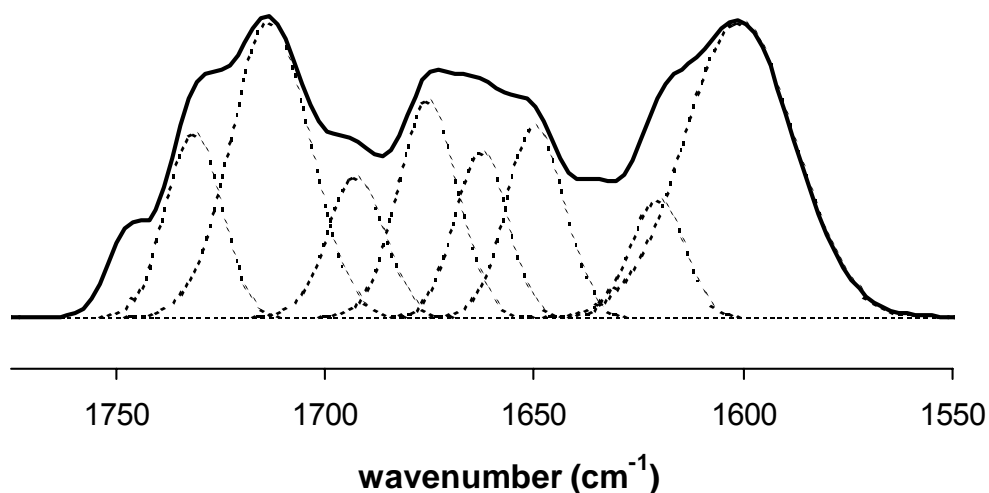


Figure 2.9: An example of peak deconvolution showing the Gaussian fit for the absorbance bands in Hyperlite® E-848.

Among these samples, the amounts of urethanes, either as free or hydrogen-bonded, differ very little. The urea species, on the other hand, vary significantly. In the case of free urea, Hyperlite® E-848 foam clearly has the least amount of free urea, whereas U-1000 and SBOP has the most amounts. For hydrogen-bonded ureas, the monodentate urea concentrations are all close in values but the bidentate urea concentrations vary substantially. For SBOP foam, the FTIR data support the observation in SAXS experiments by showing the highest concentration of free urea and the lowest concentration of bidentate urea in sample. The polyurea-based hard segments are clearly not as associated in SBOP as in Hyperlite® E-848. Phase mixing is rather pronounced in SBOP. The U-1000 foam shows a similar IR absorbance in the hydrogen-bonded urea region ($< 1680 \text{ cm}^{-1}$) to SBOP indicating phase mixing in this sample as well. The IR

spectrum of castor oil is somewhat different from either the U-1000 or the SBOP. A slightly more pronounced bidentate absorbance band (at 1640 cm^{-1}) is seen in castor oil, which is less visible in either U-1000 or SBOP. Recall the SAXS results on these foams, both U-1000 and SBOP shared nearly the same scattering profiles, while castor oil foam showed slightly higher intensities. It could potentially be the molecular-level differences that gave rise to the minor differences in SAXS profiles.

Another important issue needs to be addressed is the fact that as the molecular weight of polyol changes and the hard segment concentration remains the same, the segmental length of polyureas that comprises hard domains varies. A higher molecular weight polyol would allow longer hard segments to form while a lower molecular weight polyol would connect hard segments that are shorter in length. The difference in polyurea segmental length could provide an explanation to the observed differences in the effective volume fraction of hard domains among the samples.

2.5 Conclusion and Outlook

In this study, we synthesized four PU foams from different polyols, two petroleum polyols with different molecular weights and two natural oil polyols. It was found that other than the high molecular weight ($M_n = 6700\text{ g/mol}$) petroleum polyol, all polyols used in this study produced foams with $T_g > 0\text{ }^\circ\text{C}$. Among all samples, SBOP foam has the highest T_g of $70\text{ }^\circ\text{C}$ and is a rigid sample, while both U-1000 and castor oil foams have T_g 's around $5\text{ }^\circ\text{C}$. The differences in foam T_g 's were attributed the differences in crosslinking densities of their soft segments. Although U-1000, castor oil or SBOP is not ideal for flexible foam formulations, the results did identify that the T_g of foam is the key parameter in

determining the flexibility of PU foams. Therefore, our future investigations will aim to find ways to lower the T_g of a PU through natural oil polyol designs.

Mechanical property of the foams also varied as indicated by the DMA study. The plateau modulus is the highest for Hyperlite[®] E-848 foam synthesized using the high molecular weight petroleum polyol and the lowest for the foam synthesized using the low molecular weight petroleum polyol. SAXS and FTIR results show that the volume fraction of phase-separated hard domains plays an essential role in determining mechanical properties and is believed to be dependent upon polyol used through its influence on the segmental length of polyureas.

In the following chapters of this thesis, we took two separate approaches to better understand these natural oil polyols, their potentials and the limitations. The first route, as SBOP is not suited as the sole polyol component in flexible foam, we partially substituted a petroleum polyol in flexible foam using SBOP and explored the potentials of SBOP as a substituent component. The second route, different from the partial substitution route, was aimed to find ways to lower the T_g of a PU and thus making natural oil polyol a potential candidate as the sole polyol component in flexible foams. A series of model polyols based on natural oils were synthesized and studied to establish a structure-property relationship for natural oil polyol-based PUs.

Chapter 3¹

Partially-substituted Polyurethane Flexible Foams

Contents

3.1	Chapter Overview	52
3.2	Introduction	52
3.3	Experimental	54
3.3.1	Materials	54
3.3.2	Foam Synthesis	57
3.3.2	Characterization	60
3.4	Results and Discussion	63
3.4.1	Solvent Extraction	63
3.4.2	Foam Cellular Structures	64
3.4.3	Polymer Phase Characterization	66
3.5	Conclusion	86

¹ Part of this work has been published in Polymer **2007**; **48**: 6656-6667.

3.1 Chapter Overview

Natural oil polyol emerged in recently years as a potential alternative to petroleum resources for polyurethane synthesis. This research started by synthesizing a series of partially substituted polyurethane flexible foams using styrene-acrylonitrile copolymer filled, crosslinker and soybean oil-derived polyols. A variety of characterization techniques were used to study and compare the morphology differences between samples. It is believed that the use of soybean oil polyol changes the hard domain ordering as well as adds a second soft phase, which has a higher modulus and glass transition temperature, to the flexible foam. Different mechanism in increasing flexible foam modulus is discussed and compared here.

3.2 Introduction

Polyurethane (PU) is one the most versatile polymeric materials with regards to processing methods and mechanical properties. By proper selection of reactants, the resulting PU can range from flexible elastomers to high modulus plastics. This wide range of achievable properties makes PU an indispensable material in construction, consumer products, transportation, and medical devices [4, 90]. Similar to many polymeric materials, PU relies on petroleum oil as the feedstock for its major components, hydroxyl-containing polyol and isocyanates. Over the last decade, as the price of petroleum oil escalated, the stability and the sustainability of the petroleum market have become growing concerns. Costs of polymeric raw materials have since risen steadily as a result of rising feedstock [31]. In contrast to the less predictable petroleum market, agriculture products, such as vegetable oils, have maintained relatively stable price and supplies [91].

Developing bio-renewable feedstock for PU manufacturing and polymer industry as a whole becomes highly desirable for both economic and environmental reasons [92]. For PU manufacturing, natural oils, such as natural oils, can be potential replacements for petroleum polyols. However, with the exception of castor and lesquerella oils, natural oils do not bear hydroxyls needed to react with isocyanate to form PU. In Chapter 1.3, a number of known methods for converting natural oils to polyols are listed. There are structural variations among natural oil polyols based upon the conversion method used.

The largest PU production goes into *flexible* foam, thus the use of natural oil polyols in flexible foam production will have a substantial impact on the PU industry as a whole. A straightforward approach is to use the naturally occurring polyol, such as castor oil. Foams made solely from castor oil have been found to be in resiliency and a temperature dependent modulus [64]. In Chapter 2, we also made a flexible foam using castor oil and the results indicate a close-to-room temperature glass transition temperature (T_g) making the foam less attractive for low temperature ($< 25\text{ }^\circ\text{C}$) applications. The narrow range of achievable properties along with the relatively high cost of castor oil have turned researchers to processed oils for polyols. John and coworkers synthesized flexible foam using entirely soybean oil-derived polyol and the data indicated that improvements in both surfactant efficiency and polyol reactivity were needed [60]. In our investigation documented in Chapter 2, foam made from SBOP alone is not in any case a flexible foam but rather a rigid sample. To use processed natural oil polyol, such as SBOP, in flexible foam manufacturing, partial substitution is a potential route and has been proven quite successful [61, 62, 93]. Not only have good quality foams been made, but also higher resiliency has been achieved with these foams. Among all partially substituted foams, higher hardness/compressive modulus has been consistently observed. In the

study done by Herrington and Malsam, they replaced up to 30 % of the total polyol with SBOP and did *not* encounter common issues associated with similar oil-derived polyols, such as odor, density control, and SBOP reactivity. More remarkably, a significant load bearing increase measured by indentation force deflection (IFD) was reported [61].

In this work, we aim to uncover the reason why partial substitution using natural oil polyol is viable in flexible foam synthesis and how increases in compressive modulus are consistently achieved in these foams. A series of flexible foams were prepared by replacing up to 30 % of petroleum-derived polyether polyol with three substituent polyols: styrene-acrylonitrile (SAN) copolymer-filled, crosslinker, and SBOP polyols. A number of experimental techniques were applied to characterize the samples both macroscopically and morphologically. The effects of substituent polyols on both cellular structure and polymer phase morphology were compared. SAN copolymer-filled and crosslinker polyols were included in this work because use of either polyol is known to increase compressive modulus of flexible foam and are served as comparison basis for understanding different mechanisms in increasing compressive modulus [4].

3.3 Experimental

3.3.1 Materials

Three commercially available petroleum-derived polyols, Hyperlite[®] E-848 (Bayer Corporation), Hyperlite[®] E-849 (Bayer Corporation), and Voranol[®] 446 (Dow Chemical Company) were selected. These are typical molded flexible foam polyols. Hyperlite[®] E-848 is a propylene oxide-based, ethylene oxide capped polyol with a number average molecular weight (M_n) of 6700 g/mol and a

functionality (f_n) of 3.8 [73]. Approximately 85% of the hydroxyls in Hyperlite[®] E-848 are primary. Hyperlite[®] E-849 is a copolymer-filled polyol, based upon Hyperlite[®] E-848. It contains an estimated 43 wt% stabilized styrene acrylonitrile (SAN) particles that are approximately 0.5 μm in size. Voranol[®] 446, referred to as a crosslinker polyol, is a low molecular weight ($M_n = 570 \text{ g/mol}$) propylene oxide-based polyol with a f_n of 4.5 [41].

SBOP used in this study was synthesized by epoxidizing soybean oil followed by an oxirane ring-opening reaction using a mixture of water and methanol. Detailed synthesis procedures are described in reference [43]. An *idealized* structure of SBOP shown in Figure 2.1 has a $M_n = 1058 \text{ g/mol}$ and $f_n = 5$. The actual molecular weight of SBOP used in this study was measured by gel permeation chromatography (GPC) at room temperature using known molecular weight polyether polyols as standards. Figure 3.1 shows the GPC trace of SBOP. The calculated M_n of SBOP used in this study is 1060 g/mol, polydispersity index (PDI) = 1.04 for the large peak in figure and $f_n = 3.8$. The lower f_n in the actual SBOP is due to both variations in fatty acid substituent and oligomerization of a small fraction of SBOP during modification evidenced by a second broad peak in GPC.

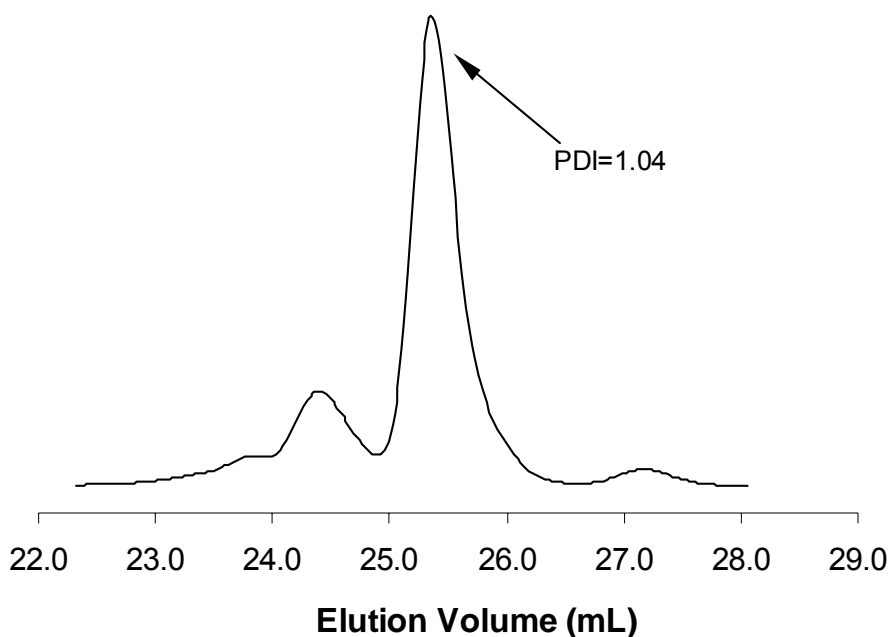


Figure 3.1: GPC trace of SBOP used in this study.

The toluene diisocyanate (TDI) used is an 80/20 mixture of 2,4 and 2,6 isomers (Grade A Mondur[®] T-80, Bayer). Isocyanate in excess of that needed to react with the OH groups on the polyols reacts with distilled water to form CO₂, which acts as the only foam blowing agent. Gelling and blowing catalysts, Dabco[®] 33LV and Dabco[®] BL-11, were obtained from Air Products and were used as received. Dabco[®] 33-LV, which accelerates the reaction of NCO with OH, is a solution of 33 wt% triethylene diamine in dipropylene glycol. Dabco[®] BL-11, which accelerates the reaction of NCO with water is a solution of 70 wt% bis (2-dimethylaminoethyl) ether in dipropylene glycol. Diethanolamine (DEOA, Huntsman) was used in small quantities as a foam stabilizing cross-linking agent.

Three surfactants were employed in this study: Niox[®] Y-10184, Dabco[®] DC-5169, and Tegostab[®] B-4690. Niox[®] Y-10184 (Momentive Performance

Materials, formerly GE Silicones) is a silicon-based, molded foam surfactant and was used in the foam formulations not containing SBOP. Dabco[®] DC-5169 (Air Products) and Tegostab[®] B-4690 (Degussa AG) were used together in SBOP foams at a weight ratio of 1:3.

3.3.2 Foam synthesis

Table 3.1 gives the formulations used to prepare the foam samples. The amount of each component was based on 100 parts by weight of total polyol and a total mixture weight of 500 g. The amounts of TDI stoichiometrically balance NCO and reactive hydrogen species, i.e. isocyanate index = 100.

Table 3.1: Foam formulations used in sample synthesis, all formulations are based on 100parts by weight of polyol*. Foam density: 32 kg/m³.

Component	control	30% SAN**	10% crosslinker	10% SBOP	30% SBOP
Hyperlite [®] E-848	100	70	90	90	70
Hyperlite [®] E-849	--	30	--	--	--
Voranol [®] 446	--	--	10	--	--
SBOP	--	--	--	10	30
TDI weight (g, Index = 100)	156.9	155.5	170.4	161.5	172.4
HS/SS ratio	0.44	0.49	0.50	0.46	0.52
HS (%)	30.0	29.7	33.0	31.1	33.4

*All formulations contain distilled water (4.2), DEOA (1.2), Dabco[®] 33-LV (0.35), Dabco[®] BL-11 (0.08) and surfactant (1.0). Surfactant used in SBOP-containing foams is a mixture of Dabco[®] DC-5169 and Tegstab[®] B-4690 at 1:3 by weight; all other foams used Niax[®] Y-10184.

** 8.5 wt% SAN particles in foam.

All ingredients, except TDI, were weighed into a 33-ounce paper cup (Model DMC-33, International Paper Company) and mixed using a 10-inch shop drill (Delta ShopMaster, Model DP-200) equipped with a 3-inch diameter mixing blade (ConnBlade Brand, Model ITC) for 24 seconds at 1100 RPM. At the end of the mixing period, pre-measured isocyanate was added to the cup and the mixing continued for additional 6 seconds. The contents were then quickly transferred to a preheated aluminum mold (38.1 cm x 38.1 cm x 11.4 cm)

controlled at $66 \text{ }^\circ\text{C} \pm 1 \text{ }^\circ\text{C}$. The foam was allowed to rise and cure for six minutes, after which the foam was removed from the mold and hand crushed to open the cell windows and prevent shrinkage of the foam. Further tests were done after the foam had aged at $25 \text{ }^\circ\text{C}$ in 50% relative humidity for a minimum of seven days.

The differences in polyol functionality and molecular weight lead to variations in hard-segment (HS) and soft-segment (SS) contents and will be discussed further in later sections. The HS and SS contents were calculated using equations (3.1) and (3.2).

$$\% \text{HS} = \frac{\text{EM}_{\text{H}_2\text{O}}(\text{EW}_{\text{H}_2\text{O}} + \text{EW}_{\text{TDI}} - \frac{1}{2} \text{W}_{\text{CO}_2}) + \text{EM}_{\text{DEOA}}(\text{EW}_{\text{TDI}} + \text{EW}_{\text{DEOA}}) + \text{EM}_{\text{OH}}(\text{EW}_{\text{TDI}})}{\text{W}_{\text{Tot}} - \text{EM}_{\text{H}_2\text{O}}(\frac{1}{2} \text{W}_{\text{CO}_2})} \quad (3.1)$$

$$\% \text{SS} = \frac{\text{EM}_{\text{OH}}(\text{EW}_{\text{OH}})}{\text{W}_{\text{Tot}} - \text{EM}_{\text{H}_2\text{O}}(\frac{1}{2} \text{W}_{\text{CO}_2})} \quad (3.2)$$

Where EM is moles of functional group, EW is equivalent molecular weight, W is molecular weight, and subscripts H₂O, TDI, CO₂, DEOA, OH and Tot refer to water, TDI, carbon dioxide, diethanolamine, polyol and total respectively. It is assumed that HS are formed via the reaction of TDI with water, DEOA, and OH on polyol, corrected for carbon dioxide loss. SS are comprised of polyols. Both HS concentrations and HS-to-SS ratios are tabulated in Table 3.1. Note that for the 30% SAN sample the weight of the SAN particles, 8%, is considered neither as HS nor SS.

3.3.3 Characterization

Solvent Extraction

Small cubic samples were cut from the center of foam buns, dried at 60 °C for 24 hours and weighed (0.1 to 0.2 grams). The dry samples were then immersed in 20 ml dimethyl formamide (DMF) for 7 days at room temperature followed by drying in a vacuum oven at 60 °C for 10 days. The weight loss after solvent extraction is reported based upon an average of 6 samples per foam.

Scanning Electron Microscope (SEM)

Foam was frozen in liquid nitrogen and cut with a razor blade into rectangular slices: 7 x 10 x 2 mm. The top surface of each slice was sputter coated with 50Å grain-sized platinum. Cellular structure images were obtained using a scanning electron microscope (JSM-6500, JEOL) operated at 5 kV. An average of 6-8 images were collected on each foam. The perimeters of cells were manually traced from the SEM micrographs using UTHSCSA ImageTool software (Microsoft Corporation). Individual cell size was then calculated by approximating the cells as circular shapes [94, 95]. Average cell diameter and cell size standard deviation were calculated from a survey of over forty cells.

Dynamic Mechanical Analysis (DMA)

Same procedures were used as in Chapter 2.3.3.

Differential Scanning Calorimetry (DSC)

Same procedures were used as in Chapter 2.3.3.

Small Angle X-ray Scattering (SAXS)

Same procedures were used as in Chapter 2.3.3.

Atomic Force Microscopy (AFM)

A two-platen hydraulic press (Carver, Auto Series, Model 3895) capable of a maximum pressure of 60 MPa was used to compress 10 x 10 x 5 mm foam samples into solid elastomeric sheets that are ~ 200 μm thick. The foam samples were placed between two 30 x 30 x 0.2 cm highly polished (grain size < 1 μm) stainless steel plates (type 304), then held under 1.2 MPa plate-pressure at 110 ± 1 $^{\circ}\text{C}$ for 3 hours [96]. The resulting elastomer sheets are semi-transparent.

Tapping mode images were obtained using an AFM (Nanoscope III Multimode, Digital Instrument) equipped with an optical microscope (Nikon) and a charge-coupled device camera. The cantilever is a standard Si cantilever with a tip radius about 100 \AA and resonance oscillating frequency of ~275 kHz. All AFM images were acquired at ambient conditions. Cantilever was operated within the repulsive regime and images were collected at a resolution of 512 x 512 pixels.

Fourier Transform Infrared with Attenuated Total Reflectance (FTIR-ATR)

An FTIR (Nicolet Series II Magna-750, Nicolet/Thermoelectron) equipped with a single bounce ATR attachment (ProfilirTM, SpectraTech) and a mercury-cadmium-telluride detector was used to collect spectra at foam surfaces. Two sets of samples, 5 x 5 x 1 cm, were cut from the center of foam buns and each set was comprised of five different foam samples. The first set was dried under vacuum at 60 $^{\circ}\text{C}$ for 48 hours prior to measurements while the second set was

measured as is. Sample drying was to ensure no water adsorbed on the foam surface after curing in 50% humidity conditions. The sample was pressed against the zinc-selenium (ZnSe) ATR crystal to ensure complete contact. A total of 512 scans were taken on each sample over the wavelength range from 4000 cm^{-1} to 400 cm^{-1} at a resolution of 4 cm^{-1} . For each foam, three ATR-IR spectra were collected at different locations of the sample to verify sample uniformity. All spectra were normalized with respect to the absorbance of the aromatic C=C stretching at 1600 cm^{-1} . Comparison between the FTIR results of two sets of foams, pre-dried and not dried, showed no difference. Deconvolution of spectrum was performed in the carbonyl region (1550 cm^{-1} to 1800 cm^{-1}) using Thermo-Galactic's GRAM32 software. Each peak was fit to a Gaussian curve at a series of fixed wavelengths given in Table 2.3.

Indentation Force Deflection Test (IFD)

One of the crucial properties of PU flexible foam is its ability to provide support under compression, commonly known as load bearing capability. This load bearing capability is measured using an indentation force deflection (IFD) test. Foam samples of $38.1 \times 38.1 \times 11.4\text{ cm}$ were tested in accordance with standard procedures described in ASTM D-3574 test B1. The sample was compressed at 5 cm/min until it reached 65% deflection. While holding the deflection constant, the foam was allowed to equilibrate for 60 seconds before the force was recorded. IFD test results are shown in Table 3.2.

3.4 Results and Discussion

3.4.1 Solvent extraction

The solvent extraction was conducted to determine polymer network connectivity in foams. The measured sol fractions of the foams are tabulated in Table 3.2. All of the foams, with the exception of 30% SAN, have less than 2% extractables. The low extractable content is remarkable in both SBOP foams. Since SBOP contains a small amount of saturated fatty acid that cannot be functionalized, one would expect an increasing sol fraction with an increasing concentration of SBOP [55]. Furthermore, SBOP is a less reactive polyol due to its secondary hydroxyl groups. However, a low sol fraction was observed consistently in both SBOP-containing foams. It appears that the concentration of non-functional polyol in SBOP is not significant and the secondary hydroxyls are reacting fast enough to incorporate SBOP into the PU network.

Table 3.2: Measured foam properties.

	control	30% SAN**	10% crosslinker		10% SBOP	30% SBOP
Sol Fraction (%)	1.31 0.20	4.75 0.37	1.52	0.17	1.31 0.27	1.38 0.18
Air Flow (scfm)	2.5	3.1	2.4		4.3	3.1
ΔC_p (J/g/°C)	0.33	0.25	0.23		0.16	0.14
G' at 25 °C (10 ⁻³ Pa)	10.5	17.7	23.2		23.5	51.8
65% IFD (kPa)	8.0	11.1	10.6		10.3	18.6

Foam made with SAN copolymer polyol has the highest extractable content and similar observations have been reported elsewhere [97]. The total concentration of SAN copolymer in 30% SAN is approximately 8 wt%. The 4.75% extractables observed can represent up to 60% of all the SAN in the foam. The extractable fraction is likely comprised of SAN particles and the soluble components in SAN copolymer polyol. This is because SAN copolymer is synthesized via dispersion polymerization of styrene and acrylonitrile monomers in the presence of unsaturated polyether polyol as a stabilizing precursor [14, 15,98]. Polymerized poly(styrene-co-acrylonitrile) forms discrete particles in foam while un-grafted and un-reacted monomers remain in the polyol mixture. Although the polymerized SAN particles are stabilized, no literature has reported chemical bond formation between the particle and the polyurethane network. The un-grafted copolymer and un-reacted monomers are incapable of chemical bonding and thus can be easily extracted [99].

3.4.2 Foam cellular structures

Performance of flexible foam requires high open cell content. Airflow (ASTM standard D3574 Test G) is the standard method measures cell openness. Sample foams were tested and the airflow data are shown in Table 3.2. All airflow values are within the standard range of open cell flexible foam [4]. Replacing base polyol with substituent polyols has little effect on cell openness.

The important parameters that affect mechanical properties of foams are cell strut thickness and length [4, 90, 100, 101]. Because direct measurements of either parameter, strut thickness or length, can be subjective, we adopted the approach of measuring cell size [102-104]. Cell strut thickness and length can be estimated from measured cell size by using equations found in Reference

[100]. Generally, in open-cell PU foams increased cell size increases foam modulus.

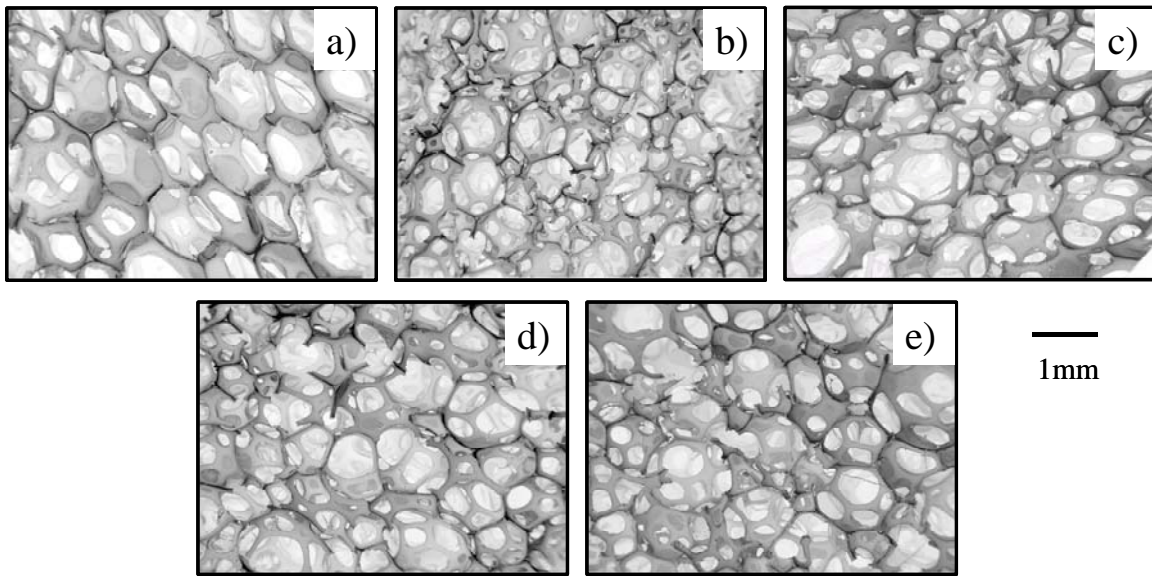


Figure 3.2: SEM images of the foam samples: (a) control, (b) 30% SAN, (c) 10% crosslinker, (d) 10% SBOP and (e) 30% SBOP.

SEM micrographs like those shown in Figure 3.2 were examined and the average cell diameter and standard deviation obtained are shown in Figure 3.3. The control foam has the largest average cell size and narrowest cell size distribution. With replacement of polyether polyol with crosslinker or SBOP, foam average cell size decreased and cell size distribution widened. Although it is seen in both SEM images and cell size analysis that SBOP and crosslinker foams have smaller cells, the size difference between either foam and control is not statistically significant. The change in SAN copolymer-containing foam is significant: the average cell size is 30% smaller than the control and cell size distribution is the broadest. However, the literature indicates that mechanical

properties, such as compression modulus, will only change slightly by such change in size [102, 105]. Thus the SEM study and cell size analysis suggest that partial substitution of polyols used here does not significantly alter cellular structure of the foam, and thus the observed foam mechanical properties changes are unlikely to be due to cell size changes.

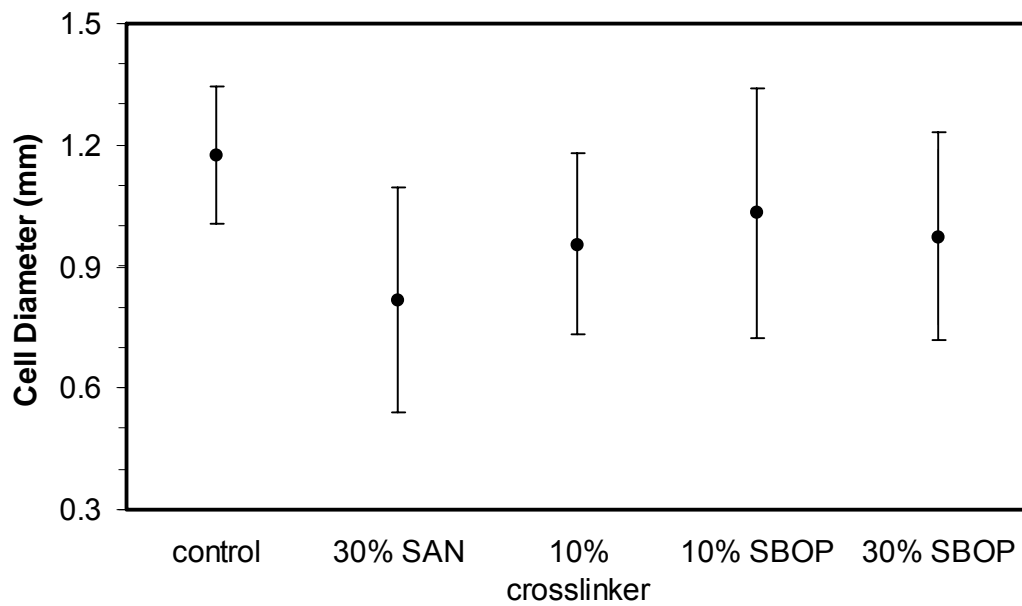


Figure 3.3: Average cell diameter and standard deviation for foams.

3.4.3 Polymer phase characterization

The polymer phase in a PU flexible foam is comprised of segmented block copolymer commonly denoted as $(A-B)_n$. The two blocks are a polyol and a polyurea. The incompatibility between the two blocks leads to a phase separated morphology consisting of polyol-rich soft domains and polyurea-rich hard domains [23, 27, 106]. Both domains have a distinct T_g and mechanical stiffness.

Dynamic mechanical analysis (DMA)

A direct approach to study the thermal and mechanical properties of the polymer phase is via DMA. Figure 3.4 shows the modulus profiles of control, 30% SAN and 10% crosslinker foams. All three G' curves are similar up to their T_g 's. At low temperatures, foams behave as a solid showing high G' values of 10^6 Pa. As temperature goes through T_g , a dramatic increase in molecular motion causes G' to decrease by nearly two orders of magnitude and reaches a plateau. Interestingly, the $\tan(\delta)$ curves of all three foams (see Figure 3.5) exhibit peaks at the same temperature. Thus, the soft phases in all three foams are polyether polyol based soft phases with a T_g of -56 °C. At temperatures higher than the soft phase T_g , plateau moduli of the foams show appreciable differences. The plateau G' values of 30% SAN is 60% higher than the control, while the plateau G' values of foam with 10% crosslinker is 80% higher. Although increases of plateau modulus are seen in both SAN and crosslinker-substituted foams, the mechanisms for the increase are different. In both Figure 3.4 and 3.5, 30% SAN foam clearly shows a second T_g at 113 ± 1 °C and beyond this transition, improvement in the plateau G' vanishes. As alluded to earlier, SAN copolymer forms discrete particles and the T_g of polymerized SAN is approximately 120 ± 1 °C [107]. SAN particles act as fillers in the polymer phase, and thus improve foam plateau modulus. The observed increase in G' , even after SAN particles soften, can be explained by a higher HS-to-SS ratio, shown in Table 2, in 30% SAN. In 10% crosslinker-substituted foam, improved plateau modulus extends over nearly the entire temperature range and is attributed to a higher concentration of HS [108]. This behavior will be further discussed in later sections.

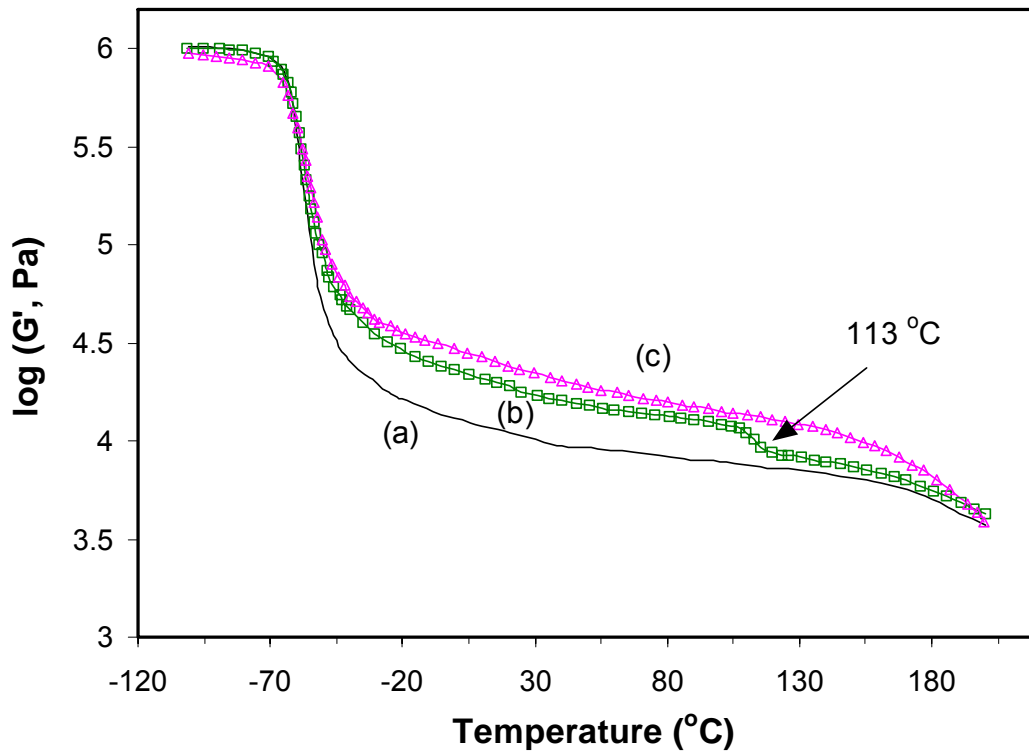


Figure 3.4: DMA results of partially substituted foams (I) showing G' as a function of temperature: (a) control; (b) 30% SAN and (c) 10% crosslinker.

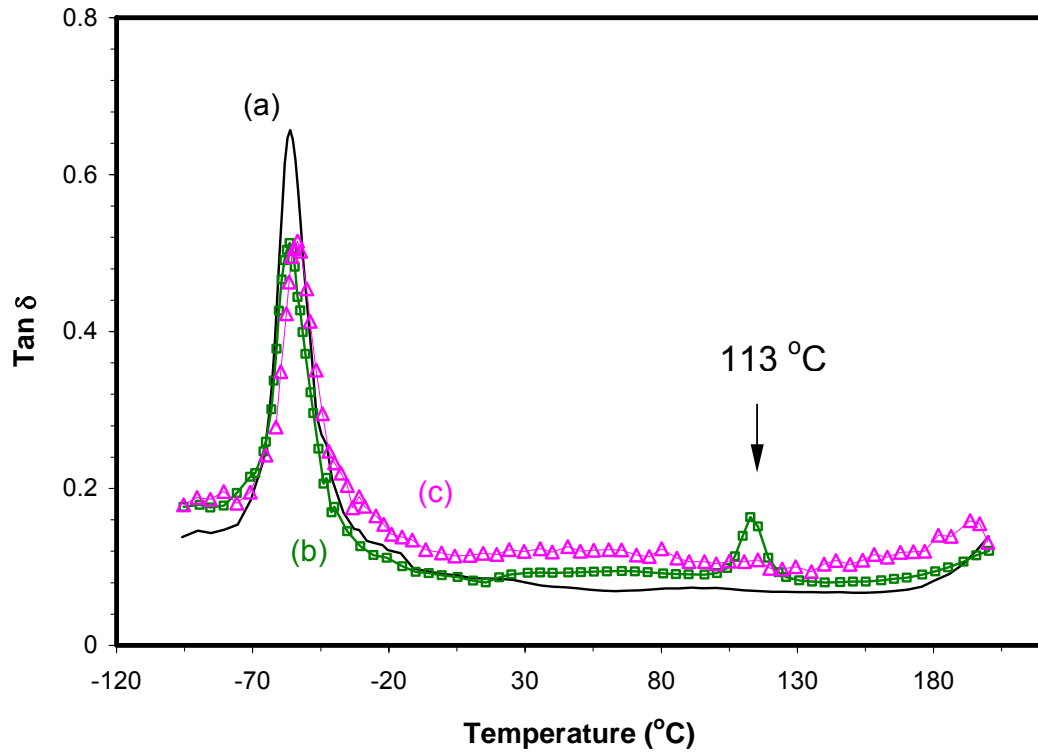


Figure 3.5: DMA results of partially substituted foams (I) showing $\tan(\delta)$ as a function of temperature: (a) control; (b) 30% SAN and (c) 10% crosslinker.

Substitution with SBOP polyol, rather than simply elevating plateau modulus, alters the DMA profiles. A slow decay of G' over a wide range of temperatures is seen in Figure 3.6. Soft phase T_g of both SBOP foams determined from $\tan(\delta)$ peaks remains the same as the control (Figure 3.7), however the $\tan(\delta)$ peak heights are significantly reduced. In both SBOP foams, a large portion (70 and 90%) of the soft phase is comprised of polyether polyol-based SS; the smaller $\tan(\delta)$ peaks indicate that these polyether polyol SS do not soften at their T_g . Especially in the case of 30% SBOP, the $\tan(\delta)$ peak height is only one-third of the control, implying a large population of polyether polyol SS is mixed with a higher T_g component, such as SBOP polyol. In Figure

3.7, 30% SBOP foam shows a very broad $\tan(\delta)$ peak around $75 \pm \text{C}$; this could indicate a second, SBOP-containing soft phase. In addition to the loss of polyether polyol-based SS, the absence of plateau regions in both SBOP foams indicates the lack of defined distance between domain spacing. Both the continuous decrease in G' and the $\tan(\delta)$ increase above $0 \text{ }^\circ\text{C}$ observed in SBOP foams argue for a distribution of phase sizes.

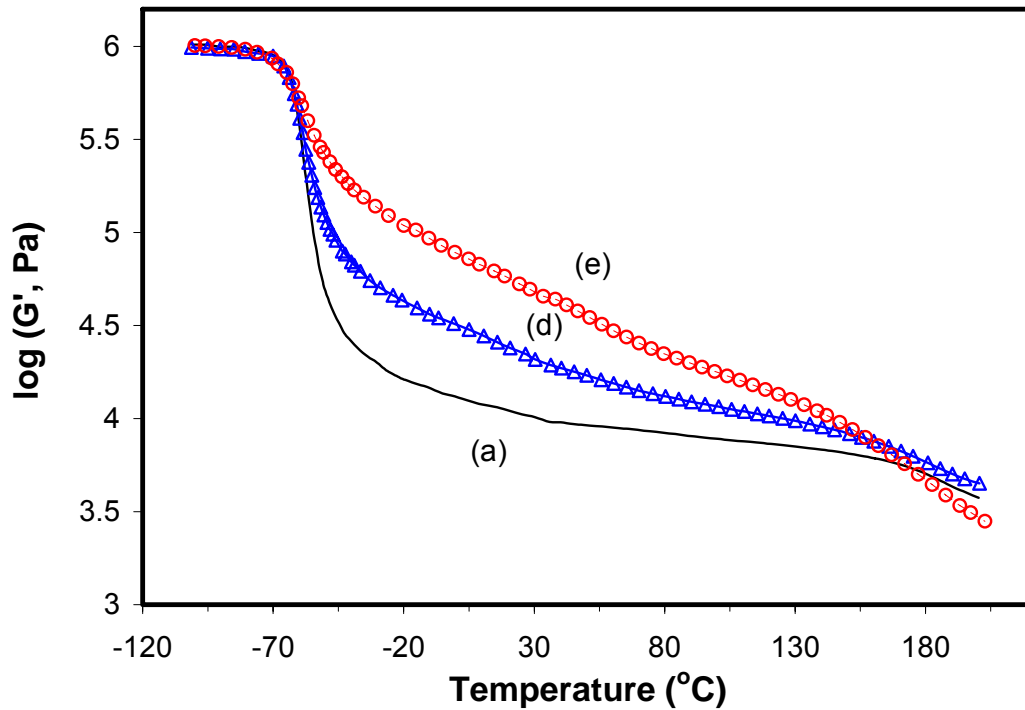


Figure 3.6: DMA results of partially substituted foams (II) showing G' as a function of temperature: (a) control; (d) 10% SBOP and (e) 30% SBOP.

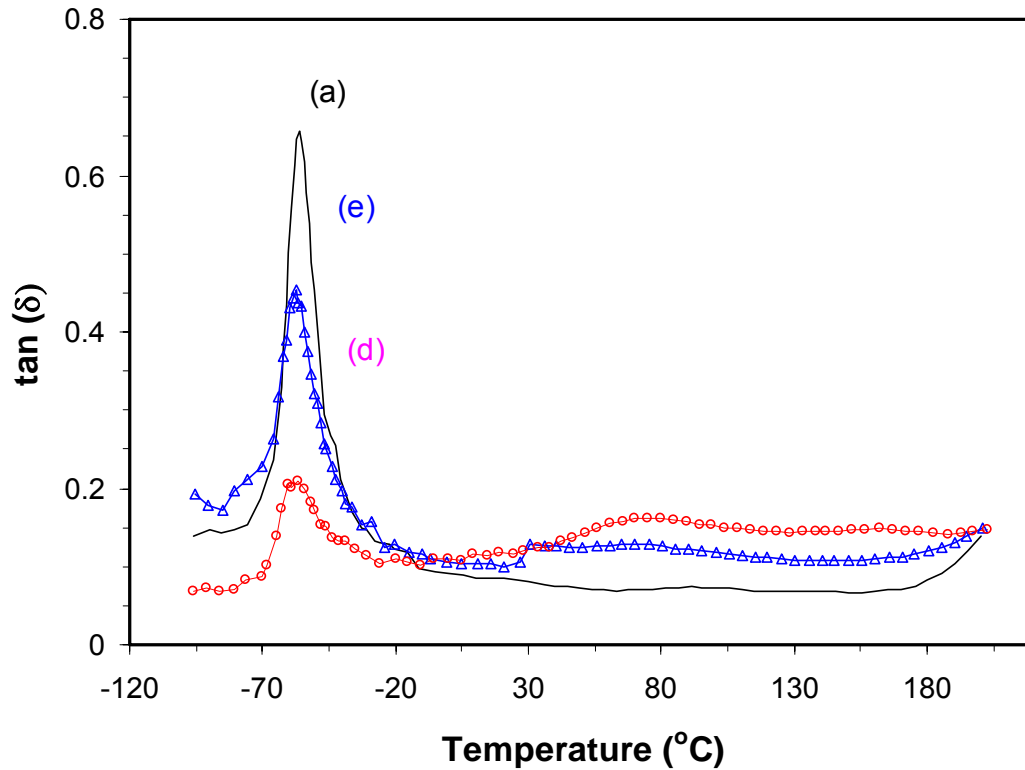


Figure 3.7: DMA results of partially substituted foams (II) showing $\tan(\delta)$ as a function of temperature: (a) control; (d) 10% SBOP and (e) 30% SBOP.

Differential Scanning Calorimetry (DSC)

DSC heating curves in Figure 3.8 reaffirmed that all four substituted foams share the same soft domain T_g as that of the control. The DSC measured T_g is $-60 \pm 1^{\circ}\text{C}$ (Figure 3.9), very similar to the temperature of the $\tan(\delta)$ peaks. As discussed above the DMA results indicate that polyether polyol-based SS may have mixed in with other components. DSC can quantify this. Since Δc_p scales with the total weight of polyether polyol-based SS undergoing a transition from a solid to a softened state, the weight fraction of pure polyether polyol soft phase can be estimated. The method for determining Δc_p is shown in the insert of Figure 3.8 and the results are tabulated in Table 3.2.

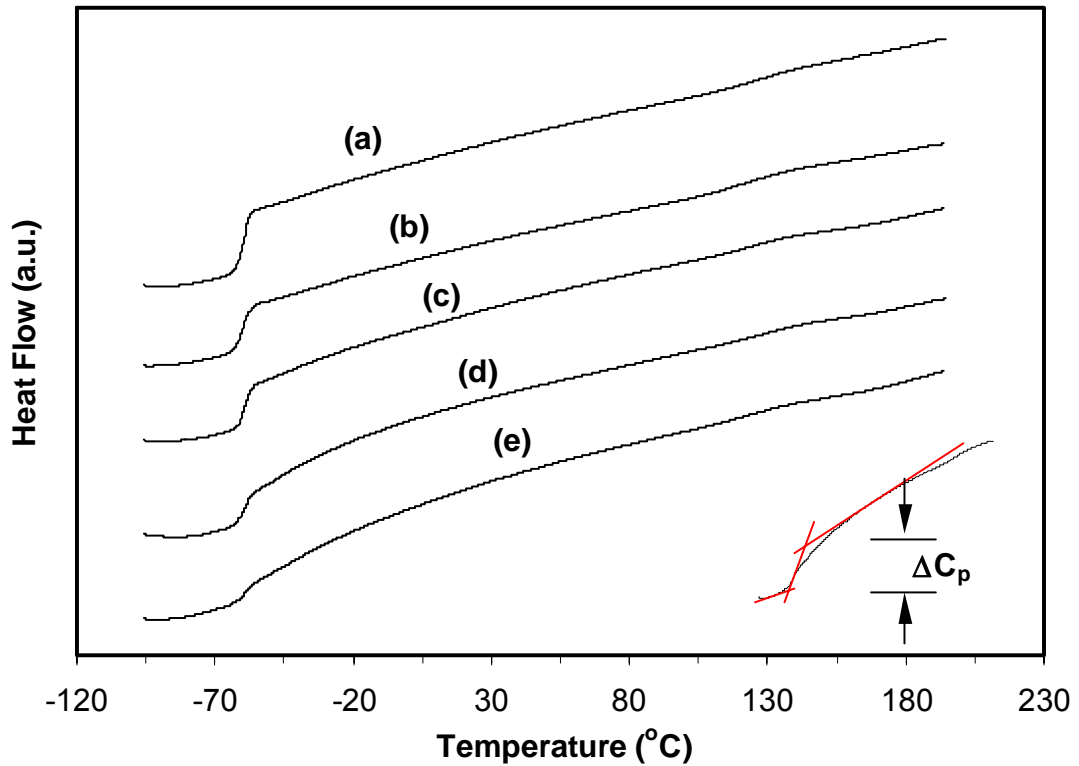


Figure 3.8: DSC traces of partially substituted foams: (a) control, (b) 30% SAN, (c) 10% crosslinker, (d) 10% SBOP and (e) 30% SBOP. The curves were shifted vertically to avoid overlapping of curves. Insert illustrates the method used to determine ΔC_p and breadth of T_g .

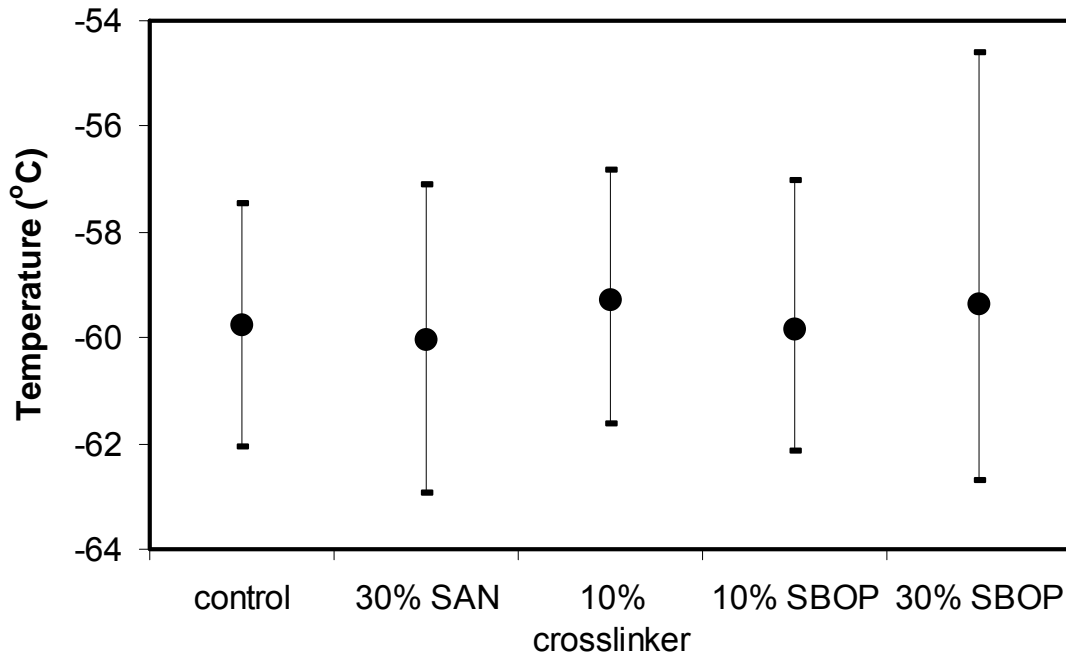


Figure 3.9: DSC results showing T_g and the breadth of glass transition. The dots indicate the glass transition temperatures. Upper and lower bars indicate the breadth of the transition.

Both SAN and crosslinker-substituted foams show a slight loss of the polyether polyol-based soft phase. The Δc_p values scale to 76% and 70% of control for crosslinker and SAN foams respectively. Given the formulations in Table 3.1, 30% SAN should contain approximately 87% polyether polyol SS in its soft phase, while 10% crosslinker foam should contain 90% polyether SS in its soft phase. Clearly, substitution of crosslinker has more impact on the purity of the polyether polyol-based soft phase than SAN, but the impact is far less significant when compared to SBOP-substituted foams. The 10% and 30% SBOP foams contain 90% and 70% polyether SS in their soft phases respectively, however, the measured Δc_p are only 48% and 42% of the control.

Polyether SS in SBOP foams are not all phase-separated; a significant fraction of them is in a phase-mixed state with SBOP and/or HS.

To better understand the loss of polyether SS fraction, we also measured T_g of each pure polyol. The T_g 's of control, SAN-containing, crosslinker, and SBOP polyols are -68, -68, -51, and -35 °C respectively. SBOP obviously has a much higher T_g than the other polyols.

Small-Angle X-ray Scattering (SAXS)

SAXS was used to determine interdomain spacing, as well as, probe the degree of phase separation. SAXS profiles of foam samples are shown in Figure 3.10. The interdomain spacing of 10% crosslinker (127 Å) is notably greater than that of control (115 Å), while other samples' remain similar to the control. Scattering signal intensity is notably different between foams. 30% SAN clearly has an enhanced signal intensity, while the two SBOP-containing foams show great reductions in signal intensities.

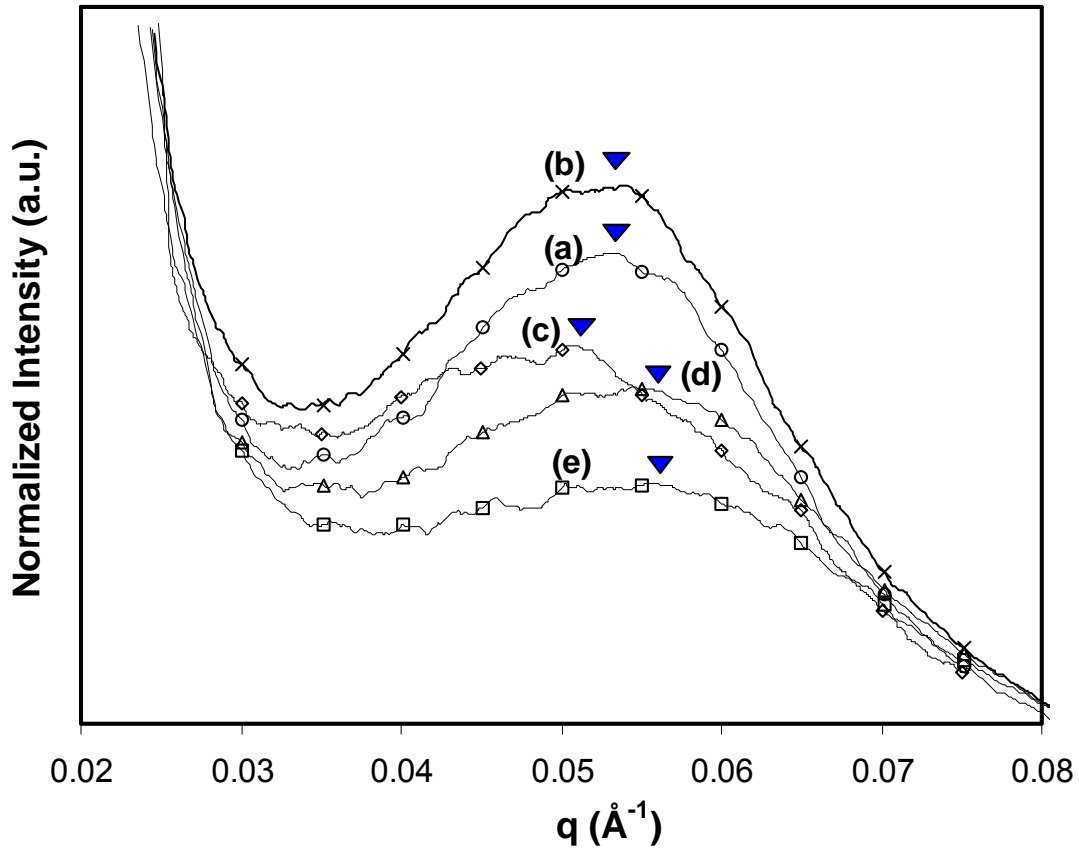


Figure 3.10: Scattering profiles of foams obtained using SAXS: (a) control (\circ), (b) 30% SAN ($+$), (c) 10% crosslinker (\diamond), (d) 10% SBOP (Δ) and (e) 30% SBOP (\square). Inverted triangles indicate average interdomain spacings.

Normalized SAXS intensity is affected by two main parameters: (1) the number of scattering objects, which is related to the volume fraction and also weight fraction of hard domains (electron dense phase) and (2) the inherent electron density contrast between the hard and soft domains [109, 110]. The observed increase in intensity of 30% SAN is attributable to the former, a higher volume fraction of hard domains/scattering objects. This is because the HS-to-SS ratio is higher in the 30% SAN polymer phase than the control. On a per volume basis, there are more scattering surfaces in SAN-containing foam than in

the control. Crosslinker and SBOP foams all have higher HS concentrations compared to control, however, SAXS intensities are much lower.

Crosslinker foam, in addition to signal intensity loss, showed a visible interdomain spacing increase of over 10 Å. Since the bulk of the soft domains are still polyether polyol-based, the interdomain spacing change is likely achieved via an increase in hard domain size. Low molecular weight crosslinker polyols can mix with the HS and form swelled hard domains, consequently, a larger hard domain size gives rise to a larger interdomain spacing [86, 111-113]. In addition, hard domains swelled with crosslinker polyol are lower in electron density than un-swelled hard domains. Therefore, the electron density contrast between soft and hard domains is reduced and 10% crosslinker foam shows a reduction in SAXS intensity.

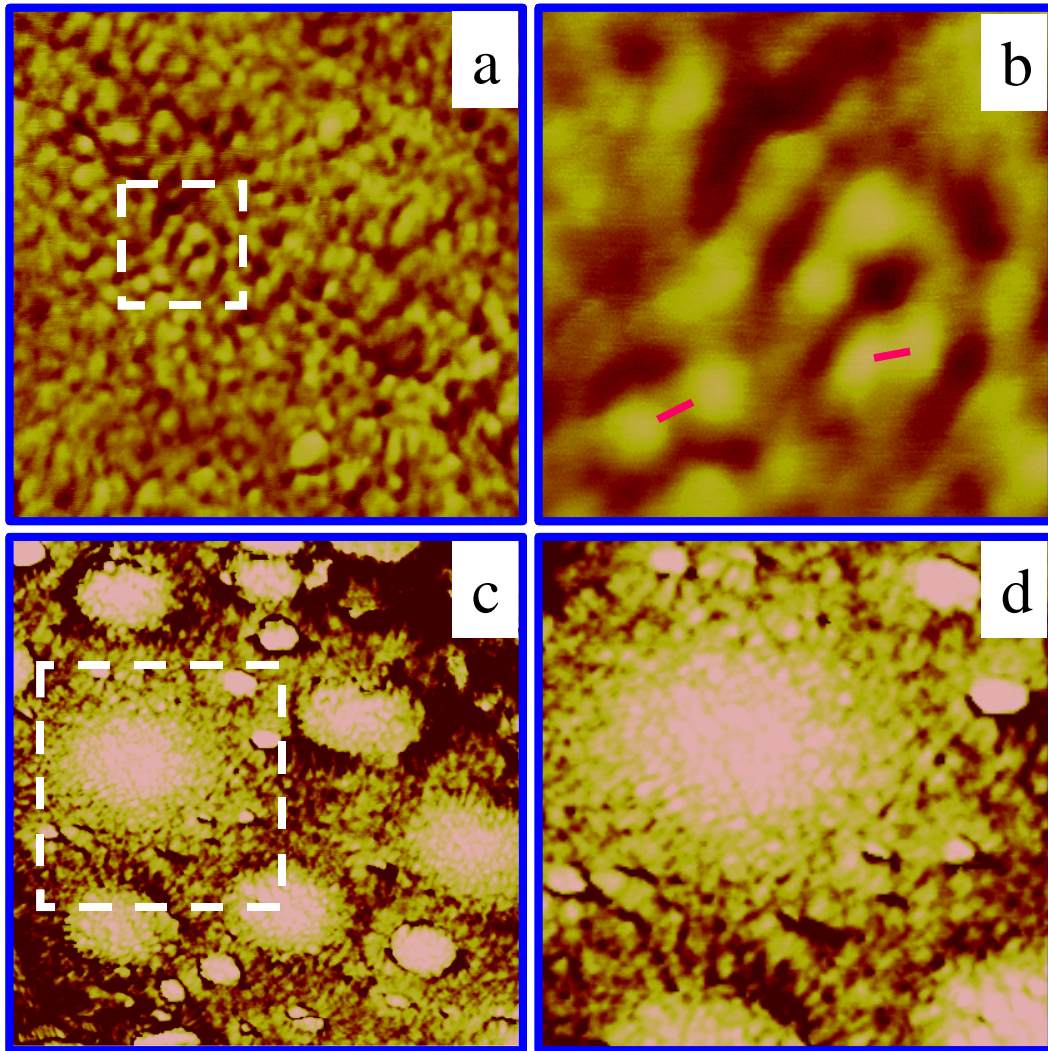
Substitution of SBOP has the most significant impact on SAXS intensity. Both scattering profiles of SBOP-containing foams show a slight decrease in interdomain spacing (higher q value) and great reductions in signal intensity. The reduction in intensity also increases as concentration of SBOP and HS increase. Implicitly, substitution of SBOP reduces the electron density difference between the hard and soft domains. Three possible scenarios are considered. First, the SBOP could mix into the hard domains, thus “diluting” electron density contrast. However, unlike in the case of 10% crosslinker foam, SBOP samples showed no signs of an increase in interdomain spacing (low q values). In fact, a small shift of the scattering profile to higher q values is observed. Thus, SBOP does not seem to swell hard domains like the crosslinker does. A second possibility is that HS are phase mixed with SS, where the hard domain is replaced by non-hydrogen bonded HS. In such a case, it would reduce the SAXS intensity. However, the results of a FTIR study, presented in a later section, indicate HS in SBOP foams are well associated through hydrogen

bonding. A third possibility is that rather than forming well-defined large hard domains, smaller hard domains may have replaced these large ones in the SBOP foams. A wide distribution of interdomain spacing could lead to a reduction in SAXS intensity. Additionally, smaller hard domain size equates to more interfacial areas per unit volume, which may explain the loss of SS observed in SBOP foams.

Atomic Force Microscopy (AFM) Images

So far, all experiments are indirect measures to the polymer phase morphology. It is desirable to “see” the hard and soft domains and thus understand the changes in morphology due to substituent polyols. This is possible using AFM.

Phase images of foams acquired via AFM are shown in Figure 3.11. Hard and soft domains are indicated by different colors. Yellow-to-white (light) colored areas correspond to high modulus regions, i.e., hard domains and brown-to-black (dark) colored areas correspond to low modulus regions, i.e., soft domains. The hardness difference between two domains is correlated to a phase scale expressed in degrees [114, 115]. For each image, the overall phase scale was adjusted to clearly illustrate foam morphology; as indicated in the captions of Figure 12. During tapping mode image acquisitions, the AFM tip was controlled to indent the sample surface by approximately 15 nm. By controlling the distance of tip-sample interaction, comparison of phase images can be made more consistently.



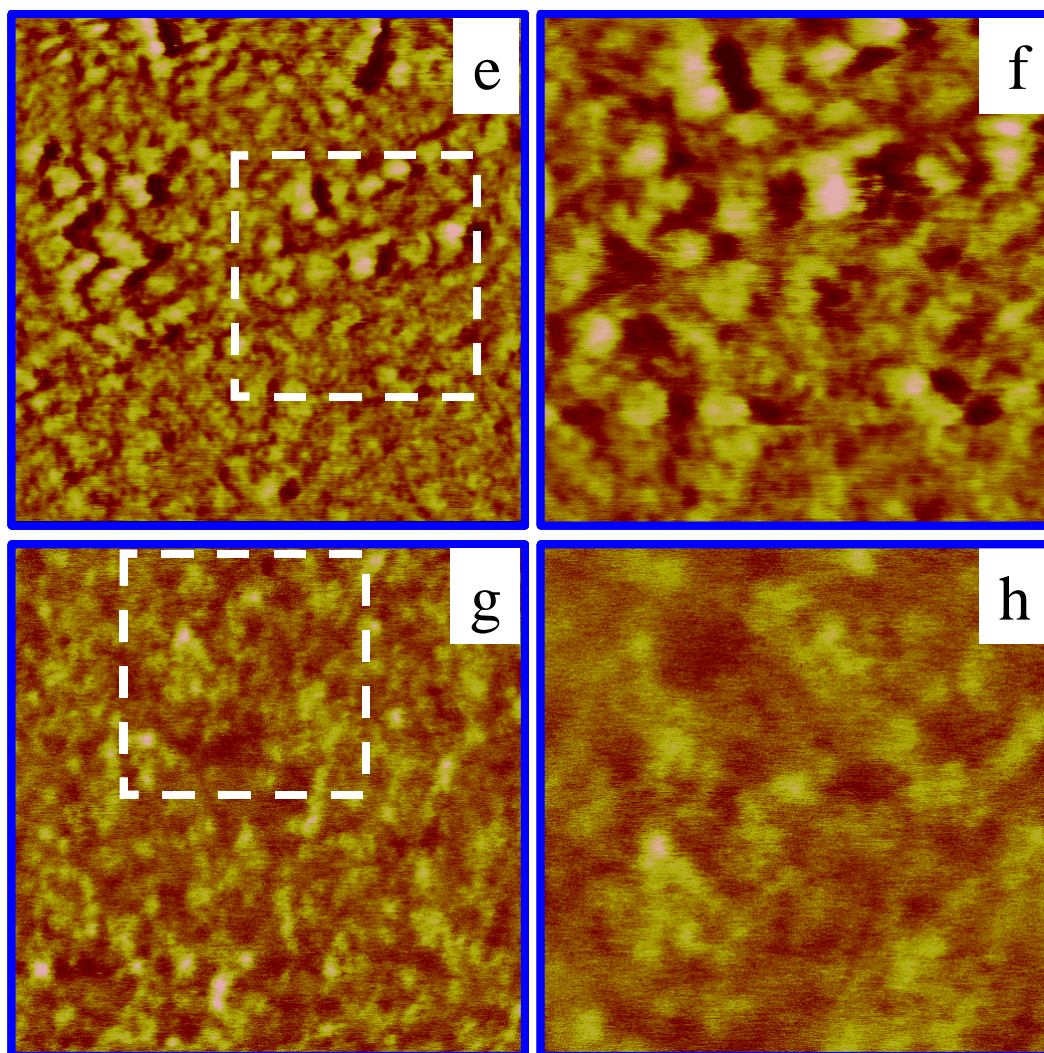


Figure 3.11: Tapping mode AFM images. Images on the right side are higher magnifications of the indicated regions on the left side. Colored bars in (b) are 100 Å in length:

Control	(a) 1 x 1 μm, 25°-scale	(b) 250 x 250 nm, 25°-scale
30% SAN	(c) 2 x 2 μm, 90°-scale	(d) 1 x 1 μm, 90°-scale
30% SBOP	(e) 1 x 1 μm, 25°-scale	(f) 500 x 500 nm, 25°-scale
30% SBOP	(g) 1 x 1 μm, 10°-scale	(h) 500 x 500 nm, 10°-scale

Control foam in Figure 3.11(a) clearly shows a two-phase, well-separated morphology. Each phase is distinguishable by color and the boundaries are visible. The image is displayed at an total phase scale of 25° , which is similar to previous findings by other studies [114, 116]. A higher magnification image of the control sample in Figure 12b showed an estimated interdomain spacing of 100-150 Å, which is in good agreement with interdomain spacing measured in SAXS, 115 Å.

Phase images (not shown here) of SAN-containing sample exhibited the same phase-separated morphology and domain spacing as the control. In addition, 30% SAN foam also exhibits a unique feature — SAN particles dispersed within the polymer phase as shown in Figure 3.11(c) and 3.11(d). These are SAN particles because they are: (1) spherical in shape, (different from the hard domains seen in the control) (2) large in size and (3) high in modulus. The measured diameters of these particles range from 0.2 to 0.7 μm , consistent with the known composition and specification of Hyperlite[®] E-849 copolymer polyol. The hardness difference between these particles and soft domains is much higher than that between hard and soft domains. The overall image phase scale is 90° for Figure 3.11(c) and 3.11(d). It is interesting to note that samples compressed at 120 °C lost this large-scale morphology presumably due to flow of the SAN particles.

Phase images of 30% SBOP display quite different morphology from the control. Figure 3.11(e) and 3.11(f) were taken at two different regions of the same sample, showing morphology variation within 30% SBOP. The most noticeable feature is that the domain boundaries in Figure 3.11(e) to 3.11(h) are blurry. In addition, a size variation of hard domains can be seen in these images. In Figure 3.11(e) and 3.11(f), some hard domains have slightly more distinguishable boundaries while the rest do not. From a sampling of different

regions on 30% SBOP foam and previous results in DMA, the slightly better phase-separated areas could be polyether polyol-based soft domain rich region. Figure 3.11(e) and 3.11(f), are displayed with an overall phase scale of 25° and the measured average phase hardness difference is only 10° . This signifies that the modulus of the soft domains increased. A similar, but more pronounced drop in phase hardness difference is observed in Figure 3.11(g) and 3.11(h). The overall phase scale is 10° and measured phase hardness difference is less than 8° . The boundaries here between the two phases are even less detectable. More importantly, hard domains appear to be smaller in size than those seen previously, especially in control.

The AFM images of 30% SBOP foam show that hard domains are smaller in size, in close proximity, and have no clear boundaries. The hardness difference between the soft and hard domains is significantly less in SBOP foams. It is expected that the 30% SBOP foam has a higher overall room temperature modulus than other foams because the soft domains in SBOP foam are relatively harder. Two possible reasons may contribute the higher modulus in SBOP foam. First: the reduced hard domain size and loss of domain boundaries. This may influence the soft phase by increasing HS/SS interface thus trapping SS at interfaces and reducing the amount of SS participating in soft domains. Second: the SBOP-based soft domain is harder. In the DMA section, we speculated that there may exist a second soft phase rich with SBOP-based SS and a T_g around 75°C .

The blurred boundaries between hard and soft domains in 30% SBOP foam also raise a question whether the amount of hydrogen bonding between HS has been altered. The following section of FTIR-ATR examines the amount of hydrogen-bonded species and molecular differences between substituted foams.

Fourier Transform Infrared (FTIR) Spectroscopy with Attenuated Total Reflectance (ATR)

FTIR-ATR spectra of the foams' carbonyl regions (1550 to 1800 cm^{-1}) are shown in Figure 3.12. Two particular absorbance regions are of interest: free species region, $> 1700\text{ cm}^{-1}$, comprised of both free urethane and free urea, and H-bonded species region, $< 1700\text{ cm}^{-1}$. Details of spectra interpretation and band assignments can be found in [74-76]. These bands are listed in Table 3.3 along with the peak areas.

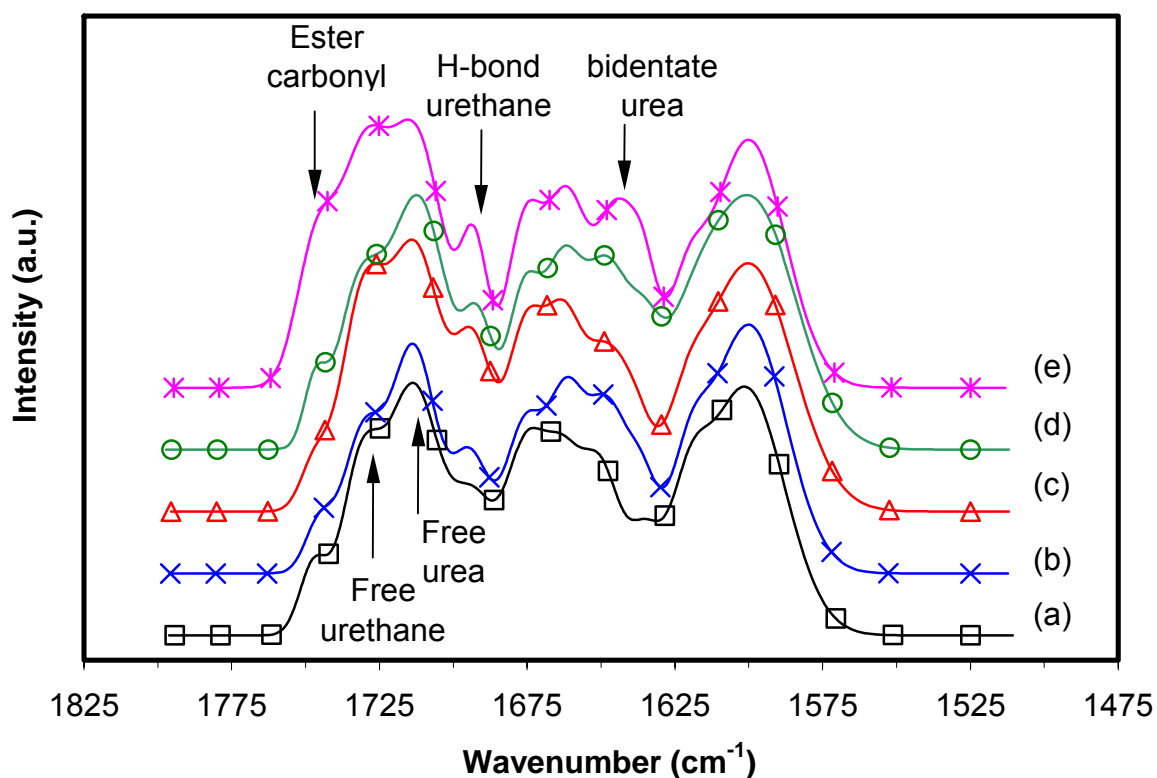


Figure 3.12: FTIR-ATR spectra of the carbonyl region: (a) control (\square), (b) 30% SAN (\times), and (c) 10% crosslinker (Δ), (d) 10% SBOP (\circ), and (e) 30% SBOP ($*$). Spectra are offset vertically.

Polyurea HS that does not participate in hard domain formation remains in the polymer as free, i.e., non-hydrogen bonded urea. These free ureas have an IR absorbance at 1713 cm^{-1} . Among all foam samples shown in Figure 3.12, 10% crosslinker shows the highest free urea absorbance band while very little variation in free urea absorbance band is seen in the other foams. These free ureas are likely the result of swelled hard domains, which agrees with the increase in interdomain spacing observed by SAXS (Figure 3.10).

Table 3.3: IR band assignments in C=O region and peak area under the bands. All areas are normalized.

	Ester Carbonyl ^(a)	Free urethane	Free urea	Monodentate urea	Bidentate urea
Wavenumber (cm^{-1})	1745	1732	1713	1676, 1662	1645
Control	0.031	0.55	0.32	0.48	0.20
30% SAN	0.024	0.54	0.31	0.47	0.22
10% crosslinker	0.020	0.57	0.42	0.42	0.16
10% SBOP	0.025	0.54	0.31	0.46	0.23
30% SBOP	0.080	0.60	0.31	0.44	0.25

^(a) Calculated band area under ester carbonyl absorbance.

The state of urethane bond provides less information on phase morphology, nevertheless, urethane still participates in hydrogen bonding via its carbonyl group. In general, more than half of the urethane bonds remain free [28]. Our foam samples show some variation in free urethane content. 30%

SAN and 10% SBOP has the least amount of free urethane followed by control, 10% crosslinker and 30% SBOP. Other than the 10% SBOP sample, the free urethane amount increases with increasing molar concentration of hydroxyls in the formulation. Note that 30% SAN and 10% SBOP closely resembles each other in the urethane composition.

Hydrogen-bonded ureas, including both monodentate and bidentate, are indications of hard domain ordering. The structure of monodentate urea is less ordered than that of bidentate urea. From control, 30% SAN, 10% SBOP to 30% SBOP, the absorbance bands shift from monodentate to bidentate urea. The shift in hydrogen-bonded urea region is in agreement with HS concentrations tabulated in Table 3.1 and is possibly a result of concentration effect. However, 10% crosslinker has the second highest HS concentration, and its IR spectrum shows the lowest bidentate urea absorbance. HS in 10% crosslinker are evidently not well associated and ordering in hard domains has been disrupted. The two SBOP-substituted foams are quite unique. The spectrum of 10% SBOP foam, as with the urethane spectrum region, resembles 30% SAN in the urea species composition. The similarity between the two spectra, 30% SAN and 10% SBOP, indicates that substituting copolymer filler or SBOP may have a similar effect on morphology. In 30% SBOP foam, the hard domains are more ordered. The peak at 1645cm^{-1} is more evident in the spectrum of 30% SBOP than in the others. Although the AFM and SAXS indicate that hard domains are smaller, FTIR indicates that the HS ordering within these domains is improved over the control. The bidentate urea peak in SBOP foam elucidates that SBOP plays a different role in polymer phase morphology from crosslinker.

Indentation Force Deflection (IFD)

The compressive properties of foams were evaluated using IFD tests and results are both plotted in Figure 3.13 and tabulated in Table 3.2. All substituent polyols have improved compression pressure considerably over the control. Conventional approaches to improve foam compression properties using copolymer-filled polyol and crosslinker showed approximately 35% increase in compression pressure. A similar amount of increase was achieved with 10% substitution using SBOP. When the amount of substituent SBOP increased to 30%, a startling 131% increase is observed. The more-than-doubled increase in compression pressure is a result of higher modulus of the foam polymer phase. A side-by-side comparison of foam shear modulus G' at 25 °C and compression pressures measured in IFD tests is shown in Figure 3.13.

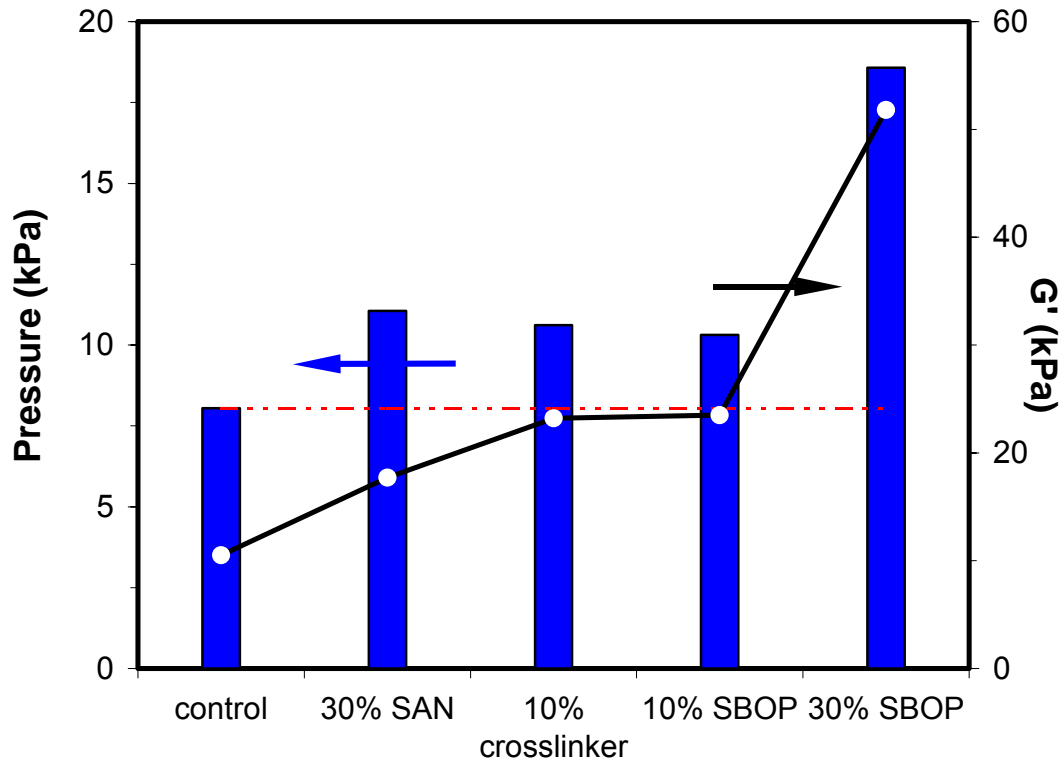


Figure 3.13: Compression properties of foams. Column data show the pressure required to achieve 65% compression (ASTM D 3574-95, test B1), and the line data show shear modulus, G' measured at 25 °C. All samples showed increases of compression pressure over control (dotted line).

3.5 Conclusion

The experimental results demonstrated that the substituent polyols used in this study are all capable of improving mechanical properties, specifically compressive properties. However mechanisms, through which the increases were achieved, are different.

Substituting SAN copolymer-filled polyol results in slightly smaller cell size and does not change phase-separated morphology in the polymer phase. The

increase in IFD test is correlated to a higher polymer phase modulus as a result of SAN particles acting as reinforcement.

The use of the crosslinker polyol alters polymer phase morphology, especially that of hard domains. This low molecular weight polyol mixes into the hard domains, disrupts hard domain ordering and alters interdomain spacing. Significant loss of HS to free ureas has been shown to result in reduction in modulus [28,117]. However, the overall concentration of HS in 10% crosslinker foam compensates for its loss of hard domain ordering. The improved modulus thus higher IFD is a result of higher HS concentration.

SBOP foams have the most interesting results. Although it is a low molecular weight polyol, the SBOP-substituted foam is morphologically different from its petroleum counterpart, crosslinker foam. The thermal analysis, DSC and DMA, shows that SBOP foams have much less than the expected amount of polyether soft domains. The DMA results further suggest that there may exist an SBOP-rich region in SBOP foams, which has a higher T_g than the polyether polyol-based soft domains. AFM images verify the possibility of two types of soft domains. In addition, AFM images show that 30% SBOP has smaller hard domains with a distribution of interdomain spacings. The observed broad peak in SAXS is, therefore, due to lower electron density contrast between hard and soft domains and a broad interdomain spacing distribution. The FTIR results indicate that SBOP-containing foams have the most ordered hard domain structures, implying a well phase-separated hard phase.

The improved polymer modulus in SBOP foam is attributed to a combination of factors: a high T_g SBOP-rich phase, high HS concentration, and improved hard domain ordering.

Chapter 4

Reaction Kinetics

Contents

4.1	Chapter Overview	89
4.2	Introduction	89
4.3	Experimental	92
4.3.1	Materials	92
4.3.2	Procedures and Characterizations	94
4.4	Results and Discussion	99
4.4.1	Hydroxyl-isocyanate Reaction	99
4.4.2	Polyol-TDI Reaction	106
4.4.3	Foaming Kinetics	110
4.5	Conclusion	126

4.1 Chapter Overview

The SBOP used in this work represents a family of natural oil polyols that contain only secondary hydroxyls. In addition, these hydroxyls are located at the mid point of polyol chains making them sterically hindered, and thus, low in reactivity. Compared to petroleum polyols, which contain either primary hydroxyls or secondary hydroxyls near chain ends, natural oil polyols are at a disadvantage kinetically. Replacing petroleum polyol with natural oil polyol in flexible foam formulation is expected to change the kinetic balance and may even affect processing. However, a 30 wt% SBOP-substituted foam, documented in Chapter 3, surprisingly showed no signs of kinetic issues. This chapter continues the investigation on partially substituted foam systems by exploring the kinetic aspect of these samples. Two sets of experiments were performed: (1) hydroxyl reactivity comparison, and (2) foaming kinetics comparison. The experimental results confirmed that the hydroxyls on natural oil polyol are at least two times less reactive than a primary hydroxyl on petroleum polyol. During foaming, the slowed urethane formation delayed the onset of phase separation in natural oil polyol-substituted foams.

4.2 Introduction

Polyurethane (PU) flexible foam formation is an intricate process involving two major competing reactions: gelling and blowing reactions (see Chapter 1.2.1). A kinetic balance between the two reactions is vital in making foams with desired cellular structures as well as producing consistent products. In this research, petroleum polyols are substituted with natural oil polyols giving rise to changes in gelling reaction kinetics and the overall kinetic balance.

Natural oil polyols are significantly different from petroleum-derived polyols. Aside from chemical nature, natural oil polyols' hydroxyls are located in

the mid point of polyol chains with the exception of those synthesized through ozonolysis route. For a natural oil polyol converted from a single oil molecule, its hydroxyls are most likely to be 5-8 covalent bonds removed from the chain ends. Such hydroxyls are sterically hindered. In addition, a significant fraction of the commercially viable natural oil polyols, such as soybean oil polyol (SBOP) used in this work, have only secondary hydroxyls. Compared to petroleum-derived polyols, which have either primary hydroxyls or secondary hydroxyls that are only one covalent bond removed from chain ends, natural oil polyols are at a disadvantage with respect to gelling reaction.

As briefly discussed in Chapter 1.2, an extreme case of a slow gelling reaction could cause foam to collapse during curing. In the previous chapter, two SBOP-substituted samples were made at 10 wt% and 30 wt% SBOP content of the total polyol without changes made in catalysts. Neither foam collapsed nor showed signs of kinetic issues. The foaming process evidently did not change as a result of substituting in the slow-reacting SBOP, however, the final morphology did change as unveiled by the characterization study in Chapter 3.

In PU flexible foam, the resultant morphology is closely associated with reaction kinetics and is determined by a complex system of reactions and phase evolution events [24, 79]. When all reactants are mixed, water and isocyanate quickly react to form ureas and polyureas, also known as hard segment (HS), while polyol and isocyanate react at a slower rate to form urethanes and polyol-based soft segments (SS) [118, 119]. At low degrees of polymerization (N), both HS and SS are soluble in the foaming mixture. As reactions proceed, the value of N increases so does the interaction parameter (χ) between the HS and the SS. At a critical reaction conversion, χN becomes large enough to drive the foaming mixture across the thermodynamic boundaries transitioning from a single-phased mixture to a phase-separated system comprised of HS-rich hard domains and

SS-rich soft domains [118-120]. Within the hard domains, hydrogen bonds are formed rapidly between neighboring HS resulting in physical crosslinks in the network [28, 74, 121]. The reactions continue after the initial phase separation as more ureas and urethanes are formed and both soft and hard domains grow in concentration and size [122]. The dynamic process of phase separation and growth comes to a halt when the hard segments vitrify. The final morphology is, therefore, a result of the dynamics among reaction kinetics, phase separation, and vitrification. The use of a slow-reacting polyol, such as SBOP, will indisputably have an effect on foam's final morphology.

A number of techniques are available to follow reaction kinetics and phase evolutions during foaming [25, 26, 74, 79, 122-124]. Among all, Fourier transform infrared spectroscopy (FTIR) emerges as method of choice because it provides information on both kinetics and phase evolution. In our experimental setup, a mid-infrared transmitting fiber was adopted in place of a conventional attenuated total reflectance (ATR) crystal to provide IR laser-sample interface. The use of IR transmitting fiber eliminates the need for a heating protocol, which is necessary, if ATR is used, to counteract the heat loss from foaming mixture to the ATR crystal [24, 80]. The substantially small mass of transmitting fiber leaves the temperature profile during foaming undisturbed and yet still provides a large surface-to-volume ratio for accurate absorbance measurements.

Four foaming experiments were followed using FTIR-fiber setup. A control foam was made entirely from a petroleum (base) polyol and three substituted foams were made by replacing 30 wt% of base polyol with crosslinker polyol, SBOP, and castor oil.

Prior to the foaming kinetics study, the reactivity of hydroxyls of small molecule alcohols was tested. Natural oil polyols are less reactive than their petroleum counterparts for two main reasons: (1) steric hindrance effect, and (2)

inherent reactivity of the hydroxyls. The small molecule hydroxyls reactivity study sheds some light on the inherent reactivity of hydroxyls and potential ways to affect their reactivity through chemical modifications. A series of low molecular weight alcohols with structural similarity to either petroleum or natural oil polyols were selected.

The hydroxyl-isocyanate reaction has been well established as a second order irreversible reaction [125-127]. However, deviations from the theoretical model have been reported on di-functional isocyanates due to substitution effect [128-130]. To avoid changes in isocyanate reactivity and stay structurally similar to toluene diisocyanate used throughout this research, a mono-functional phenyl isocyanate was selected to react with the alcohols. The reactants were pre-dissolved in a high dielectric constant solvent, N, N-dimethylformamide (DMF) to ensure a homogeneous mixture of reactants and products formed.

4.3 Experimental

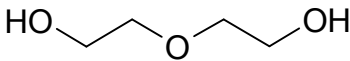
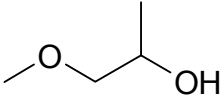
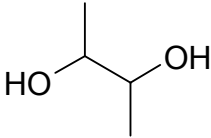
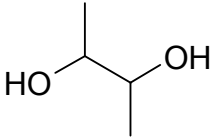
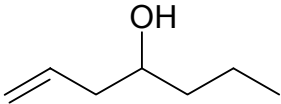
4.3.1 Materials

Alcohol-isocyanate Reaction

Phenyl isocyanate, $\geq 99\%$ purity, for reaction with alcohols and amines, was purchased from Sigma-Aldrich, and dried using activated molecular sieve for 12 hours before use.

Model hydroxyl-containing alcohols used for this study are listed in Table 4.1 along with purity and manufacturer information. All alcohols were dried using activated molecular sieve for 12 hours before use.

Table 4.1: Alcohols used in hydroxyl reactivity study.

Alcohol	Corresponding Polyol	Source
	Petroleum, ethylene oxide-capped polyol	≥99.5% (GC) Sigma-Aldrich
	Petroleum, propylene oxide polyol	≥99.7% (GC)
	Natural oil polyol, epoxidized, oxirane opened with methanol	Sigma-Aldrich
	Natural oil polyol, epoxidized, oxirane opened with water	≥99% (GC) Sigma-Aldrich
	Natural oil polyol, naturally occurring (e.g. castor oil)	≥98% Avocado

Heptadeutero-N,N-dimethylformamide (DMF-d₇), 99.5 atom% D, contains 1% tetramethylsilane (TMS) (Aldrich) was selected as solvent and dried using activated molecular sieve for 24 hours prior to use.

Polyol-TDI Reaction

Polyol isocyanate reactions were run on three polyol samples. They are Hyperlite[®] E848, Castor oil and SBOP. Dabco[®] 33-LV is the gelling catalyst used in this study at 0.25 pph loading. Details on polyols, catalyst and TDI used can be found in Chapter 2 and 3.

Foaming Kinetics

Three commercially available and one experimental polyols were used for foaming experiments: Hyperlite[®] E848 (Bayer Corporation), Voranol[®] 446 (Dow Chemical Company), Castor oil (Aldrich), and SBOP. Details on all polyols can be found in Chapter 2.3 and Chapter 3.3.

All other reactants, including toluene diisocyanate, catalysts and surfactants are fully documented in Chapter 3.3.

4.3.2 Procedures and Characterizations

Alcohol-isocyanate Reaction

The formulations used for small molecule alcohol-isocyanate reaction study are given in Table 4.2. Alcohol or phenyl isocyanate solution was prepared by measuring either reactant into a pre-dried glass vial and diluting with the proper amount of pre-dried DMF-d₇. The hydroxyl concentrations of the alcohol solutions are in the range of 0.2-0.3 mol/L. When stoichiometrically balanced amounts of alcohol and phenyl isocyanate solutions were mixed in an NMR tube the reaction time was started. The reacting mixture was then quickly transferred into a NMR apparatus for data collections. A nuclear magnetic resonance, ¹H NMR, (VI-500, Varian Inova) operated at 500 MHz was used to follow the hydroxyl-isocyanate reactions. All reactions proceeded inside NMR probe at 20 °C and 1 atmosphere pressure. The δ -scale was calibrated to TMS. ¹H NMR spectra were collected every 5 minutes for the first hour and every 30 minutes or more thereafter, pending reactant conversion. To determine the chemical shifts of groups of interest, the ¹H NMR spectra of alcohols both before and after complete conversion were collected.

Table 4.2: Formulations used for hydroxyl reactivity study.

Reactant	Quantity (mg)			
Diethylene glycol	18.20			
1-methoxy-2-propanol		37.07		
2,3-butadiol			49.77	
1-hepten-4-ol				41.20
Phenyl isocyanate	48.54	45.32	65.20	59.83

Polyol-TDI Reaction

Formulations used for polyol-isocyanate reaction are shown in Table 4.3. The amount of TDI used was stoichiometrically balanced. All reactants were first dried in a vacuum oven at 40 °C, under full vacuum for 6 hours before use. Vials used for mixing were also dried by baking them in a 120 °C oven for 3 hours and cooled to room temperature under nitrogen gas flow.

All reactants, except TDI, were mixed by hand in the pre-dried glass vial and then appropriate amount of TDI was added and hand mixed for ~ 10 seconds.

Table 4.3: Formulations used for polyol-TDI reaction study. Values in parenthesis are actual amounts of reactants used, unit: g.

Component	Hyperlite [®] E-848	Castor oil	SBOP
Hyperlite [®] E-848	100 (14.98)	--	--
Castor oil	--	100 (7.45)	--
SBOP	--	--	100 (7.97)
Dabco [®] 33-LV	0.25 (0.037)	0.25 (0.019)	0.25 (0.020)
TDI	(0.74)	(1.88)	(2.48)

The reactions were taken place under an isothermal condition at 20 °C. Data were collected using an FTIR-ATR. Details on the equipment can be found in Chapter 2. Sample was taken from the mixing vial directly without quenching and placed on ATR crystal for spectra collection. A total of 16 scans were performed on each sample in the wavenumber range of 4000 to 600 cm^{-1} . The reason that only 16 scans were taken on each sample was to avoid changes in spectra due to reaction time. Data collections were terminated after isocyanate had reached a conversion of 60% or higher.

Data analysis software used was the same as documented in Chapter 2 and the peak area corresponds to the isocyanate stretching band (2270 cm^{-1}) was integrated to produce conversion data. Internal standards used in each sample were: ether stretching band ($\sim 1100 \text{ cm}^{-1}$) for Hyperlite[®] E-848, and alkane (CH_2) bending band ($\sim 1465 \text{ cm}^{-1}$) for castor oil and SBOP.

Foaming Kinetics

Foaming kinetics study was performed on four foam formulations. Table 4.4 gives the formulations used.

Table 4.4: Sample formulations for foam kinetics study

Component	Control	30% crosslinker	30% castor oil	30% SBOP
Hyperlite [®] E848	100	70	70	70
crosslinker	--	30	--	--
castor oil	--	--	30	--
SBOP	--	--	--	30
TDI weight (g) (index=100)	78.44	97.21	86.18	84.39

All formulations contain distilled water (4.2pph), DEOA (1.2pph), DABCO[®] 33-LV (0.35pph), DABCO[®] BL-11 (0.08pph), and surfactants (1.0pph). Surfactant used in control and 30% crosslinker foams was Niax[®] Y-10184 and in the rest of the foams was a mixture of DABCO[®] DC-5169 and Tegostab[®] B-4690 at 1:3 weight ratio.

The amount of each component was based upon 100 parts by weight of polyol and total mixture weight of 250 g. The amounts of TDI used is in stoichiometric balance with active hydrogen species, i.e. TDI index = 100.

Details on mixing procedures can be found in Chapter 2.3.2.

The FTIR-fiber set up is comprised of an IR interferometer (MIDAC Corporation), a Mercury-cadmium-telluride (MCT) detector (Model HCT-12.5-0.50, Grasby Specac) cooled by liquid nitrogen, a pair of fiber holders for

positioning, and a 250 μm -diameter and 30 cm-long chalcogenide glass fiber (Amorphous Materials) composed of tellurium, selenium, germanium and antimony. A simplified depiction of the FTIR-fiber system is shown in Figure 4.1.

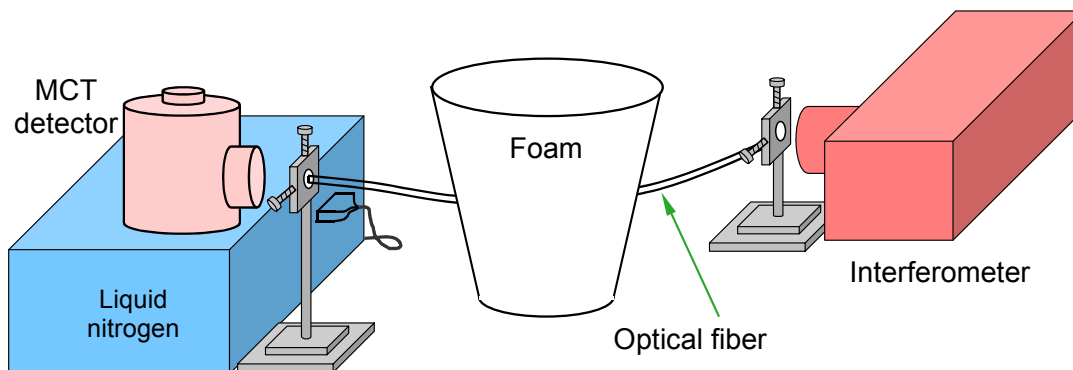


Figure 4.1: FTIR set-up used for foaming kinetics study.

Background spectrum was taken immediately before each experiment and the reaction spectra were collected every 2 seconds over the range of 4000 to 800 cm^{-1} in wavenumber at 2 cm^{-1} resolution. Data analysis was performed using Grams/AI software (Thermo Scientific). Due to the temperature rise during foaming, the baseline at 980 cm^{-1} shifted upward to an intensity of approximately 14 % of the intensity of ether (C-O-C) absorbance at 1100 cm^{-1} at reaction time, $t = 5$ minutes. The spectra were baseline corrected by fitting a quadric equation to five data points, where no infrared absorbance should be observed: 4000, 3750, 2500, 1800, and 980 cm^{-1} . The spectra were then normalized with respect to the area of the C-O-C stretching band, 1026 and 1127 cm^{-1} .

Temperature rise during foaming was measured by placing a type J thermocouple (0.25mm diameter, Omega Engineering Inc., details are available

in Chapter 2.3.3) in the center of a foam bun and recording the analogue signals at a frequency of 1 Hz.

4.4 Results and Discussion

4.4.1 Hydroxyl-isocyanate Reaction

The ^1H NMR spectra were taken of both reactant and product to differentiate and assign chemical shifts. Figure 4.2, as an example, shows the spectra of diethylene glycol and its urethane product. The characteristic chemical shift at $\delta = 3.6$ ppm, a triplet assigned to the α -hydrogen on diethylene glycol, shifts up field to $\delta = 4.2$ ppm as its hydroxyls react with phenyl isocyanate. Chemical shifts selected to monitor the other hydroxyl-isocyanate reactions are: $\text{CH}_3(\text{OH})\text{CH}_2\text{CH}_2\text{OCH}_3$ ($\delta = 1.08$ ppm, singlet) shifts to $\delta = 1.20$ ppm after reaction; $\text{CH}_3\text{CH}(\text{OH})\text{CH}(\text{OH})\text{CH}_3$ ($\delta = 3.46$ ppm, multiplet) shifts to $\delta = 4.68$ ppm after reaction, and $\text{CH}_2=\text{CHCH}_2\text{CH}(\text{OH})\text{CH}_2\text{CH}_2\text{CH}_3$ ($\delta = 3.56$ ppm, multiplet) shifts to $\delta = 4.87$ ppm after reaction. The time evolution of the ^1H NMR spectra for diethylene glycol-phenyl isocyanate reaction is shown in Figure 4.3. The peak areas under the chemical shifts were measured for conversion, x , calculations. Diethylene glycol-phenyl isocyanate reaction, as the example, the integrated area between $\delta = 3.4$ and 3.8 ppm were measured as well as the area between $\delta = 4.2$ and 4.4 ppm. The expression used for calculating conversion, p , is shown in Equation 4.1:

$$p = \frac{2A}{A+B} \quad (4.1)$$

where A is the area under δ from 4.2 to 4.4 ppm and B is the area under δ from 3.4 to 3.8 ppm.

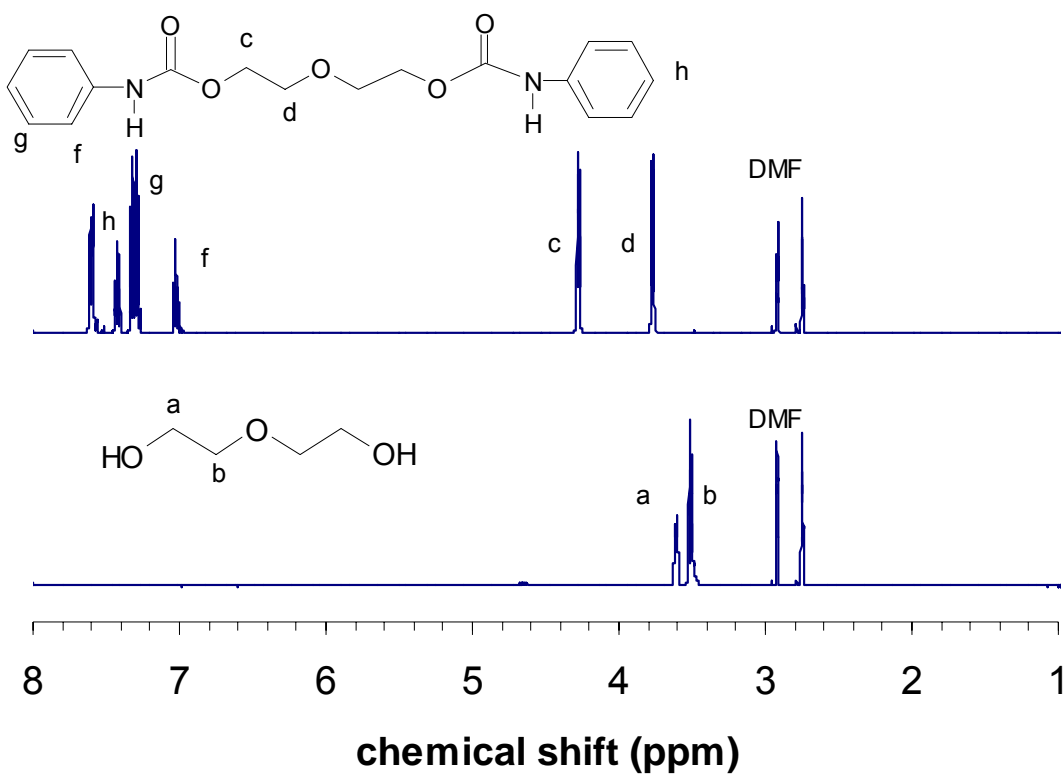


Figure 4.2: ^1H NMR spectra of diethylene glycol (bottom) and the urethane-derived thereof by reaction with phenyl isocyanate (top).

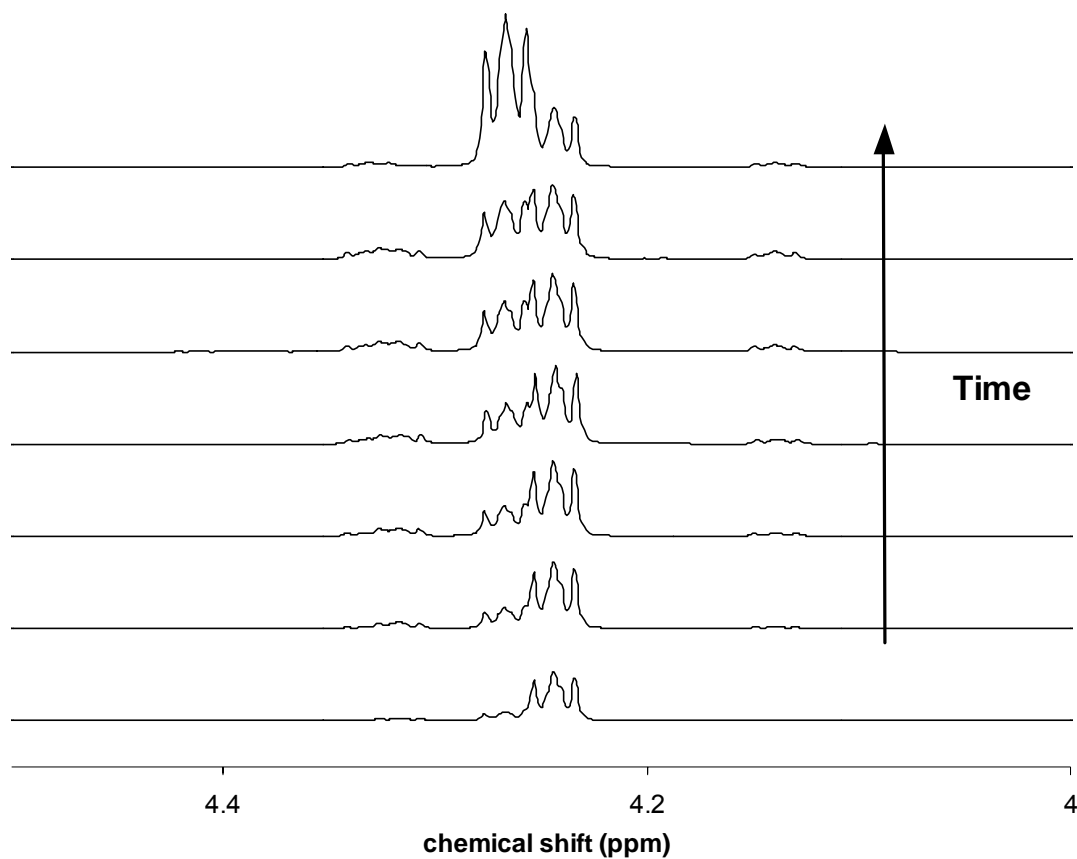


Figure 4.3: ^1H NMR spectra of diethylene glycol-phenyl isocyanate reaction at different times.

Since hydroxyl-isocyanate reaction follows a second order reaction, its kinetic expression can be written as:

$$\frac{dP}{dt} = k[\text{OH}][\text{NCO}] \quad (4.2)$$

where P, [OH] and [NCO] are the concentrations of urethane product formed, hydroxyl and isocyanate groups, respectively, k is the reaction constant, and t is reaction time. For a stoichiometrically balanced hydroxyl-isocyanate reaction, as in all the cases here, Equation (4.2) can be further simplified to:

$$\frac{p}{1-p} = k[OH]_0 t \quad (4.3)$$

where p is conversion of either reactant at any given time and [OH]₀ is the initial concentration of hydroxyls.

Using conversion, p, obtained from integration of the peak areas, one can calculate the reaction rate constant by plotting the left-hand side of the equation 4.3 with respect to time, t. In Figure 4.4, the experimental data were plotted for all four reactions. The calculated reaction constant, k, for each reaction is tabulated in Table 4.5.

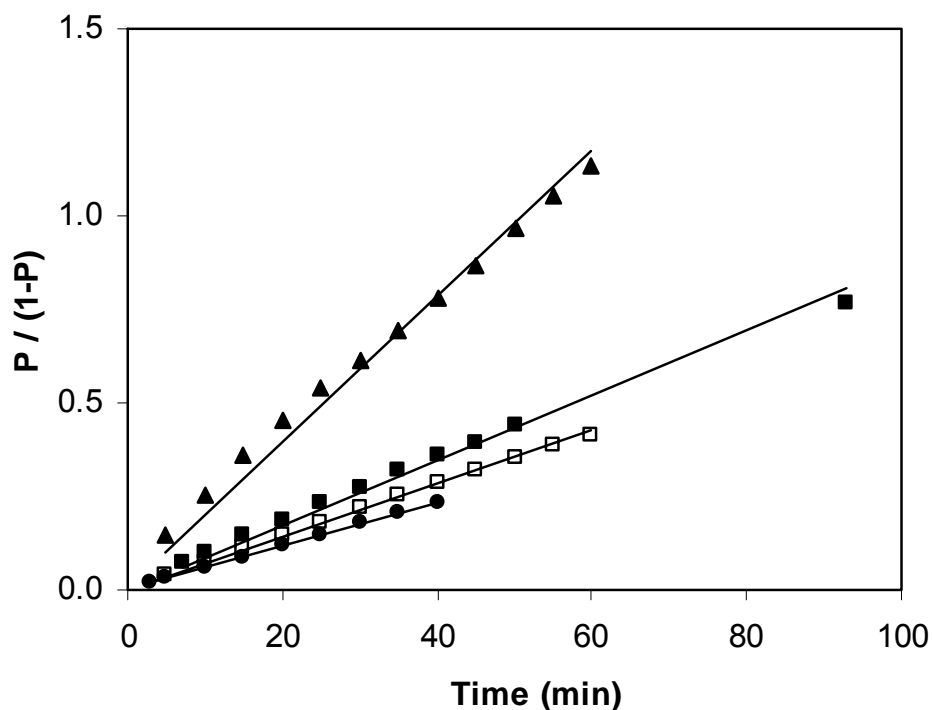
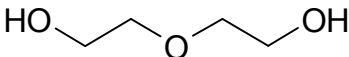
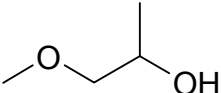
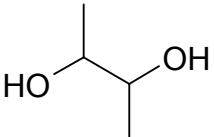
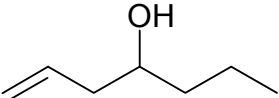


Figure 4.4: Second order kinetic plots used to calculate reaction constants: diethylene glycol-phenyl isocyanate (●), 1-hepten-4-ol-phenyl isocyanate (■), 2,3-butadiol-phenyl isocyanate (□), 1-methoxy-2-propanol-phenyl isocyanate (▲). Solid lines are the linear fit to the experimental data.

Table 4.5: Reaction constants for hydroxyl-isocyanate reactions in DMF.

Alcohol	Reaction constant, k , ($\text{L}\cdot\text{mol}^{-1}\text{min}^{-1}$)
	0.099
	0.049
	0.045
	0.061

It is not surprising that the primary hydroxyl in diethylene glycol is more reactive than the secondary hydroxyls. Davis and Farnum have shown that a primary hydroxyl is three times as reactive as a secondary hydroxyl, and is one-hundred times as reactive as a tertiary hydroxyl [131]. In the tabulated data, the primary hydroxyl in diethylene glycol is only twice as reactive as the secondary hydroxyl alcohol, 1-methoxy-2-propanol, which is lower than the difference Davis et. al. have reported. The reason a smaller reactivity difference is obtained here can be attributed to a solvent effect. Dyer and coworkers synthesized urethanes in a xylene solution by reacting either n-butanol or s-butanol with phenyl isocyanate [132]. The observed reaction rate of n-butanol is slightly over two-times that of s-butanol, lower than the three-time reactivity difference seen by Davis et. al. [133]. Later studies suggested that solvents, especially aprotic

solvents change the apparent reaction rate by solvating the hydroxyl-isocyanate complex formed, and allowing a fast urethane bond formation [134, 135]. The rate-determining step was found to be the rearrangement of the hydroxyl-isocyanate complex, thus, solvent effect does *not* change the relative reactivity of the alcohols. The reactivity data obtained are valid indication of relative reactivity of the hydroxyls. The reactivity ranking is, therefore: diethylene glycol > 1-hepten-4-ol > 1-methoxy-2-propanol > 2,3-butadiol.

Among the three secondary hydroxyl alcohols, both 2,3-butadiol and 1-methoxy 2-propanol are the same in reactivity, which suggests that the oxirane opening agent, either water or methanol, has little to no effect on the reactivity of SBOP. A slightly surprising result is the reactivity of 1-hepten-4-ol. The reaction rate constant, k , of this alcohol is approximately 24 % higher than the other secondary hydroxyl alcohols and is only 38 % lower than the primary hydroxyl alcohol in diethylene glycol. This improved reactivity in 1-hepten-4-ol is likely due to the presence of the double bond. Since a hydroxyl reactivity is largely determined by the electron-withdraw tendency of the substituent group attached, the presence of a double bond stabilizes the electrons, thus making the neighboring hydroxyl more reactive [136].

From the reactivity data of the four selected alcohols, it is clear that the natural oil polyols will be, at least, two times less reactive than the primary hydroxyls in petroleum polyols. In the following section, we will further explore the reactivity change as polyols are reacted with TDI and the last section of this chapter will focus onto foaming kinetics change in partially substituted flexible foams.

4.4.2 Polyol-TDI Reaction

The isocyanate conversions as functions of time for the three reactions of TDI with different polyols are plotted in Figure 4.5. Each formulation contains 0.25 pph dibutyltin dilaurate as a catalyst, details on the formulation can be found in Table 4.3.

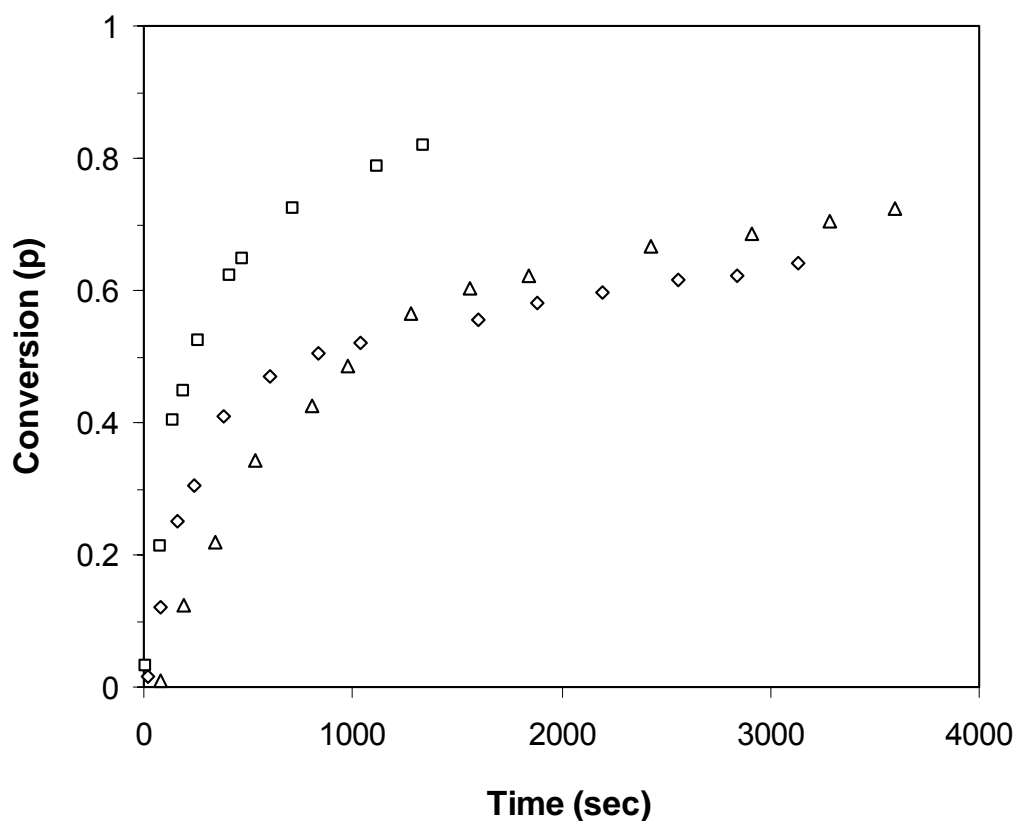


Figure 4.5: Isocyanate conversion (p) as a function of time during hydroxyl-isocyanate reaction at 25 °C by FTIR-ATR: Hyperlite® E-848 (□), castor oil (◇), and SBOP (△).

The Hyperlite[®] E-848 reaction with TDI shows the highest NCO conversion rate over the first 500 seconds, followed by the reaction of SBOP with TDI, and castor oil reaction with TDI has the lowest NCO conversion rate. The differences in rates can be explained by both steric hindrance effect and the presence of only secondary hydroxyls in natural oil polyols. In the case of Hyperlite[®] E-848, 85% of the hydroxyls are primary hydroxyls making a relatively high isocyanate conversion rate expected.

Early study on polyether polyols reaction with TDI showed that a para-isocyanate is 2-3 times more reactive than an ortho-isocyanate [129]. However, as either catalyst is added or the reaction temperature is raised to greater than 100 °C, the reactivity difference between ortho- and para-isocyanates diminishes [137-139]. The kinetics of a polyol reaction with TDI can be expressed as Equation 4.4.

$$-\frac{d[NCO]}{dt} = k_1[OH][o-NCO] + k_2[OH][p-NCO]$$

$$-\frac{d[NCO]}{dt} = k_1[OH](0.6)[NCO] + k_2[OH](0.4)[NCO] \quad (4.4)$$

$$-\frac{d[NCO]}{dt} = (0.6k_1 + 0.4k_2)[OH][NCO]$$

where k_1 and k_2 are the reaction constants of hydroxyl reactions with ortho- and para-isocyanate, respectively. In commercial TDI, 40 mol% of isocyanates are on the para-position while the rest 60 mol% are on the ortho-position [73]. Thus, the expression in Equation 4.4 could also be written explicitly as a function of [NCO]. For a stoichiometrically balanced reaction, as for all the polyol-TDI reactions performed here, Equation 4.4 can be solved to give isocyanate

conversion as a function of reaction time, shown in Equation 4.5, where p is conversion of isocyanate and $[NCO]_0$ is the initial concentration of isocyanate.

$$\frac{1}{[NCO]_0} \frac{p}{1-p} = (0.6k_1 + 0.4k_2)t \quad (4.5)$$

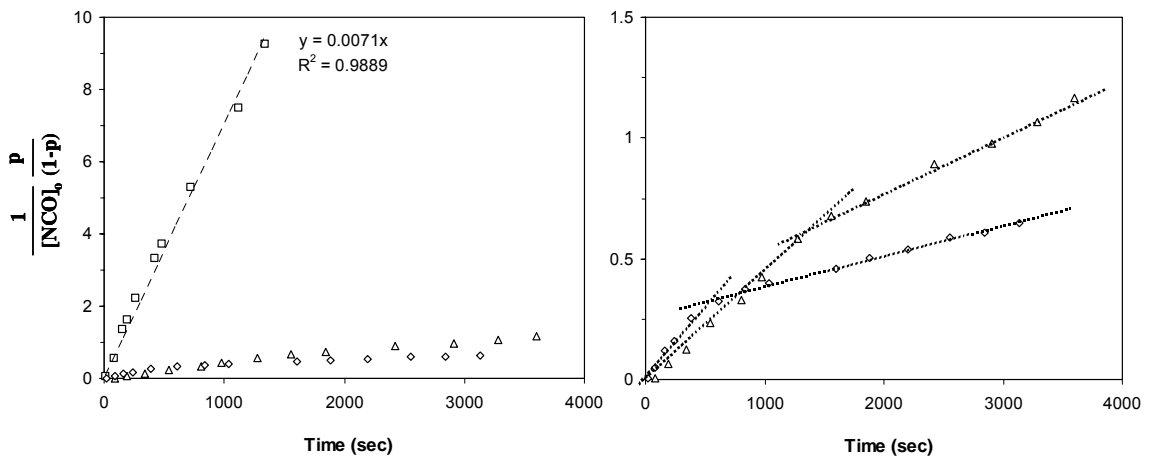


Figure 4.6: Plots for obtaining reaction constants of polyol reaction with TDI. Dashed lines are linear fits to the experimental data. Left plot shows Hyperlite[®] E-848 (\bar{N}), and right plot shows both castor oil (\bar{D}), and SBOP ($\bar{\diamond}$).

The experimental data were plotted as suggested by Equation 4.5, shown in Figure 4.6. A linear relationship between the reaction time (t) and the isocyanate conversion function is observed for Hyperlite[®] E-848 reaction with TDI. Thus, a single reaction constant sufficiently describes the reaction kinetics of Hyperlite[®] E-848 polyol reaction with TDI. For the two natural oil polyol reactions, instead of a single linear fit, two linear fits were used to fit the experimental data, as shown in Figure 4.6 (right). One may speculate the two rates represent ortho- and para- isocyanate reaction with polyol. However,

based on Equation 4.5, the difference between k_1 and k_2 will not give rise to a deviation away from a linear relationship. The apparent decrease in reaction rate is likely due to substitution effect. As one isocyanate on TDI is reacted, the reactivity of the other isocyanate group is expected to decrease by approximately 3 times [124]. In addition, the change in line fit slopes occurred between 45-55 mol% isocyanate conversions suggesting most of the TDI molecules are partially substituted. Slopes of the linear fits are tabulated in Table 4.6, where k is slope of the first linear fit, and k' is the slope of the second linear fit.

Table 4.6: Reaction constants for polyol reactions with TDI.

	k (L mol ⁻¹ s ⁻¹)	k' (L mol ⁻¹ s ⁻¹)	k/k'
Hyperlite [®] E-848	70.7	70.7	1.0
SBOP	6.7	1.2	5.6
Castor oil	4.4	2.6	1.7

The overall reactivity of un-substituted TDI reaction with Hyperlite[®] E-848 is over 10 times higher than that TDI reaction with SBOP, and nearly 16 times higher than TDI reaction with castor oil. Between the two natural oil polyols, we expected castor oil to be more reactive than SBOP based on previous small molecule study. However, SBOP is shown to be 50% more reactive than castor oil with TDI. Steric hindrance played a significant role in changing polyol reactivity not only between the primary and secondary hydroxyls but among secondary hydroxyls in different chemical environment as well. For the natural oil polyols, a reduced secondary reaction constant, k' , was also observed. The k' value for castor oil reaction with substituted TDI is more than 2 times the constant of SBOP reaction with substituted TDI. This is a rather important finding

because the reactivity of polyol with substituted TDI directly determines whether the polyol will be participating in the network formation. During foaming, water reaction with TDI is faster than polyol reaction with TDI, converting TDI to partially substituted TDI for reaction with polyol. Hyperlite[®] E-848 is thus kinetically advantageous as its reaction constant remains the same in case of both substituted and un-substituted TDI. In addition the reaction constant is the highest in Hyperlite[®] E-848 polyol among all three polyols tested making it highly likely to participate in PU network formation. Both natural oil polyols, castor oil and SBOP, on the other hand are at least 10 times less reactive than Hyperlite[®] E-848. In addition, the reaction constant of either natural oil polyol reaction with substituted TDI is more than 30 times lower than Hyperlite[®] E-848 making it crucial to examine their reactivity during foaming. Between the two natural oil polyols, castor oil reacts nearly two times faster with substituted TDI than SBOP. During foaming, castor oil could have an advantage over SBOP and will be examined in the following section.

4.4.3 Foaming Kinetics

Figure 4.7 shows the chemical structures of important species involved in kinetic reactions and phase separation. The ureas generated from the blowing reaction can remain as (1) free urea, or evolve to (2) mono-dentate urea, single hydrogen bonded, or (3) bidentate urea, double hydrogen bonded. At the onset of phase separation, the concentration of bidentate urea increases considerably, and is generally used as an indication of phase separation [140, 141]. Most of the urethanes generated from the gelling reaction are likely to remain as free urethanes while a small portion of them evolve to hydrogen-bonded urethanes [28].

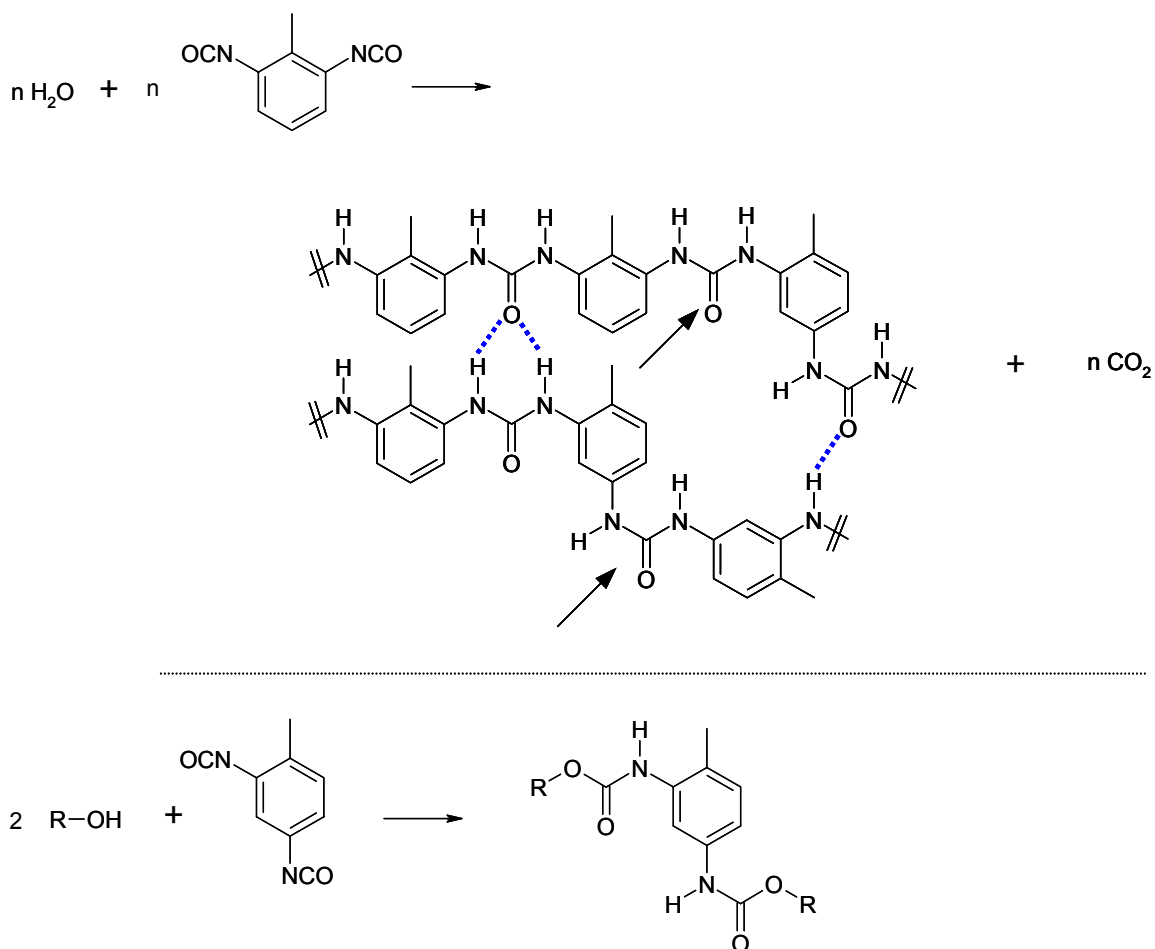


Figure 4.7: Chemical structures of a bidentate urea, shown as double hydrogen-bonded (dashed lines), a monodentate urea, shown as single dotted line, and free ureas, indicated by arrows. The reactions illustrated are the blowing reaction (top) and the gelling reaction (bottom).

Adiabatic Temperature Rise

The overall reaction progress is indicated by the consumption of isocyanate as both the blowing and the gelling reactions deplete isocyanate to form urea and urethane, respectively. Foam formulations can be found in Table 4.2. Figure 4.8 shows the typical three-dimensional FTIR spectra obtained in the

absorbance range of 2150 to 2350 cm^{-1} . The asymmetric stretching of the NCO group has a strong absorbance peak at 2270 cm^{-1} as seen in Figure 4.8. As reactions proceed, the peak intensity decreases. A second method for monitoring the isocyanate conversion is through the temperature rise monitoring and was employed here as well. Details on calculating isocyanate conversion from the temperature rise during foaming can be found in Chapter 2.3.

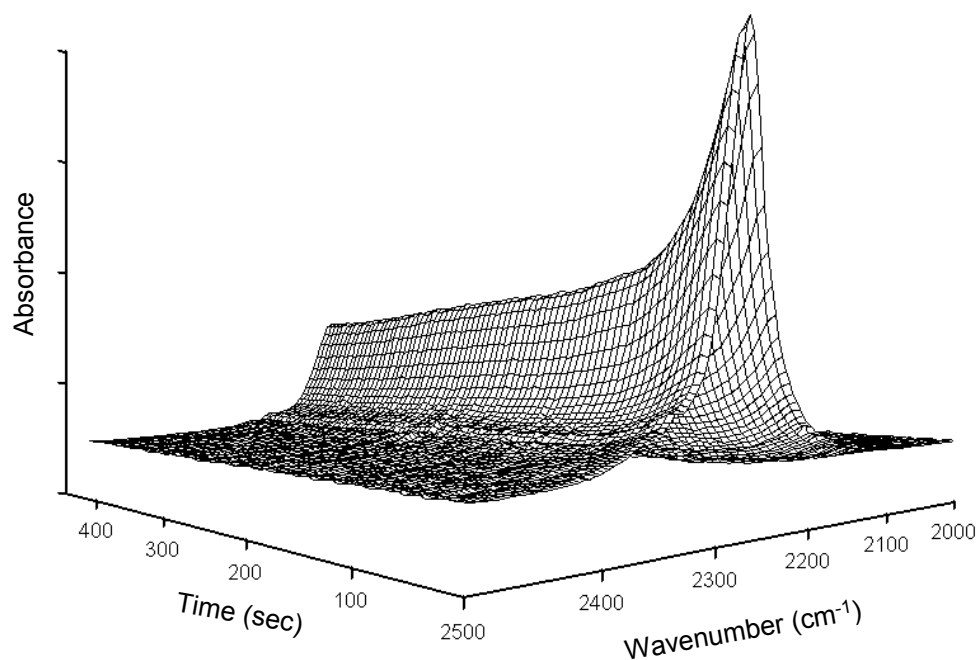


Figure 4.8: Three-dimensional surface of the isocyanate absorbance band for control foam.

The isocyanate conversions obtained using both FTIR and the temperature rise method are plotted in Figure 4.9. Both curves are in a good

overall agreement and captured the fast consumption of the isocyanate at the early stages of foaming. Later data analysis will primarily use the FTIR data.

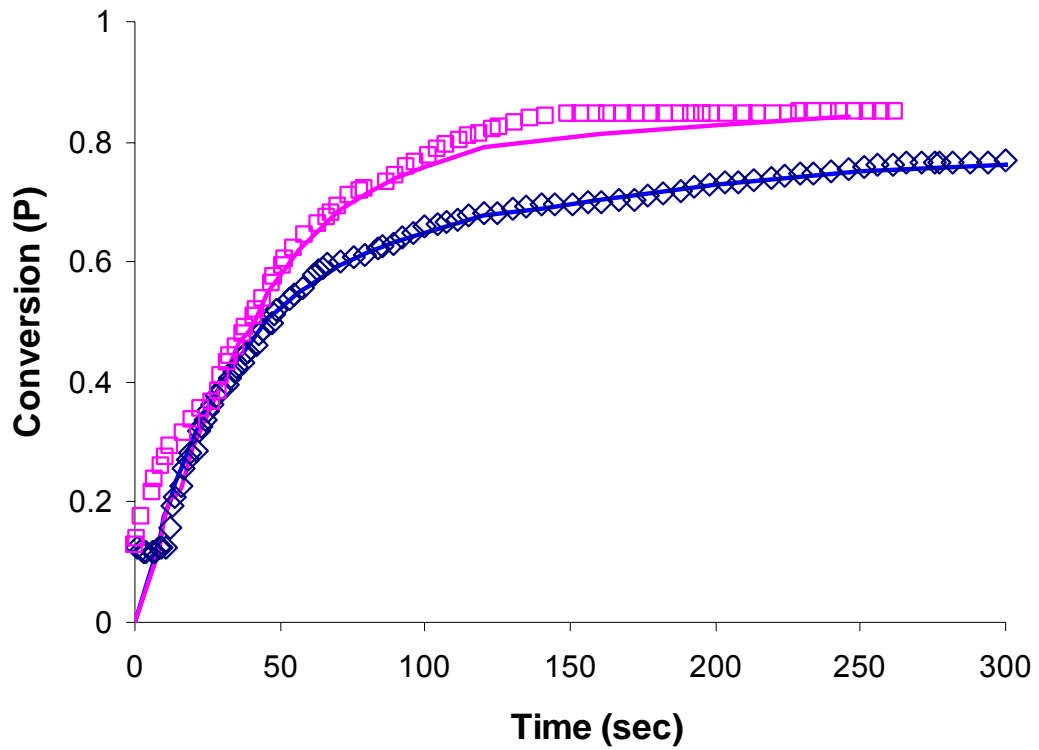


Figure 4.9: Isocyanate conversion calculated from temperature rises (open symbols) and extrapolated from FTIR data (solid line). The plot shows control (◇) and 30% crosslinker (□).

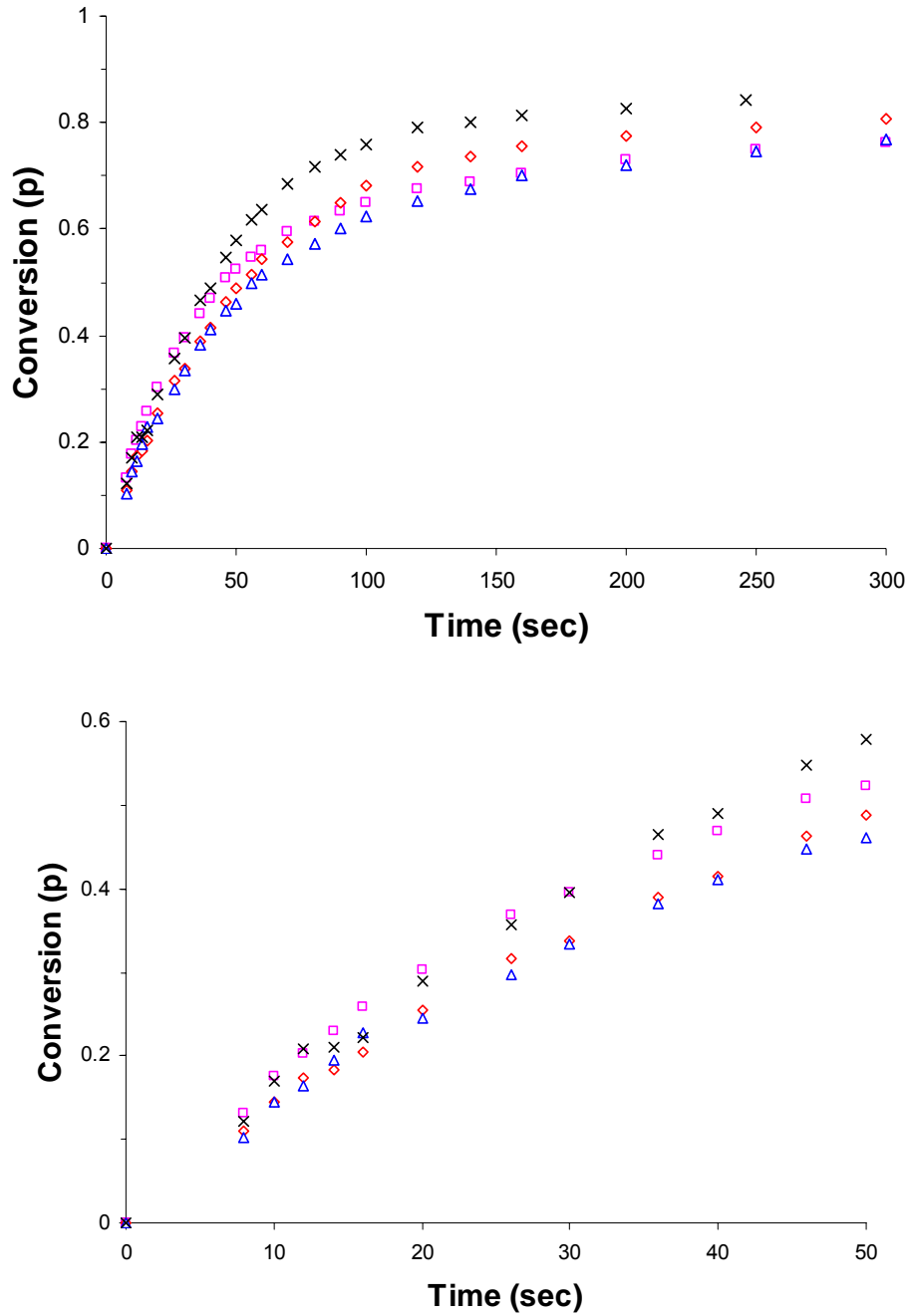


Figure 4.10: Isocyanate conversion during foaming: control (□), 30% crosslinker (x), 30% SBOP (◇), and 30% castor oil (△). Bottom enlarged scale of the first 50 seconds of foaming.

Figure 4.10 shows that initial rates of isocyanate conversion in control and crosslinker are nearly identical, whereas the rates in SBOP and castor oil are lower, by approximately 15 %, but identical between these two foams. At longer times, the crosslinker shows the highest conversion of isocyanate followed by SBOP, where castor oil and control share nearly an identical conversion.

The higher isocyanate conversion rate as well as a higher overall isocyanate conversion observed in 30% crosslinker sample is somewhat expected, since 30% crosslinker has the highest concentration of active hydrogen species, which include both water and polyol. The apparent rate of depletion rate of isocyanate is directly related to the content of active hydrogen species. Succeeding 30% crosslinker, 30% SBOP and 30% castor oil foams have the second and third highest active hydrogen species contents, and control has the lowest content of active hydrogen species. If only considering the reactant concentration differences, both natural oil polyol-containing samples are expected to have higher isocyanate conversion rates than control. However, the observed rates in both 30% SBOP and 30% castor oil foams are lower than control, which could be a sign of a slowed water-isocyanate reaction or a significantly slowed polyol-isocyanate reaction, or a combination of the two. By examining the isocyanate conversion alone is not adequate to draw conclusions, thus we will focus attention to the IR spectra in the carbonyl region for an answer.

One notable characteristic of the conversion data plotted in Figure 4.10 is all samples have an isocyanate conversion lower than unity. Among all, 30% crosslinker has the highest isocyanate conversion of 85 % at 250 seconds of reaction time, while the rest of foams all reached approximately 80 % conversion. Vitrification of the hard domains has likely hindered the isocyanate conversion in foam [74].

The carbonyl region (1630 to 1750 cm^{-1}) of the IR spectra is rich with information on urethane, urea formations as well as phase morphology evolutions. Two general regions are of interest: Region I, 1775 - 1700 cm^{-1} and Region II, 1700 - 1625 cm^{-1} . Region I is comprised of the absorbance bands of free species, both free urethane and free urea. Region II is comprised of the absorbance bands of hydrogen-bonded species. Detailed IR band assignments can be found in Table 2.3 in Chapter 2 [80]. Morphology development during foaming can be associated with changes in the characteristics of the hydrogen-bonded species, especially the ureas. Figure 4.11 shows the typical FTIR spectra evolution as a function of time for control sample.

Region I of the FTIR spectra shows the earliest increase in the intensity, which starts as soon as the reactants are mixed. Region II of the FTIR spectra shows a later rise in the intensity, which lags by approximately 30 seconds. As reactions continue, the absorbance bands in Region II, where hydrogen-bonded species are, shift towards lower wavenumber indicating changes in morphology. All four foams are similar in the respect that the aforementioned characteristics are seen in all samples, however, differences in species formation rates exist.

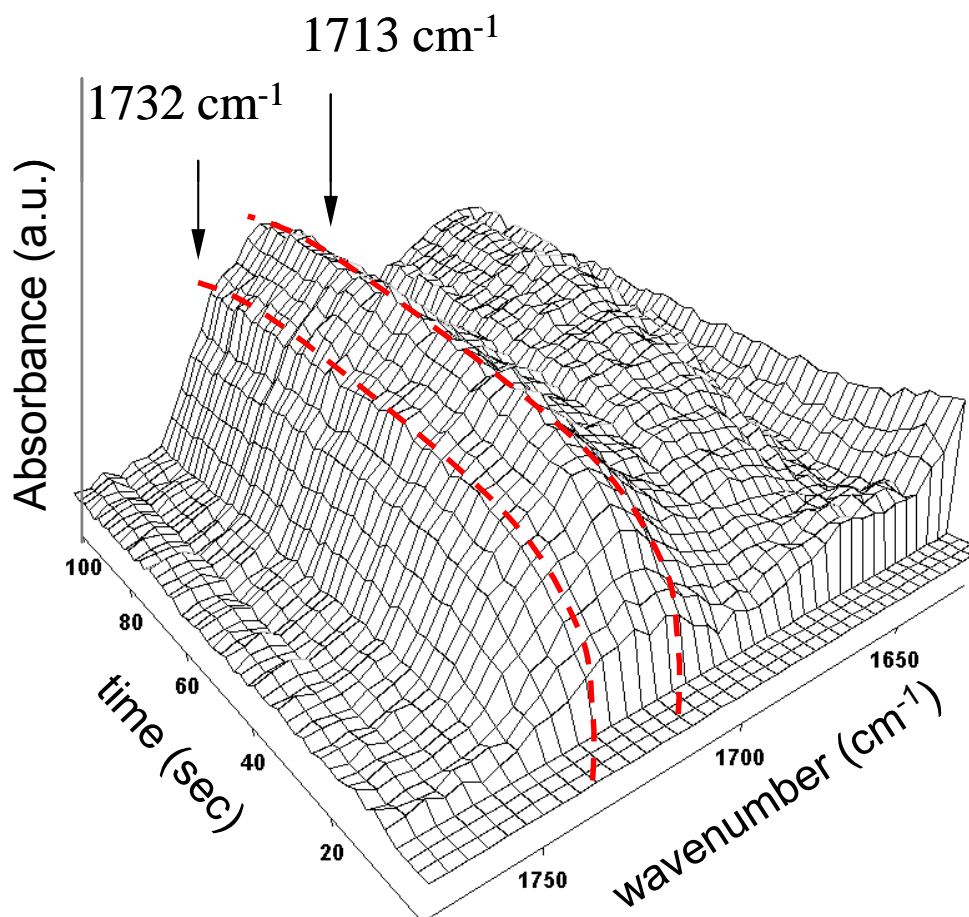


Figure 4.11: Time resolved FTIR spectra of control foam. The three-dimensional plots show only the carbonyl regions (1775-1625 cm⁻¹) and the dashed lines are indicative of the positions of free urethane (1732 cm⁻¹) and free urea absorbance bands (1713 cm⁻¹).

From Figure 4.11, it is clear that both free urethane and free urea were formed at the early stage of foaming as the dashed lines tracing both 1713 and 1732 cm⁻¹ absorbance bands show the rises of the band intensities [26, 80]. The band intensity changes of the free urethane (1732 cm⁻¹) and free urea (1713 cm⁻¹) formation are compared among samples. From the previous NMR study, we

have demonstrated that natural oil polyols are at least two times less reactive than the base polyol. The free urethane formation is analyzed and the intensity as a function of time is plotted in Figure 4.12.

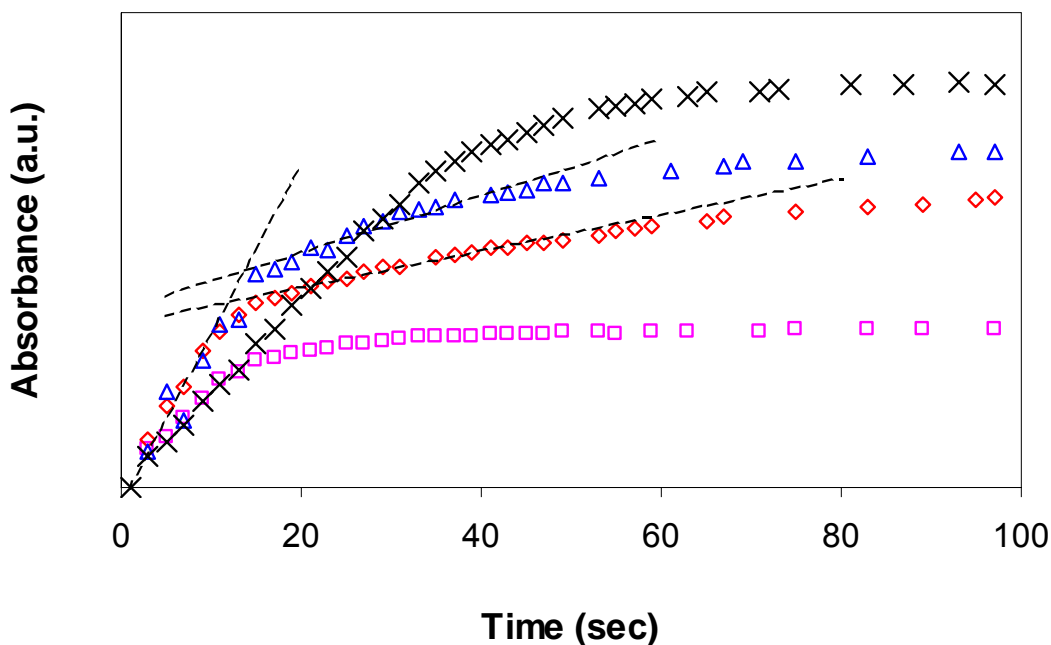


Figure 4.12: Free urethane absorbance (1732 cm^{-1}) change as a function of time for: control (■), 30% crosslinker (x), 30% SBOP (◇), and 30% castor oil (△).

During the first 20 seconds of reaction time, Figure 4.12, a linear rise of the free urethane absorbance is observed for all four samples, which indicates a constant rate of free urethane formation. The rates at which the free urethanes are formed vary somewhat. Two distinct rates are seen: the rate shared between control and 30% crosslinker is lower than the rate shared between the two natural oil polyol-containing foams. As stated earlier that natural oil polyols, SBOP and castor oil, are slow-reacting polyols, a higher slope, thus a higher free

urethane formation rate observed in natural oil polyol-substituted foams is counter-intuitive. The matter of the fact is that the hydroxyl concentrations among the four formulations vary quite some due to the difference in substituent polyol's molecular weight and f_n . The free urethane formation rate is not only a function of the reactivity constant more importantly a function of the reactant concentrations. The apparent initial rates of free urethane formation as well as the rates that are normalized with respect to hydroxyl concentrations are tabulated in Table 4.7. Control sample containing mostly primary hydroxyls, as expected, has the highest free urethane formation rate after normalization, while the two natural oil polyol-containing foams have slightly lower rates with castor oil showing slight kinetic advantages over SBOP polyol. 30% crosslinker foam, surprisingly, has the lowest free urethane formation rate after normalization, which is only 28% of the free urethane formation rate in control. This surprisingly low rate could be attributed to a high concentration of secondary hydroxyls. As the crosslinker used is a poly(propylene oxide) polyol, its hydroxyls are all secondary. Replacing 30 wt% of base polyol with crosslinker polyol leads to an 88-mol% secondary hydroxyl content, which is the highest among the samples. The significantly low free urethane formation is likely a reflection of high secondary hydroxyl content. The linear free urethane formation rate continues in 30% crosslinker foam for an additional 20 seconds after control has already reached a plateau. The overall free urethane in 30% crosslinker is the highest among all foams, which is expected as this formulation has the highest hydroxyl content as well.

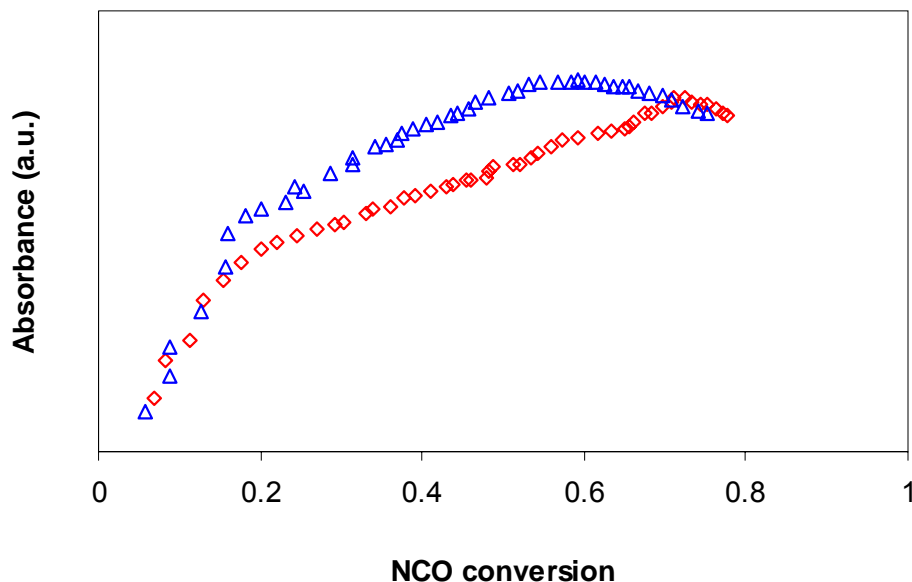


Figure 4.13: Free urethane absorbance change as a function of isocyanate conversion for 30% SBOP (\diamond) and 30% castor oil (\triangle).

The two natural oil polyol-containing foams have an interesting characteristic that after the first 20 seconds of reaction a second slope in the free urethane absorbance is observed. The presence of a second slope in the free urethane formation is not observed in either control or 30% crosslinker foams and is attributed to the reaction of natural oil polyol with TDI. The two slopes are more distinct as the same data is plotted as a function of isocyanate conversion, shown in Figure 4.13. The second slopes in 30% SBOP and 30% castor oil are 0.3×10^{-3} and $0.5 \times 10^{-3} \text{ s}^{-1}$, respectively, without normalization. Compared to the free urethane formation rate during the first 20 seconds in control, the second rate in 30% SBOP is approximately one-sixth of the rate in control, while 30% castor oil is merely one-third of the rate in control. There is an apparent difference between the free urethane formation rates in castor oil and SBOP containing foams. The second free urethane formation rate in castor oil is nearly

twice that of SBOP, which agrees with the polyol-TDI study before, where castor oil showed a more-than-two-time higher reaction constant than SBOP.

Table 4.7: Extrapolated relative reactivity data in the unit of Intensity/s.

	Relative reactivity ($\times 10^{-3}, \text{s}^{-1}$.)		
	Free urethane ^a	Free urea ^a	Bidentate urea ^b
Control	1.7 (47) ^c	2.5 (8.3) ^c	0.04
30% crosslinker	1.8 (13)	2.3 (8.9)	--
30% SBOP	2.5 (26)	2.5 (8.8)	0.06
30% castor oil	2.8 (36)	2.5 (8.7)	0.08

^a Only the first 20 seconds of reaction data was used to extrapolate the relative reactivity.

^b Data were extrapolated from the linear growth region of bidentate ureas.

^c The number in parenthesis indicates the rate after normalization with respect to the initial concentration of hydroxyl or water.

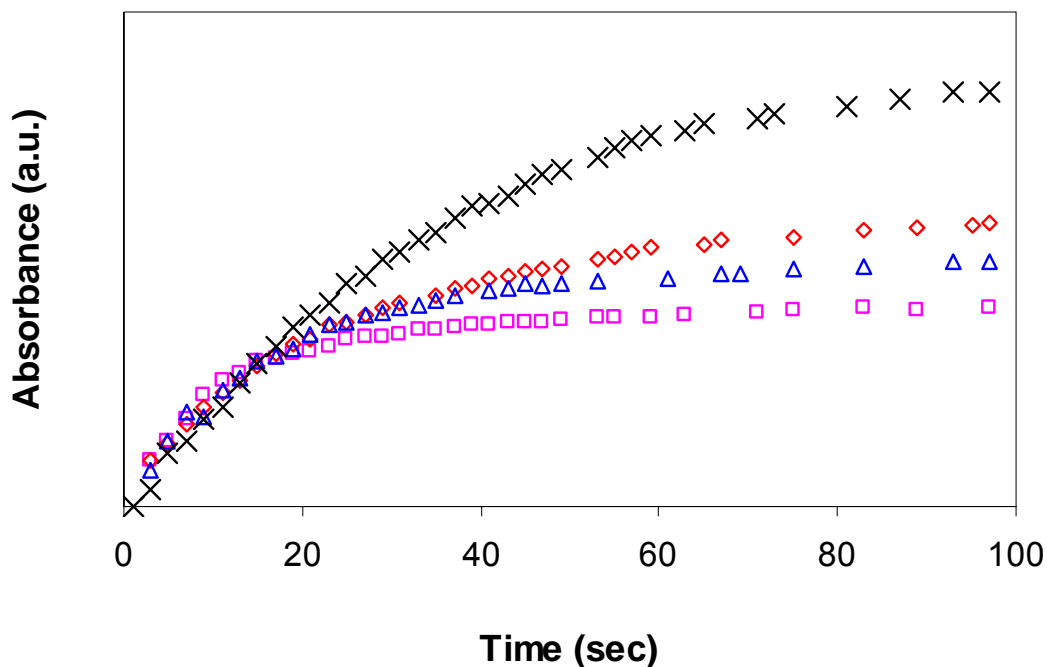


Figure 4.14: Free urea absorbance (1713 cm^{-1}) change as a function of time for: control (N), 30% crosslinker (x), 30% SBOP (D), and 30% castor oil (D).

The reaction rate of water with isocyanate is not significantly affected by substituting in different polyols as shown in Figure 4.14. Over the first 20 seconds of reaction, the free urea absorbance bands all increase at nearly the same rate. Even after normalization, the difference between the free urea formation rates is less than 10%. One notable fact is that the substituted foams all have higher free urea formation rates than control, and 30% crosslinker foam has the highest free urea formation rate. This is an encouraging result because it indicates that substituent polyols, especially natural oil polyols, do not hinder water-isocyanate reaction. On the other hand, the lower free urethane formation rates in substituted foams imply a shift in the reaction balance between the gelling and the blowing reactions as base polyol is replaced.

30% crosslinker foam stands out in Figure 4.14 as its free urea absorbance continue to rise, whereas the same absorbance of the other three foams begin to level off at approximately 20 seconds. The morphology evolution in flexible foam involves phase separation and the formation of hydrogen bonds between polyurea hard segments. The continuous rise of the free urea concentration in 30% crosslinker implies that most of the polyurea hard segments formed in this foam do not participate in the formation of hydrogen-bonded species. Thus, phase separation is likely hindered. In the following section, we will examine the bidentate urea formation to detail the morphology development differences among the foams.

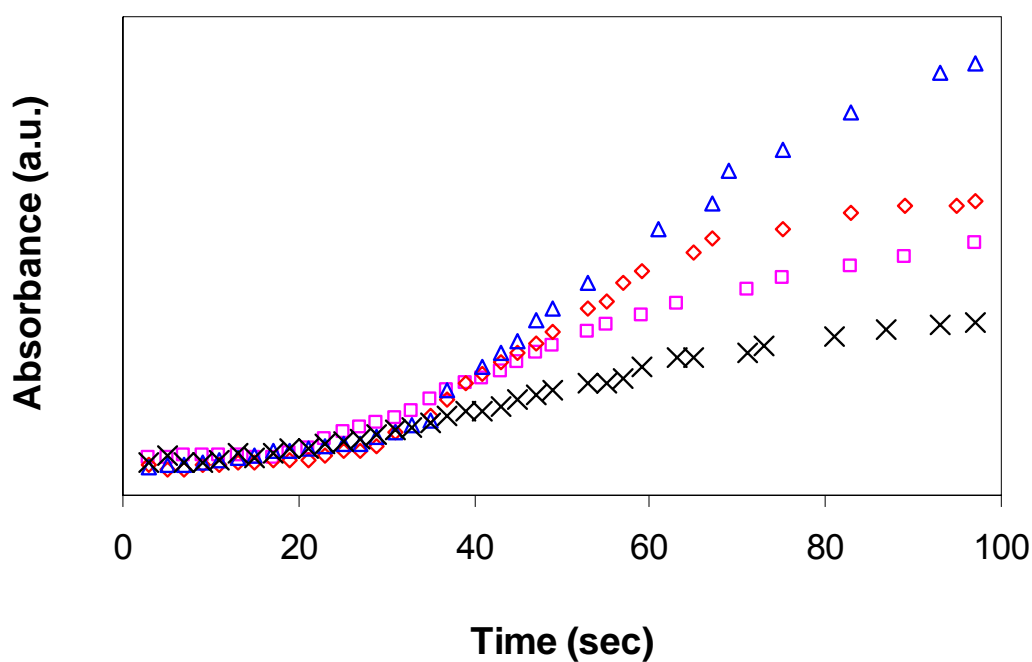


Figure 4.15: Bidentate urea absorbance (1640 cm^{-1}) change as a function of time for: control (□), 30% crosslinker (×), 30% SBOP (◇), and 30% castor oil (△).

Figure 4.15 shows the changes in absorbance of bidentate ureas. For control, as the free urea absorbance band reaches a plateau at approximately 20 seconds, seen in Figure 4.14, a significant rise in the bidentate urea absorbance band is observed in Figure 4.15. The same phenomenon, exchanging between a rise of free urea absorbance and a rise of bidentate urea absorbance, is seen in 30% SBOP and 30% castor oil as well. However, 30% crosslinker shows only minor change in bidentate urea concentration. As suggested by the free urea formation profile in Figure 4.14, there is little phase separation in 30% crosslinker foam. Among the three samples that did phase separate, a timing difference is noticed. For comparison purposes, Figure 4.16 re-plotted the bidentate urea absorbance as a function of isocyanate conversion.

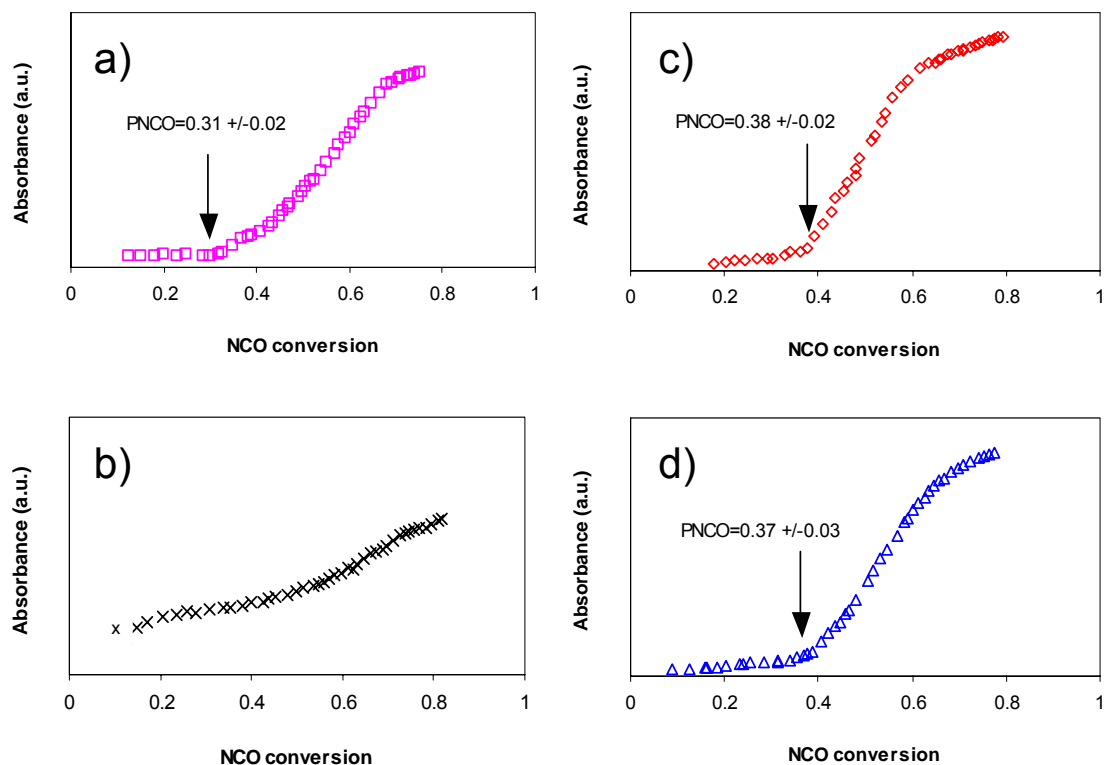


Figure 4.16: Bidentate urea absorbance change as a function of isocyanate conversion: (a) control, (b) 30% crosslinker, (c) 30% SBOP, and (d) 30% castor oil.

The onsets of phase separation, marked by a rapid rise in bidentate urea concentration, are labeled in Figure 4.16. In control, the phase separation occurs at approximately 30 % isocyanate conversion. When either SBOP or castor oil was substituted into foam formulations, the phase separation is delayed by 15 seconds to nearly 40% isocyanate conversion.

Phase separation varied significantly as different substituent polyols were used. In the case of 30% crosslinker foam, the phase separation seems to be eliminated, whereas the two natural oil polyol foams delayed the phase separation. At the onset of phase separation in control, $t = 20$ seconds, all four

foams had nearly the same concentrations of free ureas, shown in Figure 4.14, and the concentration of free urethane is the lowest in control. Because phase separation is determined by the value of χ_N , thus the difference in the timing of phase separation could be an indication of lower miscibility between the hard segments with control soft segments than either SBOP or castor oil soft segments, and crosslinker soft segments are likely the most miscible with hard segments. For the crosslinker polyol, previous studies have suggested that it is the low molecular weight of this polyol makes it soluble among hard segments and hinders hydrogen bond formation and phase separation [63, 86, 111-113].

An addition issue was not touched upon is the cell opening in these foams as it is an important aspect in foam processing. Zhang and coworkers have proposed that cell opening is triggered by urea phase separation [142]. In both 30% SBOP and 30% castor oil foams, the delayed phase separation could have a significant implication on cell opening. Therefore, foams made with high content of natural oil polyols may require additional assistance in cell opening.

4.5 Conclusion

The small molecule alcohol reaction with phenyl isocyanate showed secondary hydroxyls is approximately two times less reactive than the primary hydroxyls. Among all secondary hydroxyls, 1-hepten 4-ol, which is structurally similar to castor oil, showed a higher reaction constant than 1-methoxy 2-propanol, which is structurally similar to SBOP.

Polyol reaction with TDI further extended the understanding of urethane formation during foaming. Among the polyols tested, Hyperlite[®] E-848 showed the highest reaction constant that is more than 10-time higher than either natural oil polyol. Furthermore, the reaction constant remains the same up to 80%

isocyanate conversion suggesting negligible change in reactivity for Hyperlite[®] E-848 reaction with substituted TDI. For the two natural polyols, not only the reaction constants were found to be much lower than Hyperlite[®] E-848, but a decrease in reaction constant was also observed at 45-50 mol% isocyanate conversion. The second reaction constants in both natural oil polyol reactions with TDI were attributed to reactions with substituted TDI.

Foaming kinetics study focusing on different species formations and morphology development showed that substituting base polyol with SBOP, castor oil, or crosslinker polyol did not change the free urea formation rate, however, the urethane formation as well as phase morphology development were significantly altered. Free urethane formation rate were seen to have slowed as a result of adding in slow-reacting polyols. When 30 wt% of base polyol was substituted with either SBOP or castor oil, the phase separation was delayed for 15 seconds or 10% addition isocyanate conversion. The delay in phase separation was attributed to the low molecular weight of the natural oil polyols, which requires a higher conversion to obtain sizeable SS. Nonetheless, the presence of phase separation as well as higher bidentate urea formation rates in natural oil polyol-containing samples suggest that the interaction parameter χ between HS and natural oil-polyol based SS is higher than between HS and petroleum SS. The absence of phase separation in 30% crosslinker foam was attributed to both its low molecular weight effect as well as its miscibility with the HS.

Chapter 5

Effects of Molecular Weight and Molecular Weight Distribution

Contents

5.1	Chapter Overview	129
5.2	Introduction	129
5.2.1	Theoretical Models	130
5.3	Experimental	134
5.3.1	Materials	134
5.3.2	Synthesis	135
5.3.3	Characterization	144
5.4	Results and Discussion	147
5.4.1	The Effect of Molecular Weight	147
5.4.2	The Effect of Molecular Weight Distribution	165
5.5	Conclusion	173

5.1 Chapter overview

In Chapter 2, castor oil and SBOP were used as the sole polyol component in flexible foam formulations. Instead of the intended flexible foams, semi-flexible and rigid foams were obtained. We attributed the loss of flexibility in either sample to its unusually high glass transition temperature (T_g) and hypothesized that the polyol molecular weight played an essential role in determining the T_g . In this chapter, we expanded on our previous hypothesis by investigating the effect of polyol molecular weight on foam thermal and mechanical properties. A series of natural oil-based polyols with increasing molecular weight were synthesized and evaluated to assess the hypothesis. A relationship between the polyol structure and PU T_g was developed based on experimental results. The focus of latter parts of this chapter was shifted onto the effect of molecular weight distributions on PU properties, as natural oil polyols have a higher polydispersity index (PDI) than their petroleum counterparts. Understanding the effect of molecular weight distribution will allow effective use of natural oil polyols in formulations.

5.2 Introduction

Polyurethane (PU) flexible foam, as alluded to in early chapters, is a family of crosslinked polymers. The gelling reaction of di-functional isocyanates with multi-functional polyols creates covalent crosslinks in a PU network, while the blowing reaction of isocyanate with water produces polyurea segments that can associate through hydrogen bonding to form physical crosslinks. A block of PU flexible foam is, in fact, one single molecule with infinitely high molecular weight. Properties of a crosslinked polymer, such as PU, are dependent upon its degree of crosslinking and hard segment concentration [82].

In Chapter 2, foams synthesized from castor oil and SBOP were semi-flexible and rigid samples leading to the conclusion that neither polyol is an appropriate candidate as the sole polyol component for flexible foam synthesis. The unusually high T_g 's measured from both samples provided the explanation for the observed rigidity in these foams. In SBOP foam, the measured T_g is 45 °C above room temperature making it a glassy polymer at 25 °C. The high T_g of PU foam is hardly unique to natural oil polyol samples. The foam synthesized from a 1000 g/mol polypropylene oxide-based polyol, Softcel[®] U-1000, also showed a T_g of 3 °C, which is close to the T_g of castor oil foam, as detailed in Chapter 2. Compared to the Hyperlite[®] E-848 foam, which was synthesized from a 6700-molecular-weight polypropylene oxide-based polyol, and have a T_g of – 60 °C, the polyol molecular weight is seemingly a key factor that influences the T_g of a foam, and more importantly, a critical parameter needs to be fine-tuned for designing natural oil polyols suited as the sole polyol component in flexible foam synthesis.

5.2.1 Theoretical Models

The presence of crosslinks in a polymer is believed to restrict segmental mobility of the polymer network and thus cause an increase in T_g . Fox et. al. examined a series of crosslinked polymers and suggested that there is a linear dependency of T_g and crosslinking density, as shown in Equation 5.1 [81, 143].

$$T_g(n) = T_g(\infty) + \frac{K}{M} \quad (5.1)$$

where $T_g(n)$ and $T_g(\infty)$ are the glass transition temperatures of crosslinked and un-crosslinked polymers, respectively. K is a constant and M is the average molecular weight per crosslink. Literature data obtained on rubber vulcanizates and vinyl-divinyl copolymers systems with low crosslinking density agreed well with the model proposed by Fox, however, deviation from the linearity was observed in systems with higher crosslinking densities [144, 145]. In these cases, DiBenedetto's equation was shown to be a more accurate model, Equation 5.2 [146].

$$T_g(n) = T_g(\infty) \left[\frac{\frac{\varepsilon_o - c_o}{\varepsilon_\infty - c_\infty} x + 1}{1 - (1 - \frac{c_o}{c_\infty})x} \right] \quad (5.2)$$

where ε and c are the lattice energy and segmental mobility, respectively, x is the crosslinking density, defined as the fraction of all segments that are crosslinked and is associated with crosslinking density of the network ($x < 1$), and the subscript ∞ and o are indicative of un-crosslinked and fully crosslinked polymers. Stutz et. al. further explored the DiBenedetto model by taking into account the effect of losing chain ends to crosslinks and proposed Equation 5.3 [147].

$$T_g(n) = T_g(\infty) \left(\frac{K_1 x}{1 - x} + 1 \right) \quad (5.3)$$

where K_1 is a constant, associated with lattice energy in DiBenedetto's model. Another model developed based on the work of Gibbs and DiMarzio was proposed by Hale et. al., which takes into account for non-Gaussian distribution

in polymer chain configurations [148]. This model for a fully cured system can be rewritten as Equation 5.4.

$$T_g(n) = T_g(\infty) \left(\frac{K_2 x}{1 - K_2 x} + 1 \right) \quad (5.4)$$

where K_2 is a fitting parameter dependent upon the polymer system used, and x is a measure of the crosslinking density and $x < 1$.

Because crosslinking systems can be formed by different types of reactions, Shefer et. al. examined the different models for predicting T_g and concluded that for networks formed by the copolymerization of di- and multifunctional monomers, such as in PU flexible foams studied here, both Hale and Stutz models produced good agreements between theoretical predictions and experimental results [149]. Later, Bicerano and coworkers surveyed a series of crosslinked polymers and proposed an equation based upon previous study findings to describe the relationship between the number of repeating units between crosslinks and network T_g , shown in Equation 5.5 [150]. This equation is the model used in this chapter to better understand the relationship between natural oil polyols and their T_g 's.

$$T_g(n) = T_g(\infty) \left(1 + \frac{\alpha}{n} \right) \quad (5.5)$$

where α is an empirical fitting parameter, and n is the number of monomer units between crosslinks. In systems that compositional differences need to be

accounted for, authors further proposed that the α term in Equation 5.5 can be replaced by c/N_{tot} term, where N_{tot} is the number of free rotating bonds in a monomer unit, a composition dependent term, and c is an empirical fitting parameter.

As indicated by all models, an increase in the number of repeating units between crosslinks, or a decrease in crosslinking density, lowers the T_g of a network. Therefore, increasing the distance between hydroxyls offers a potential route to lower the T_g of PU synthesized from natural oil polyols. To examine the effect of crosslinking density on T_g , a series of model polyols with varying distance between the hydroxyls were synthesized through esterification reaction of ricinoleic acid following procedures described by Petrovic et. al. [151]. Ricinoleic acid is a hydroxyl-bearing fatty acid found in castor oil. The T_g 's of resultant collapsed foams were measured thereof.

Another issue we focused our attention on is the molecular weight distribution effect on foam properties. The reason that the molecular weight distribution effect becomes of interest is because the synthesis scheme of esterification yields polyols with wide molecular weight distributions. The measured PDIs of the experimental polyols synthesized for this study are 1.3 or higher. Putting the values in perspective, commercially available petroleum polyols generally have PDIs of 1.05 or lower, as measured in our GPC experiments. More importantly, to obtain high molecular weight ($MW > 2000$ g/mol) natural oil polyols economically, a wide distribution of molecular weight ($PDI > 2$) and a wide distribution of the number of covalent bonds between polyol hydroxyls will likely accompany. As aforementioned molecular weight of polyol plays a critical role in determining polymer properties, a high PDI value in natural oil polyol will inevitably have an effect on foam properties. Understand how PDI may alter the properties of a PU foam can aid in natural oil polyol selection during

the formulation step. For this study, we purposely mixed two different molecular weight natural oil polyols to alter the PDIs. PU samples synthesized from these polyols mixtures were evaluated using DMA, DSC, and X-ray scattering techniques.

5.3 Experimental

5.3.1 Material

Medical grade castor oil purchased from Walgreen was used as the source for monomers. Trimethylol propane (TMP), used as the initiator for polyols, was purchased from Sigma-Aldrich. Methanol, ACS reagent, was purchased from Fisher Scientific (Pittsburg, PA). Potassium methoxide (CH_3OK), purity 95-99%, was purchased from Alfa Aesar (Ward Hill, PA). Diethyl ether, ACS reagent, was purchased from Sigma-Aldrich and was used as received. Fascat[®] 4350, a proprietary butyltin compound used as transesterification catalyst, was obtained from Arkema Inc. (Philadelphia, PA).

A commercially available Arcol[®] F-3022 (Bayer Corporation) was obtained from Bayer and used as a comparison basis to the natural oil-based polyols. Arcol[®] F-3022 is a glycerol-initiated, polypropylene oxide-based tri-functional polyol. Arcol[®] F-3022 has a molecular weight (M_n) of 3000 g/mol and a functionality (f_n) of 3. TDI used is an 80:20 mixture of 2, 4 and 2, 6 isomers (Grade A Mondur[®] T-80, Bayer Corporation). Gelling and blowing catalysts used were DABCO BL-11 and DABCO 33-LV and were both obtained from Air Products and Chemicals (Allentown, PA). Details on the catalysts can be found in Chapter 2. Distilled water was reacted with TDI to form polyureas within the PU network.

5.3.2 Synthesis

Model Polyol Synthesis

Model polyol synthesis was carried out at Cargill research labs in Wayzata, MN by Wei Zhang and was observed and recorded here by the author. Monomer units of methyl ricinoleate were first obtained by transesterification reaction of castor oil with methanol. A total of 500 grams of raw materials, 30:1 molar ratio of methanol to castor oil, was charged into a 1000ml round-bottom boiling flask and the large amount of excess methanol was used to ensure the completion of transesterification reaction. CH_3OK in the amount of 1 wt% of castor oil, ~ 2.45 gram, was added to the flask as the catalyst. The reaction was carried out under refluxing conditions for 3 hours with temperature controlled at 65-70 °C. After the flask was cooled to room temperature, water was charged into the reactor to remove the catalyst, CH_3OK . The wash was repeated several times as the water layer was discarded each time and the pH value of the mixture finally reached 7. The residual water was then removed via a rotary evaporator operated at room temperature.

The captured methyl esters were purified by fractional distillation to obtain only the ricinoleic acid methyl esters (RME) for further synthesis steps. The methyl ester mixture was heated to 230 °C and a one-atmospheric vacuum was applied to the distillation column. Because castor oil is comprised of different types of fatty acid esters, the methyl ester mixture obtained above contained approximately 3% saturated fatty acid methyl esters, such as palmitic and stearic acids esters, 90% ricinoleic acid methyl esters, and 7% unsaturated fatty acid esters, such as oleic and linolenic acid ester [52, 152, 153]. Due to the differences in boiling temperature between the functional (ricinoleic acid) and the non-functional (the rest) methyl esters, where the ricinoleic acid methyl ester has a higher boiling temperature than the rest, the distillates were divided into three

fractions [154, 155]. The first fraction, approximately 15-wt% of the total methyl esters, was comprised largely of non-functional methyl esters and some methyl ricinoleate, and was collected and discarded. We controlled the first fraction of distillates to be 15 wt% of the total methyl esters for it ensures the second fraction, approximately 65-70 wt% of the total methyl esters, contains only the desired ricinoleic acid methyl ester. Based on literature data, 97 wt% or higher of the second fraction is comprised of ricinoleic acid methyl ester [156]. And the second fraction of the distillates was collected and kept for further uses. The remaining mixture, approximately 15-20 wt%, of the methyl esters was discarded as it contained undesired oligomers and some remaining methyl ricinoleate.

The poly-condensation reaction was carried out in a 1000ml round-bottom boiling flask equipped with a fractional distillation column. Approximately 150 grams of the ricinoleic acid methyl ester obtained previously was first charged into the flask and then a specified amount of TMP, as shown in Table 5.1, and approximately 0.75 grams of catalyst, Fascat[®] 4350 were added to the reactor. The amount of TMP used was calculated based upon the targeted molecular weights of 1000, 2000, 3000, 4000 and 5000 g/mol, and the amount of catalyst used was 0.5 wt% of the total reaction mixture. Table 5.1 details the reactants used and the properties of the polyols synthesized. The reaction mixture was heated to 220 °C with continuous stirring under atmospheric pressure. Methanol formed was collected via distillation column and was used as an indication for reaction conversions. For all polyols, the polycondensation reaction was allowed to take place at 220 °C under one atmospheric pressure for one hour followed by applying a vacuum slowly to remove methanol byproduct and promote polyol formation. The reaction time under vacuum were 1 hour for the 1K and 2K polyols and up to 3 hours for the 5K polyol [151, 157]. The final vacuum reading on the reactor was approximately 2-3 mmHg. The model polyols synthesized

were titrated using ASTM standard test D4274 method A (testing method details see next section) to determine their hydroxyl numbers and both gel permeation chromatography (GPC) and vapor pressure osmometry (VPO) experiments (see next section) were run to determine the molecular weights. The GPC traces of polyols are shown in Figure 5.2. There are notable differences between f_n measured experimentally and the theoretical value of “3”. The reason that the measured f_n is lower than expected can be attributed to dehydration, especially in the case of 2K and 3K samples, where polyols have a similar molecular weight to the theoretical value but lower f_n . The rest of the polyols, besides dehydration, may also contain small amounts of mono-functional alcohols produced by polycondensation reaction between methyl ricinoleate. This is because not only the f_n is lower than expected, the molecular weights are also lower in these samples.

Table 5.1 A: Reactant details and polyol properties.

Sample	1K	2K	3K	4K	5K
Molar ratio RME/TMP	3.1	6.7	10	14	17
Theoretical M_n (g/mol)^a	1002	2010	2934	4054	4894
OH number (mg KOH/g)	144.6	66.9	41.2	34.1	23.0
M_n by GPC (g/mol) (f_n)^b	1512 (3.90)	2322 (2.77)	2978 (2.19)	3400 (2.07)	4395 (1.80)
M_n by VPO (g/mol) (f_n)^b	1090 (2.81)	2046 (2.44)	2967 (2.18)	3565 (2.17)	--
Polyol T_g (°C), $T_g(\infty)$	-67.8	-70.8	-72.2	-72.5	-74.5
ΔC_p (J/g/°C)	0.74	0.68	0.71	0.65	0.68

^a The value was calculated based on TMP-to-RME ratio in reactor.

^b The f_n of a polyol was calculated using both OH number and M_n measured.

Table 5.1 B: Properties of additional polyols: castor oil and Arcol[®] F3022.

Sample	Castor oil	Arcol[®] F3022
M_n (g/mol)	930	3000
f_n	2.7	3.0
Polyol T_g (°C), T_g(∞)	-64	-70
ΔC_p (J/g/°C)	0.88	0.74

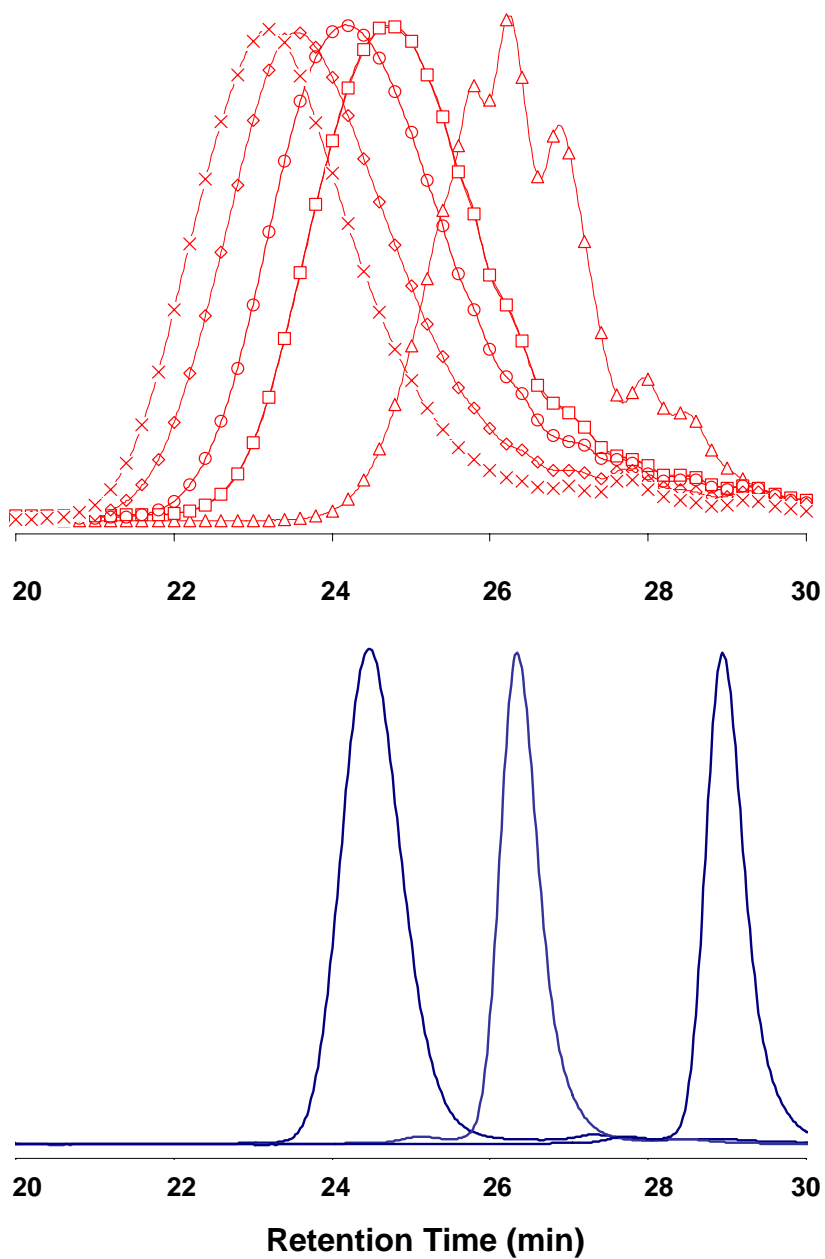


Figure 5.2: GPC trace of model polyols synthesized (top). From right to left in the top figure are: 1K (Δ), 2K (\square), 3K (\circ), 4K (\diamond), and 5K (\times). Bottom GPC traces are those of, from right to left: RME, castor oil and Arcol[®] F3022.

Collapsed Foam Sample Synthesis

Sample formulations are shown in Table 5.2 and 5.3. The formulations were based on 100 parts of total polyol and a total reactant weight of 20 grams. Hard segment content in each sample was within the range of 28.1-28.8 wt%. All ingredients, except TDI, were weighted into a 50mL polypropylene beaker and hand mixed with a metal spatula for 1 minute in a 55 °C silicone oil bath. The pre-measured TDI was then added into the beaker and mixed by hand continuously and vigorously to rupture gas bubbles formed. The mixing was continued for an additional minute or up to 7 minutes until the mixture became viscous and the rate of bubble formation had slowed. The viscous mixture was then transferred to a rectangular mold (80 x 20 x 2mm) sandwiched between two Teflon sheets backed by steel plates. The mold assembly was placed in a two-platen hydraulic press (Carver, Auto Series, Model 3895) and held under 700 lbf (~ 15 psi) at 70 °C for 2 hours. Sample was then placed in a curing oven at room temperature cured for an additional 48-hours before further testing.

Table 5.2: Collapsed foam formulations for single-polyol systems.

	2K	3K	4K	Castor oil	Arcol[®] F3022
1K	--	--	--	--	--
2K	100	--	--	--	--
3K	--	100	--	--	--
4K	--	--	100	--	--
Castor oil	--	--	--	100	--
Arcol [®] F3022	--	--	--	--	100
Water	3.5	4.0	4.15	1.84	3.75
TDI (g, index =100)	5.98	6.04	6.07	5.94	6.05
Dabco [®] BL-11	0.06	0.06	0.06	0.06	0.06
Dabco [®] 33-LV	0.08	0.08	0.08	0.08	0.08
T _g (n) by DSC	-52.33	-65.77	-69.11	9.24	-57.22
ΔC_p (J/g/°C)	0.30	0.32	0.27	0.47	0.46

Table 5.3: Collapsed foam formulations for molecular weight distribution study.

	1K	2K-4K	Castor oil- 5K
1K	100	--	--
2K	--	50	--
3K	--	--	--
4K	--	50	--
5K	--	--	50
Castor oil	--	--	50
Arcol [®] F3022	--	--	--
Water	2.2	3.5	4.0
TDI (g, index =100)	5.99	5.98	6.04
Dabco [®] BL-11	0.06	0.06	0.06
Dabco [®] 33-LV	0.08	0.08	0.08

5.3.2 Characterization

Polyol characterization

Hydroxyl Determination was carried out at Cargill research labs in Wayzata, MN by Wei Zhang and was observed and documented here by the author. The hydroxyl determination followed ASTM standard test D4274, Method A. Acetic anhydride, purity > 99.5 %, was purchased from Sigma-Aldrich and diluted with pyridine, purity of 99.8% anhydrous, purchased from Sigma-Aldrich. The concentration of the acetic anhydride solution was 1.02 mol/L. Hydrochloric acid, ACS reagent, was purchased from Sigma-Aldrich and dissolved in pyridine to make a solution of 0.5 mol/L concentration. Phenolphthalein indicator solution

was prepared by dissolving 1 gram of phenolphthalein in 100 mL of pyridine. Sodium hydroxide, ACS reagent, was purchased from Sigma-Aldrich and prepared to a solution by dissolving sodium hydroxide in pyridine. The final solution of sodium hydroxide had a concentration of 0.5 mol/L.

A sample of approximately 200 mg of polyol was taken from the reactor and reacted with 1mL of the pre-prepared acetic anhydride solution. The residual anhydride was reacted by adding 2 mL of the hydrochloric acid solution to the sample. Titration of the entire solution was performed by first adding 1 mL of the pre-prepared phenolphthalein indicator solution and titrating immediately with the pre-prepared sodium hydroxide solution. The hydroxyl number was then determined using Equation 5.6. A blank solution was also titrated using the same method aforementioned.

$$\text{HydroxylNumber} = \frac{(B - A)N \times 56.1}{W} \quad (5.6)$$

where A and B are the amounts of NaOH required for titration of the sample and the blank, L, respectively. N is the molar concentration of NaOH solution, mol/L, and W is the total weight of polyol measured, g.

Gel Permeation Chromatography (GPC) was performed onsite at the University of Minnesota, Minneapolis, MN. All model polyols as well as RME, castor oil, and Arcol[®] F3022 were tested. Approximately 2-3 mg of a polyol was dissolved in 3 mL of tetrahydrofuran (THF), ACS reagent, purchased from Sigma-Aldrich. The polyol molecular weight and PDI were measured via a Waters 590 GPC (Milford, MA, USA) equipped with three phenomenex Phenogel[™] columns that contains 5- μ m sized beads. An internal refractive

index detector (Waters 410) was used to measure the polyol molecular weights and PDIs. Five commercial polyols were used as the standards, and they were Arcol[®] 31-28, Arcol[®] LHT-42, Arcol[®] LG-56, Arcol[®] LHT-112, Arcol[®] LHT-240, and Arcol[®] LG-650 with respective molecular weights of 6000, 4100, 2950, 1500, 700, 260 g/mol, as provided by the manufacturer.

Vapor Pressure Osmometry (VPO) measurements were performed at Pittsburg State University at Pittsburg, KS on 1K through 4K polyols using a vapor pressure osmometer (Osmomat 070, UIC Inc., Joliet, IL, USA). Approximately 10-50 mg of a model polyol was dissolved in 10 mL of anhydrous toluene, ACS reagent purchased from Sigma-Aldrich. For each polyol, four samples were prepared with varying polyol concentrations. The sample solutions were allowed to stabilize overnight before measurements were taken.

VPO experiments were performed at 60 °C and the equilibration time was set at 3 minutes. Two syringes filled with blank toluene solvent and four syringes filled with the prepared polyol solutions were loaded into osmometer. All syringes were then warmed up to 60 °C before experiments were started. All measurements were taken after 3 minutes of equilibration time.

For molecular weight determination, standard solutions of Benzil were prepared in anhydrous toluene with concentrations of: 20, 40, 64 and 88 g/L. The standards were allowed to stabilize overnight before any measurements. A calibration curve was generated by running the standards with two blank toluene samples in the osmometer following the procedures described above.

Dynamic Mechanical Analysis (DMA)

DMA experiments were performed on the collapsed foam samples. A rectangular piece of sample (10 x 50 x 2 mm) was cut from the collapsed foam.

Torsion test attachments were used to fix either end of the rectangular sample to the rheometer and testing parameters and conditions can be found in Chapter 2.3.3.

Differential Scanning Calorimetry (DSC)

Same procedures were used as in Chapter 2.3.3.

Small-Angle X-ray Scattering (SAXS)

Same procedures were used as in Chapter 2.3.3.

Fourier Transform Infrared Spectroscopy (FTIR)

Same procedures were used as in Chapter 2.3.3.

Tensile Tests

Tensile experiments were carried out on sample cutouts (10 x 7 x 2 mm). For each sample, three test specimens were measured. The tensile test apparatus used was a Minimat miniature mechanical testing device (Model MMT-2000, Rheometric Scientific, Piscataway, NJ, USA). Cyanoacrylate adhesive (KrazyGlue[®], Elmer's Products, Inc., Columbus, OH) was used to attach either end of the sample to the grips. The extension rate was set as 5 mm/min and the stress-strain curve was recorded.

5.4 Results and Discussion

5.4.1 The Effect of Molecular Weight

Model Polyols

The purpose of this study is to establish a relationship between the crosslinking density of a natural oil-based PU and its T_g . Such relationship will aid polyol selections and shed light on whether natural oil polyols could be

potentially used as the sole polyol component in flexible foam synthesis. Based on studies of crosslinked polymers, altering crosslinking density, or equivalently the number of covalent bonds between crosslinks, offers control over the network T_g [81, 147, 158, 159]. For this work, our main objective is to lower the T_g of a natural oil polyol-based PU. Therefore, to achieve this objective, we increased the number of covalent bonds between crosslinks in the PU and examined its effect on the T_g 's of resultant PU.

The model polyols synthesized have different number of covalent bonds between hydroxyls and based upon the measured molecular weight and functionality, the calculated number of covalent bonds between two hydroxyls are detailed in Table 5.4. There are some differences in molecular weights measured using GPC or VPO, and thus disagreements on the calculated number of covalent bonds between hydroxyls are seen in the table. Between the two sets of measurements, the VPO data was believed to be more accurate than the GPC data. This is because GPC measurements rely on hydrodynamic volume of a molecule to determine its molecular weight and using petroleum polyols as standards to estimate natural oil polyol molecular weights could lead to inaccuracy due to solubility differences. Furthermore, polyols are branched polymers, making GPC measurements even less reliable. VPO measurements, on the other hand, are associated with the number concentration of a solute making the measurements less ambiguous. Additionally, the f_n calculated from GPC results for the 1K model polyol is 3.90 greater than the theoretical value of 3.0 (Table 5.1), reassures the decision to consider only the VPO data. Due to a low functionality of 1.8, the 5K model polyol was not included in parts of this study as the PU produced is a un-crosslinked polymer. The 1K polyol, although has a functionality greater than 2, its multi-modal molecular weight distribution, seen in Figure 5.2, makes the results ambiguous. Castor oil was, therefore,

included in the molecular weight effect study as a replacement to the 1K model polyol.

Table 5.4: The number of covalent bonds (n , in Equation 5.5) between two neighboring hydroxyls.

	n, by theoretical M_n^a	n based on GPC M_n^b	Crosslinked Fraction (%)^c	n based on VPO M_n^b	Crosslinked Fraction (%)^c
Castor oil	27	--	90	--	90
1K	30	46	129.9	32	93.6
2K	65	73	92.3	64	81.3
3K	97	95	72.9	94	72.6
4K	135	109	68.9	114	72.2

^a Calculated from TMP:RME ratio by assuming $f_n = 3.0$.

^b Calculated by assuming the crosslinked fraction of a polyol is comprised of ricinoleic acid repeating unit.

^c The ratio of measured functionality (Table 5.1) over theoretical functionality of 3, which estimates the fraction of polyol that is in a crosslinked network.

Differential Scanning Calorimetry (DSC)

Equation 5.5 suggests that the T_g of a crosslinked polymer is related to the T_g of its un-crosslinked form. Therefore, DSC results on both un-crosslinked polyols and crosslinked PU collapsed foams are shown in Figure 5.3 and 5.4. Included also in the figures are the DSC curves of Arcol[®] F3022 polyol and its resultant PU collapsed foam. Arcol[®] F3022 is a petroleum polyol and was used as a comparison basis for this study.

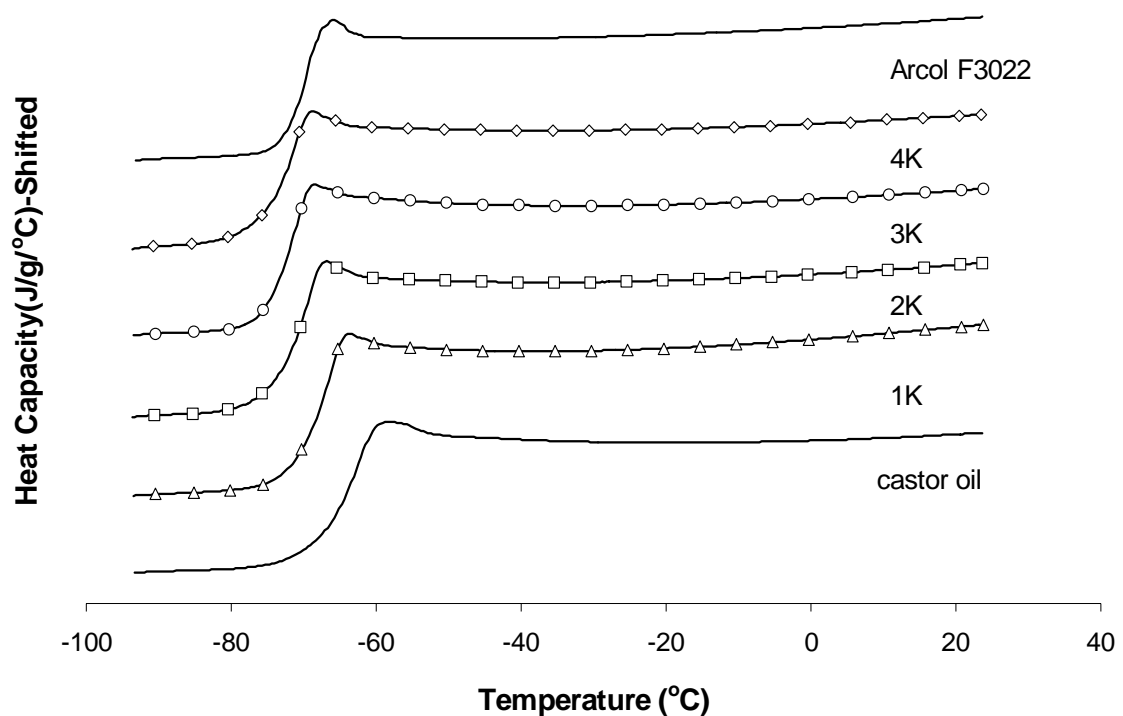


Figure 5.3: DSC curves of model polyols. From bottom up: castor oil (solid line), 1K (Δ), 2K (\square), 3K (\circ), 4K (\diamond), and Arcol[®] F3022 (solid line). The curves were shifted vertically to avoid overlapping.

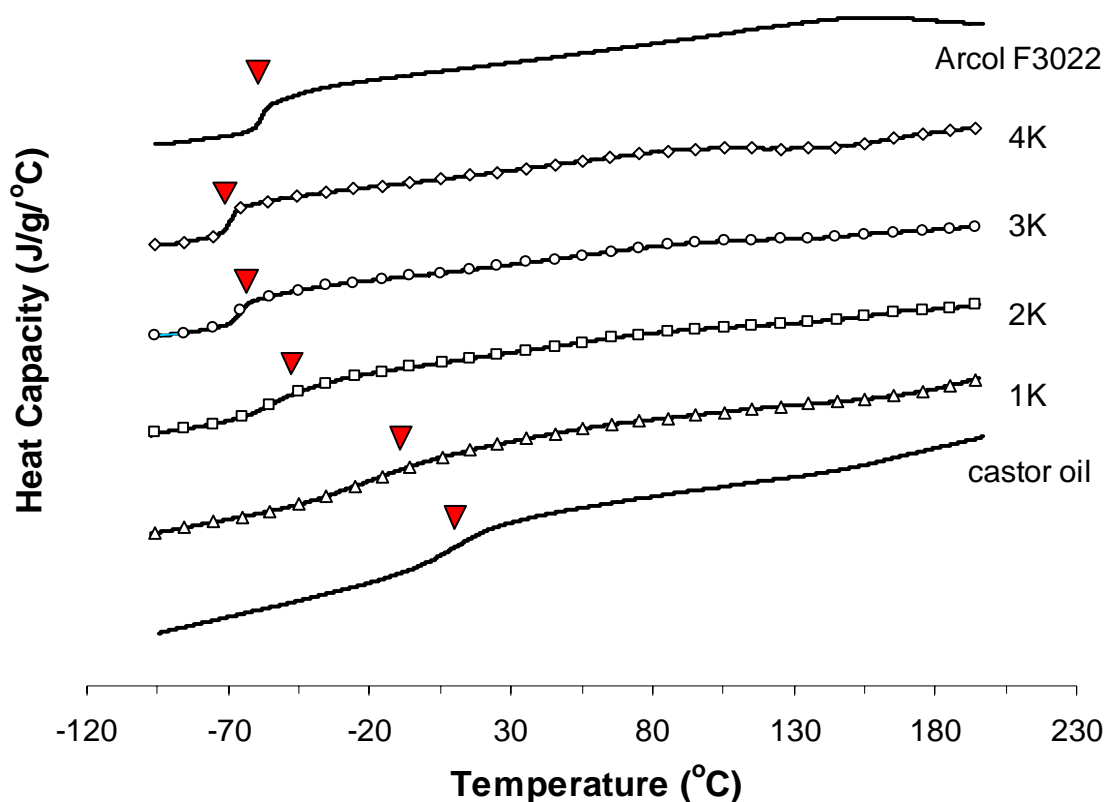


Figure 5.4: DSC curves of collapsed foams. From bottom up: castor oil (solid line), 1K (Δ), 2K (\square), 3K (\circ), 4K (\diamond), and Arcol[®] F3022 (solid line). The DSC curves were shifted vertically to avoid overlapping. The inverted triangles are indicative of the T_g 's.

The T_g 's of the un-crosslinked polyols, although are seen to be inversely related to the molecular weight, do not vary significantly, see Table 5.1. Castor oil, among all polyols, has the highest T_g of -64 °C followed by 1K with T_g of -67 °C, 2K with T_g of -71 °C, and the rest of the polyols share a T_g of -72 °C. The T_g of collapsed foam, on the other hand, varies substantially. Low molecular weight polyol PU, such as castor oil, shows a high T_g of 9 °C; while high molecular weight polyol PU, such as 4K, has a low T_g of -69 °C. An inverse

relationship between the polyol molecular weight and the T_g of PU is evident. To verify whether Equation 5.5 adequately describe a natural oil polyol PU system, the term, $T_g(n)/T_g(\infty)-1$, was plotted against $1/n$. $T_g(n)$, $T_g(\infty)$ and n data were taken from Table 5.1, Figure 5.4 and Table 5.4, respectively. From the mathematical expression, a linear plot with an intercept at (0,0) is expected. Figure 5.5 shows the T_g data points used to generate the plot and the quality of a line fit that was forced through the origin of coordinates. The 1K model polyol was not plotted in this graph as briefly discussed earlier that its wide distribution in molecular weight makes the data ambiguous and will be discussed in the later parts of this chapter.

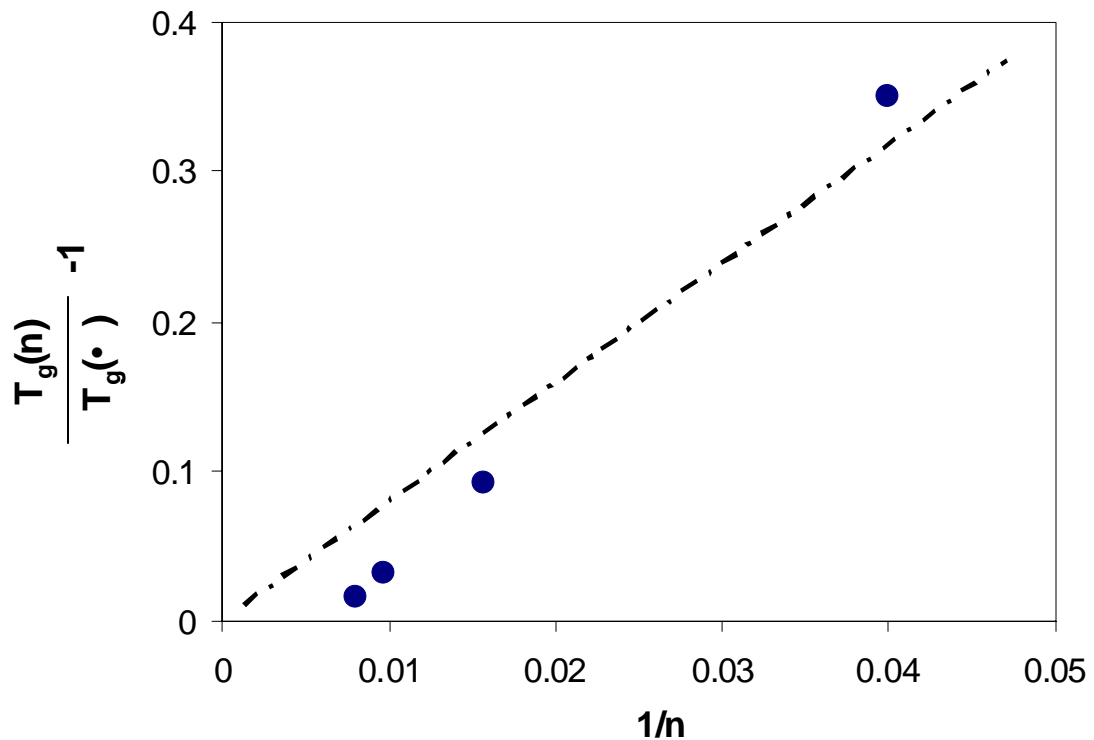


Figure 5.5: A line fit to the T_g data of castor oil, 2K, 3K, and 4K samples forced through the origin of coordinates.

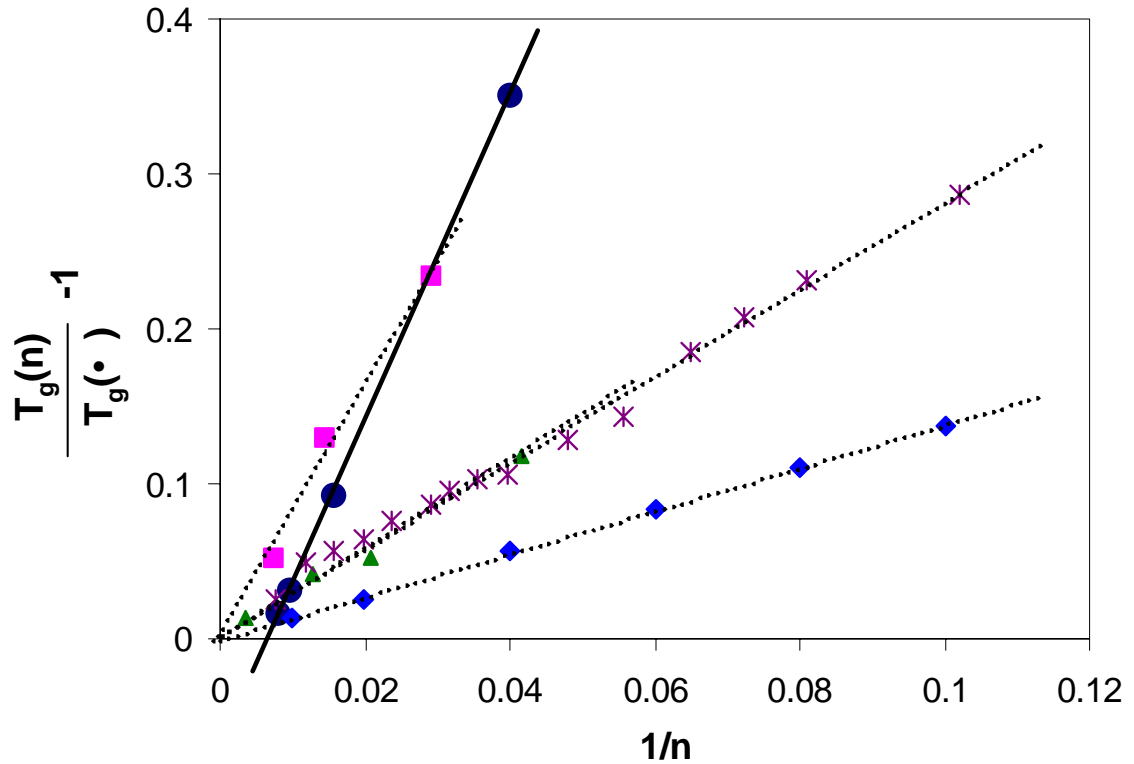


Figure 5.6: Plots of T_g values for different crosslinked polymers, showing the validity of Equation 5.1. These crosslinked polymers are: polyethylmethacrylate (\blacklozenge), polystyrene divinylbenzene ($*$) [147, 150], polymethylmethacrylate (\blacktriangle) [160], polyurethane (\blacksquare) [150], and natural oil polyol-based polyurethane (\bullet) (this work).

Figure 5.5 shows that by forcing a line fit through the origin of coordinates, the fit is a low quality description of the data. To substantiate Equation 5.5, the T_g data of a number of different crosslinked polymers were plotted in Figure 5.6, along with the model polyol PU data. All crosslinked polymer systems, other than the model polyol PUs, show a good agreement between the theoretical model and the experimental results.

The reason that model polyol results deviate from Equation 5.5 can be associated to the structural characteristics of these natural oil polyols. Compared to the crosslinked polymers listed above, natural oil polyols are crosslinked in the midpoints of the polymer chains leaving a 6-carbon chain ends free of covalent bonds. Zlanatic and coworkers studied PU elastomers based on a triolein polyol with and without its dangling chains, and found a 6.5-°C difference in the T_g 's of PUs [161]. Based on the experimental data on the model polyol systems used in this work, we believe that these dangling chains on natural oil polyols are acting as a plasticizer to lower the T_g . Mathematically, this hypothesis can be expressed as Equation 5.6, where the T_{adj} is added to the Bicerano model to account for the plasticizing effect of dangling chains.

$$T_g(n) = T_g(\infty)\left(1 + \frac{\alpha}{n}\right) - T_{adj} \quad (5.6)$$

Fitting the modified equation, Equation 5.6, to the experimental data, a better fit is found in Figure 5.6 and the T_{adj} term was determined to be approximately 13.8 °C. Compared to the 6.5 °C difference in the triolein-based PUs, the plasticizer effect observed in the model polyol system is more pronounced. There are two possible reasons. The first reason is that the T_g 's of un-crosslinked triolein polyols with and without dangling chains are unknown. Therefore, the 6.5 °C observed by Zlanatic is not equivalent to the term, T_{adj} . In addition, the systems studied by Zlanatic et. al. are elastomers based on methylene di-phenyl diisocyanate (MDI) making them less comparable to the flexible foam systems studied here. The second reason that the plasticizer effect is more pronounced in the model system could be due to the un-functionalized

fraction of polyols. The measured functionalities of model polyols are lower than the theoretical value of “3”, Table 5.1, suggesting a small fraction of the polyol chains do not bear hydroxyls. The un-functionalized polyol chains can act as plasticizer more effectively, thus has led to the observation of a 13.8 °C T_{adj} term.

One may question the necessity of a T_{adj} term here for data fitting and recommend the model of Bicerano, Equation 5.5. As the values of $T_g(\infty)$ are somewhat ambiguous, we used both n and $T_g(n)$ terms obtained in this study and allowed the value of $T_g(\infty)$ to vary. To obtain a linear fit in the form of Equation 5.5, the $T_g(\infty)$ term was determined to be -89.5 °C, which is nearly 20 °C lower than the $T_g(\infty)$ measured. Based on our knowledge of polyols, it is unlikely to obtain a polyol with such low T_g , thus we believe the term T_{adj} is necessary to describe the experimental results.

Between the crosslinked polymers listed in Figure 5.6, the slope of the line fit also varies, which indicates flexibility difference between the polymer chains, as mentioned earlier. The T_g data of PU flexible foam systems based on Voranol polyols not only fits the model Equation 5.5, but also has a slope that is 22% lower than the model polyol PUs. Voranol polyols are petroleum-derived polyols, comprised of polypropylene oxide. Potentially, a difference in free volume between the two types of polymer chains, propylene oxide (Voranol) and hydrocarbon (model polyol), has caused the observed difference in the line fit slope.

The model polyols are at a disadvantage in terms of polymer chain flexibility. For every one-degree decrease in the PU T_g , 28% more number of covalent bonds between crosslinks is required in the model polyol system than in a Voranol polyol. However, the plasticizing effect found as a result of dangling

chains lowers the T_g systematically by 13.8 °C giving model polyols some advantage in controlling T_g .

Dynamic Mechanical Analysis (DMA)

Aside from lowering T_g , mechanical properties of PU is another significant aspect in determining whether natural oil polyols can be used as the sole polyol component in flexible foam. All collapsed foam samples were tested in DMA experiments and the results are shown in Figure 5.7 and 5.8.

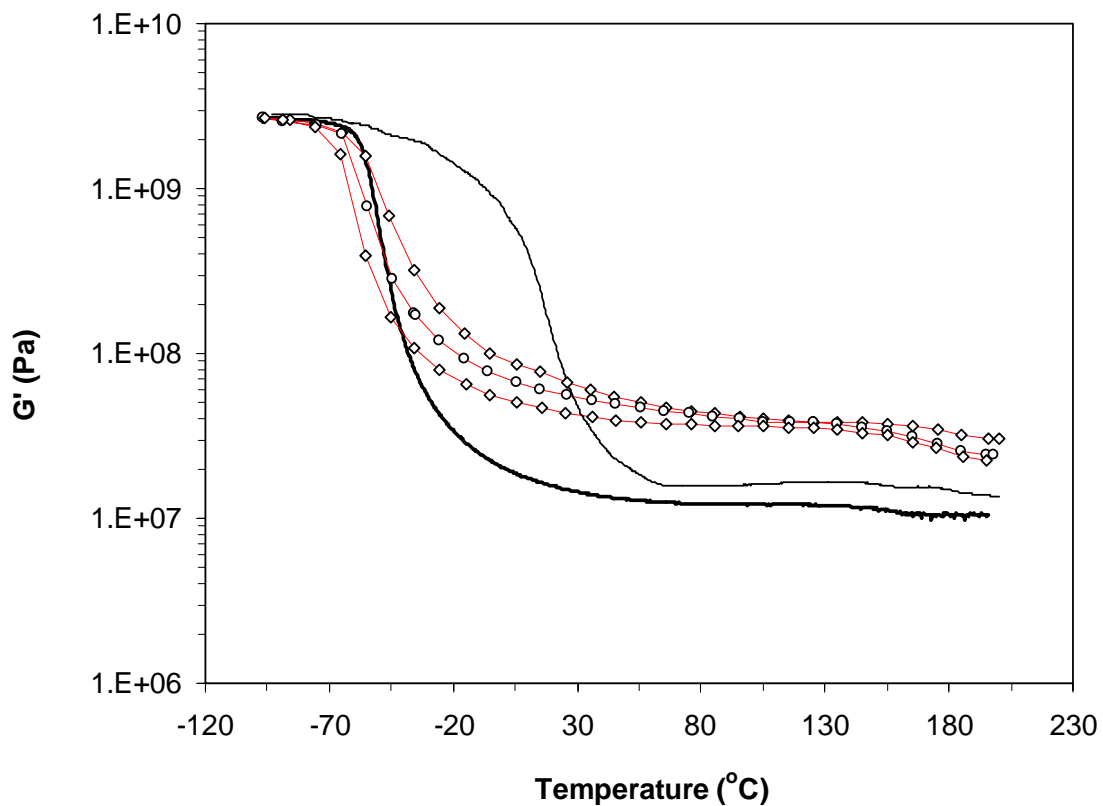


Figure 5.7: DMA curves of collapsed foam samples. From top down: Castor oil (solid line), 2K (\square), 3K (\circ), 4K (\diamond), and Arcol[®] F3022 (solid line).

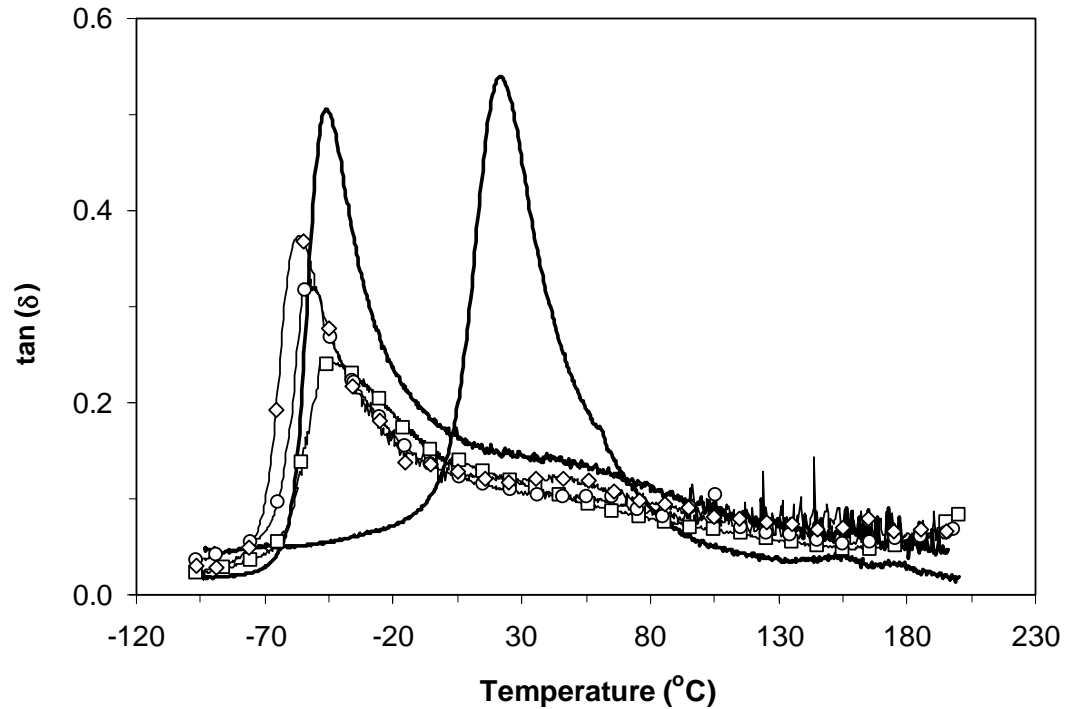


Figure 5.8: $\tan(\delta)$ curves of collapsed foam samples: 4K (\diamond), 3K (\circ), Arcol[®] F3022 (solid line), 2K (\square), and castor oil (solid line, peaked at 30 °C)

The G' data on collapsed foams are similar to the G' data on foamed samples, seen in Chapter 2, where the polymers are glassy at low temperatures and rubbery at high temperatures. The difference between a collapsed foam and a foamed sample is that the absolute G' values are higher in collapsed foam due to an increase in density [162]. To put this into perspective, Figure 5.9 shows the DMA results on both castor oil foam and castor oil collapsed foam. The shifted G' values nearly overlap each other in the bottom figure of 5.9.

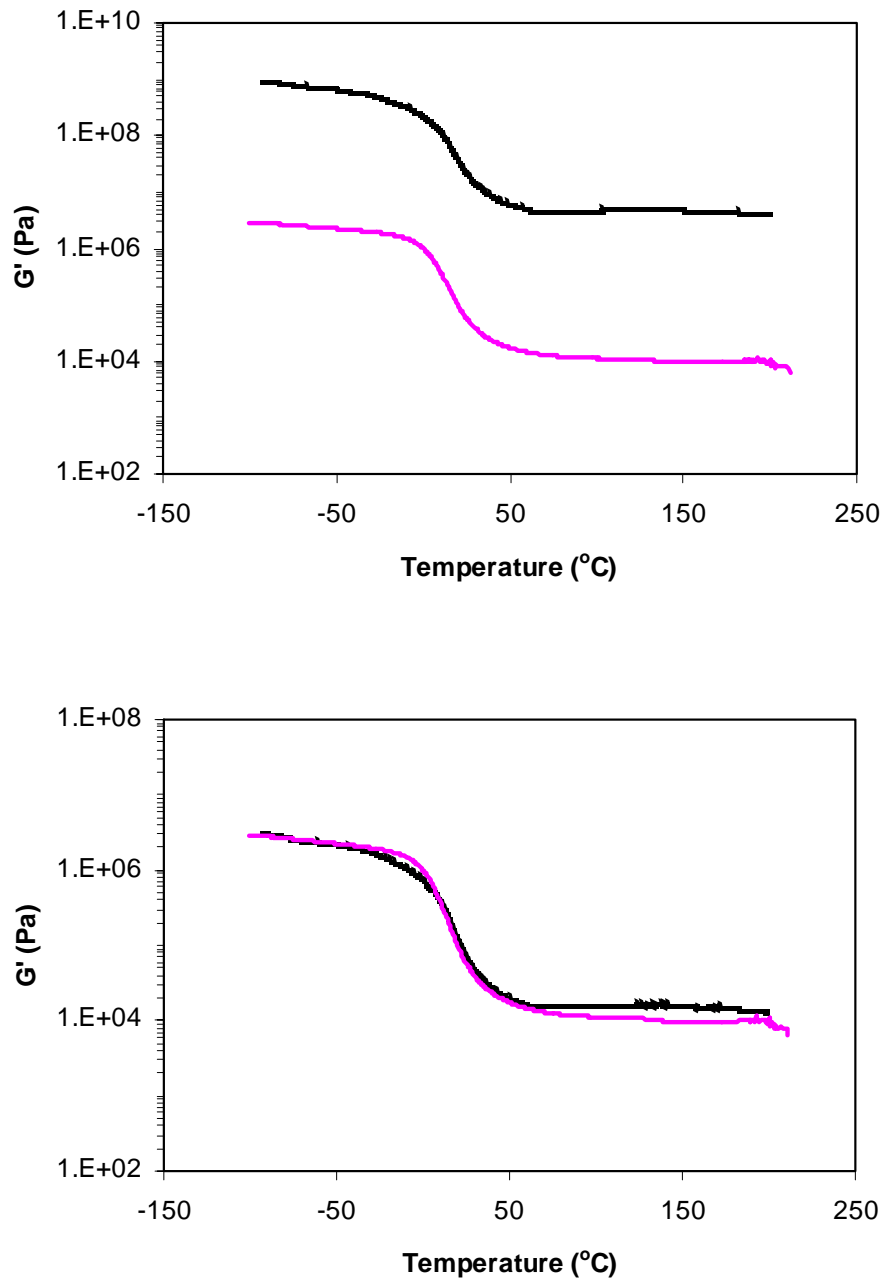


Figure 5.9: DMA curves of both collapsed foam and foamed sample based on castor oil. The top figure shows the un-shifted data while the bottom figure shows the matching between the G' values after shifting the data vertically.

The DMA results on samples differ in two areas. First, the temperature, at which the transition from glassy state to rubber state, T_g , decreased with increasing model polyol molecular weight. Three model polyols, 2K, 3k and 4K, even show lower T_g 's than the Arcol[®] F3022 sample, which was made from a 3000 g/mol petroleum polyol. Castor oil having the lowest molecular weight and thus the lowest number of covalent bonds between crosslinks shows the highest T_g of 23 °C, which was taken as the peak position of $\tan(\delta)$ curve, Figure 5.8. The T_g results seen here in DMA tests are consistent with the results seen in DSC experiments, and suggest an increasing number of covalent bonds between crosslinks has a negative effect on the T_g . Both the 2K model polyol sample and the Arcol[®] F3022 sample share nearly the same T_g making model polyols with higher number of covalent bonds between hydroxyls promising candidates for flexible foams. The second difference among the samples is the plateau modulus. Arcol[®] F3022 foam shows the lowest plateau G' values, followed by castor oil foam. The three model polyol-based foams shared similar plateau modulus and are higher than either Arcol[®] F3022 or castor oil. As discussed in Chapter 2, plateau modulus is largely determined by the properties of the hard domains, such as hard domain volume fraction and/or segmental length of the polyureas that comprises the hard domains, and may to a lesser extent influenced by the crosslinking density of the soft domains [83, 83, 86]. Between castor oil and Arcol[®] F3022 samples, the segmental length of polyureas is shorter in castor oil making the volume of each hard domain in castor oil small. The higher plateau modulus in castor oil than Arcol[®] F3022 can hardly be explained by smaller hard domains leading us to consider the effects of crosslinking molecular weight in these two samples (27 and 103 in castor oil and Arcol[®] F3022, respectively). Interestingly enough, the number of covalent bonds between crosslinks in the three model polyols spreads over the value found in Arcol[®] F3022, ranging from 64 to 114, and yet the modulus observed in these

samples are at least two times that of the Arcol[®] F3022 (at $T = 100$ °C). Evidently, neither the crosslinking density nor the hard domain packing alone can adequately explain the results. It is rather the combination of both hard domain properties as well as crosslinking density in the soft domains that influenced the plateau modulus. In the following sections, we will turn the attention to molecular level details, using both X-ray scattering and FTIR techniques, to further explore the source of property differences.

Small Angle X-ray Scattering (SAXS)

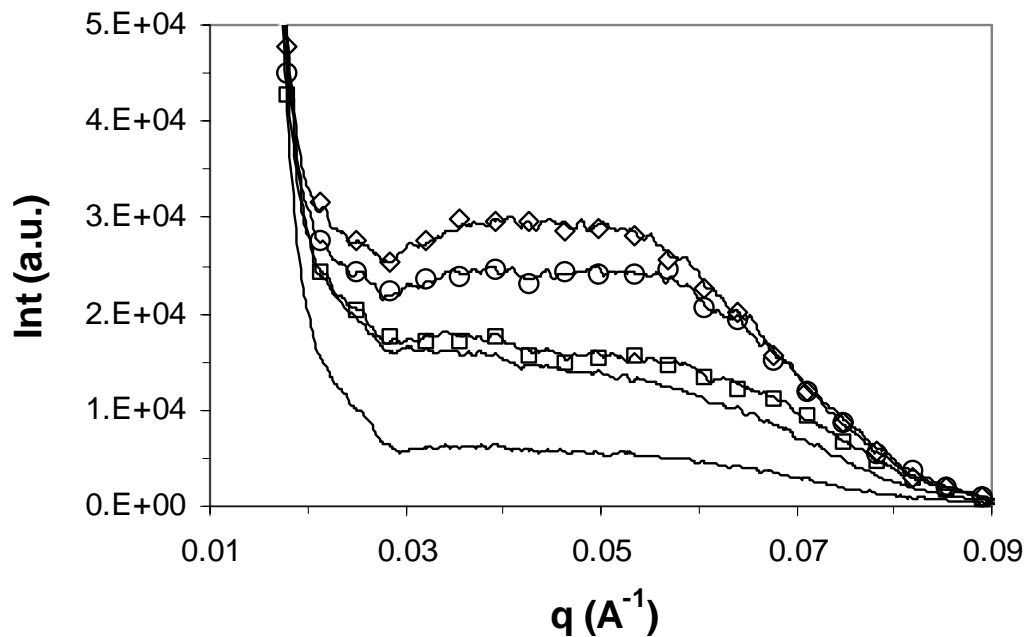


Figure 5.10: Scattering profiles for collapsed foams. From bottom up: castor oil (solid line), Arcol[®] F3022 (solid line), 2K (\square), 3K (\circ), and 4K (\diamond).

Figure 5.10 shows the scattering profiles of samples. Castor oil collapsed foam shows a low scattering profile, as have been reported in Chapter 2 on a

foamed castor oil sample as well. Arcol[®] F3022, although has a more pronounced scattering peak than the castor oil sample, shows comparably low scattering intensity than the model polyol samples. Among 2K, 3K and 4K sample, the scattering intensity increases with increasing polyol molecular weight. Because all samples were formulated to contain the same amount of hard segments, the change in scattering intensity must be associated with the electron density distribution or the degree of phase separation. It could be that the model polyols have produced more phase-separated samples than Arcol[®] F3022 polyol, since all model polyol samples show higher scattering intensity than the Arcol[®] F3022 sample.

The scattering intensity change might provide an explanation to the differences in plateau modulus. For a better phase-separated sample, a higher volume fraction of hard domain is expected, therefore, the higher plateau modulus in 2K through 4K samples could be attributed to an increase in the volume fraction of hard domains compared to Arcol[®] F3022. The high plateau modulus in castor oil, however, cannot be explained by hard domain properties, as the sample barely shows any scattering patterns. For castor oil, it could be the crosslinking density that gives rise to the high plateau modulus.

Fourier Transform Infrared Spectroscopy – Attenuated Total Reflectance (FTIR-ATR)

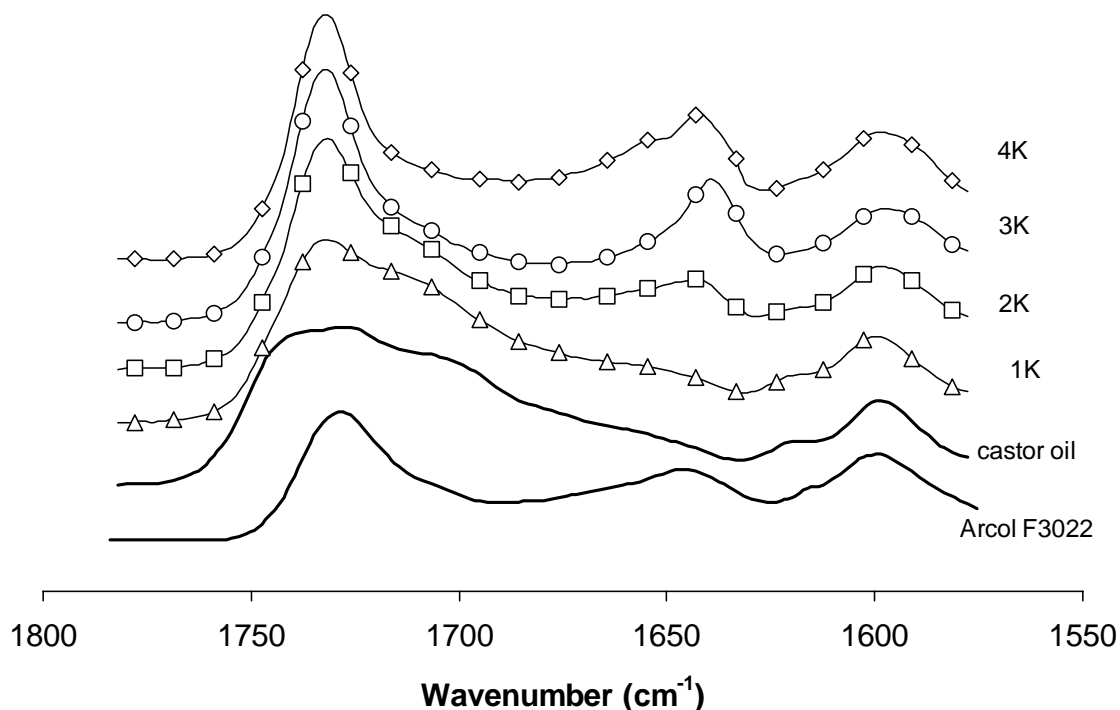


Figure 5.11: FTIR-ATR results on collapsed foam samples. From bottom up: Arcol[®] F3022 (solid line), castor oil (solid line), 1K (Δ), 2K (\square), 3K (\circ), and 4K (\diamond).

In Figure 5.11, the FTIR-ATR results are plotted and the molecular-level differences among samples are further investigated. The absorbance band assignments can be found in Chapter 2, Table 2.3. Castor oil sample in Figure 5.11 shows very little amount of hydrogen-bonded ureas (from 1680 to 1640 cm⁻¹), whereas Arcol[®] F3022 sample shows a small peak at 1640 cm⁻¹ indicating the presence of bidentate ureas. For the model polyol PUs, the bidentate urea peak at 1640 cm⁻¹ continues to increase as molecular weight of the polyol increases

and suggests a bidentate urea concentration increase as a function of polyol used. Considering both the X-ray results in the previous section and FTIR data, the volume fraction of hard domains is higher in the model polyol samples than in Arcol[®] F3022 and increases with increasing model polyol molecular weight. Between the 3K and 4K samples, not only that the peak of bidentate urea increases with increasing polyol molecular weight but also a rise in the intensity of monodentate urea ($1670\text{-}1650\text{ cm}^{-1}$) is observed, which are associated with loosely packed hard domains [28]. The high plateau modulus observed in DMA for the model polyol PUs, Figure 5.7, is, therefore, a result of increased volume fraction of hard domains.

Tensile Properties

Tensile tests on collapsed foam samples were performed to examine their elongation/tensile properties. Figure 5.12 shows the test results. Among all collapsed foam samples, the extrapolated tensile moduli are close in values for 2K, 3K, 4K, and castor oil samples, whereas Arcol[®] F3022 has the lowest tensile modulus. This result is consistent with the observations made in DMA tests, where at room temperature Arcol[®] F3022 has the lowest G' modulus. Detailed tensile/elongation properties are tabulated in Table 5.5, which averages the results of three specimens per sample.

Table 5.5: Tensile/elongation properties of collapsed foams.

Sample	Tensile Modulus (MPa) ^a	Stress at break (MPa) ^b	Elongation at break (%) ^c
Arcol [®] F3022	9.8	4.16 ± 0.3	52 ± 6
Castor oil	17.0	6.79 ± 0.7	93 ± 5
2K	16.7	5.8 ± 1.2	59.2 ± 10
3K	15.8	6.2 ± 0.8	69.2 ± 7
4K	15.5	4.8 ± 1.5	40.2 ± 4

^a Tensile modulus values reported is the average value of three samples.

^b Stress at break shows the average value of the three samples and the variation term is reflective of the largest deviation from the average.

^c Data taken is the average of three samples and the variation term is reflective of the largest deviation from the average.

Castor oil sample is unique for it shows the longest extension at break as well as a strain hardening at approximately 80% strain. This strain hardening behavior is not seen in any other samples, which likely broke before the strain-hardening state was reached. The extrapolated tensile modulus of 4K collapsed foam is found to be nearly 60% higher the tensile modulus of Arcol[®] F3022, which agrees, to some extent, with the G' data, where 4K sample has a G' value twice of the Arcol[®] F3022 sample. All model polyols and castor oil samples share similar tensile modulus and order of their tensile modulus is consistent with the order of their G' values found in DMA. Elongation properties vary substantially among the samples. Castor oil sample broke at the highest elongation with the highest stress at elongation, followed by 3K, and 4K has the lowest elongation and stress at break. There is not a clear trend in properties at

break, however, the relatively poor elongation in 4K could be attributed to its low functionality, which provides less crosslinks and thus poor performance in tensile tests.

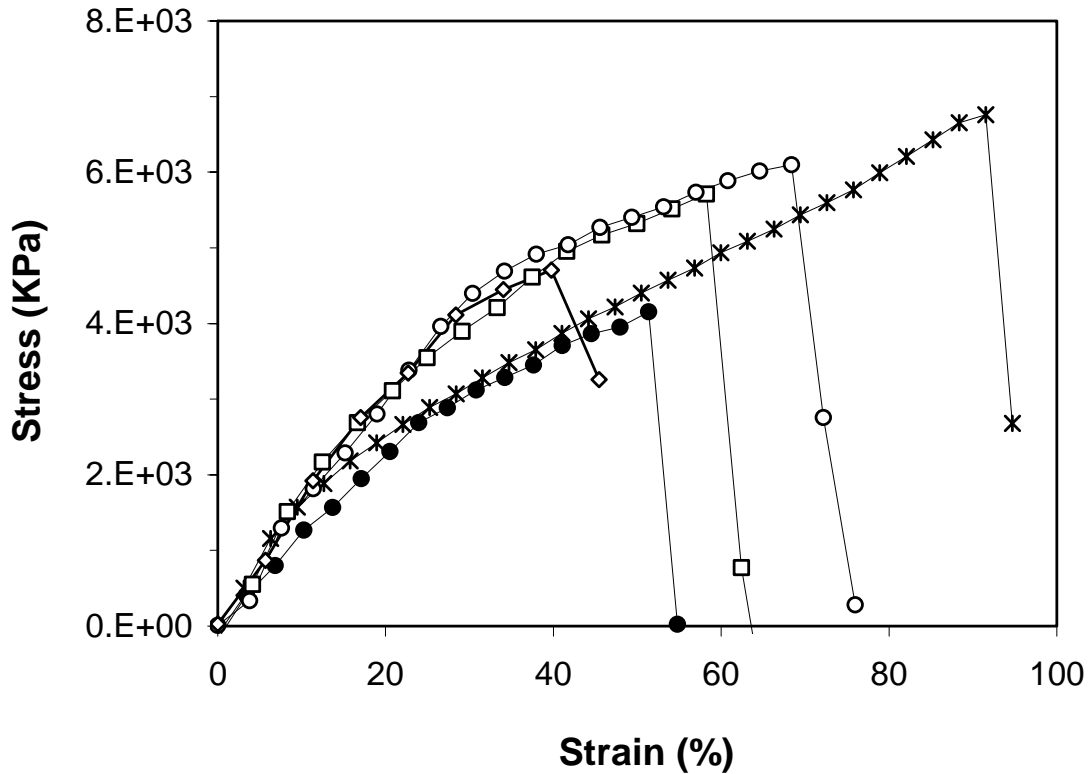


Figure 5.12: Stress-strain curves of collapsed foams measured at 25 °C: Arcol® F3022 (●), castor oil (*), 4K (◇), 3K (○), and 2K (□).

5.4.2 The Effect of Molecular Weight Distribution

The second focus of this study is the molecular weight distribution effect on PU samples. Two sets of samples were examined. The first set of PUs were synthesized from 1000-molecular weight polyols, castor oil and 1K-model polyol,

and the second set of PUs were synthesized from three 3000-average molecular weight polyols, (1) 3K model polyol, (2) 50/50 by weight of castor oil, 5K model polyol, and (2) 50/50 by weight 2K, 4K model polyols. From the GPC traces shown in Figure 5.2, 1K model polyol is comprised of different molecular weight species and has a PDI of 1.4. Compared to castor oil, which has a PDI of 1.03, there is a significant difference between the two polyols in their molecular weight distribution. The second set of PUs, the molecular weight distribution was broadened even further. From 3K to 2K-4K to castor oil-5K, the PDIs are 1.30, 1.40, and 2.18, respectively.

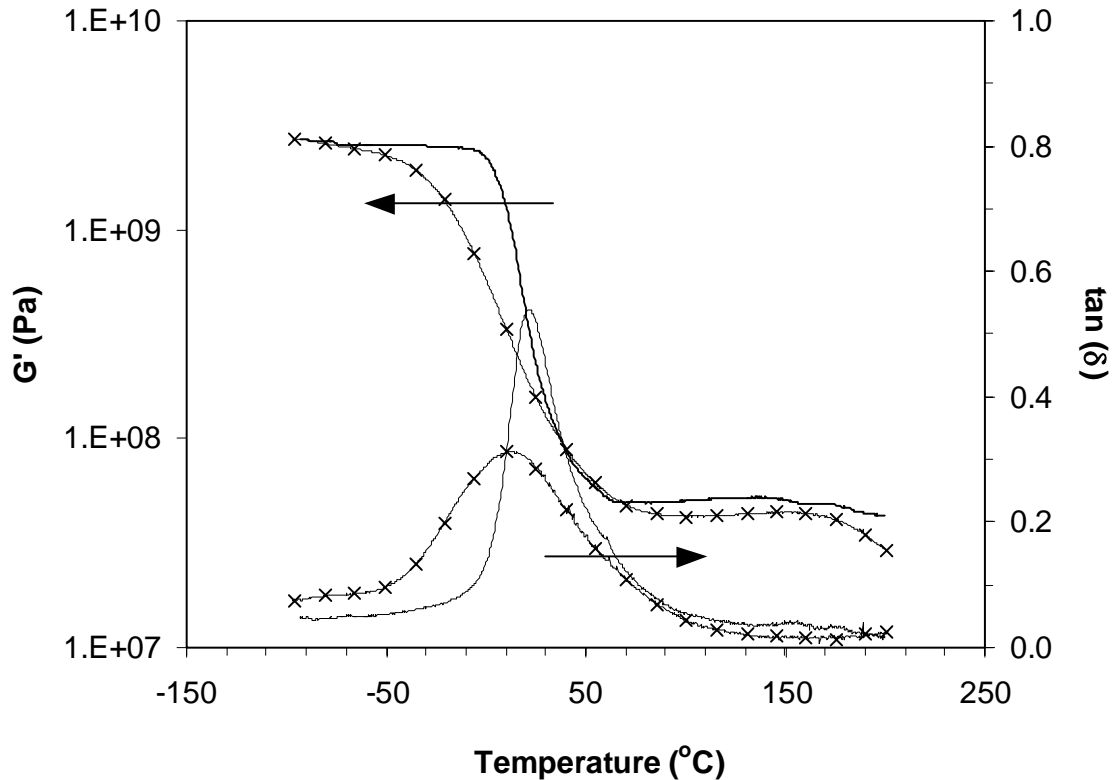
1K vs. Castor Oil

Figure 5.13: DMA curves of collapsed foams showing G' and $\tan(\delta)$ traces: castor oil (solid line), and 1K (x).

Figure 5.13 shows the DMA results of PUs synthesized from castor oil and 1K model polyol. The most visible differences between the two samples are the distribution and the peak position of the $\tan(\delta)$ curves. The low PDI polyol-derived PU, castor oil, has a sharp $\tan(\delta)$ peak with narrow distribution, whereas the high PDI polyol-derived sample, 1K, has a less pronounced $\tan(\delta)$ peak. The broadening in $\tan(\delta)$ peak in 1K is the result of a distribution in the number of covalent bonds between crosslinks. In the case of 1K polyol, it is comprised of polyols with different molecular weight, thus PU derived from 1K model polyol

has a distribution of the number of covalent bonds between crosslinks. As temperature increases, in Figure 5.13, different polyol segments become mobile at different temperatures resulting in broadening of the $\tan(\delta)$ peak and a slower decrease in G' values than castor oil sample over T_g . The $\tan(\delta)$ curves also differ in their peak positions, where 1K sample shows a $\tan(\delta)$ peak approximately 10-°C lower than the castor oil sample. Comparing the differences between the two polyols, a fraction of the 1K polyol has higher molecular weight than castor oil, Figure 5.2. The lower T_g in 1K is likely associated with the fraction of high molecular weight species, which has a higher number of covalent bonds between crosslinks, thus lowered the overall T_g .

The other noted difference between the two samples is the G' plateau modulus. Castor oil has a slightly higher plateau modulus than the 1K PU by approximately 15% of 1K plateau G' value. Although the difference is minor, it could indicate the effect of molecular weight distribution on plateau modulus, and foam hardness. This change in plateau modulus will be further examined in the next set of PUs.

Molecular Weight Distribution of Model Polyol Systems

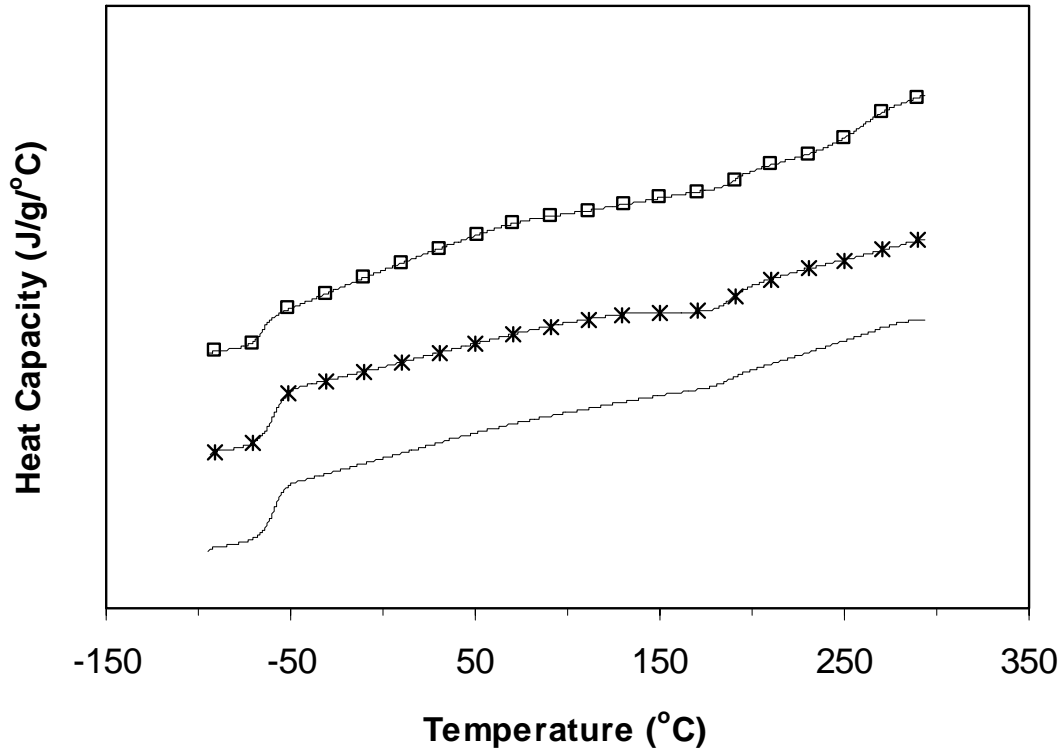


Figure 5.14: DSC curves of collapsed foams. From bottom up: 3K, 2K/4K (*), and castor oil/5K (\square). The curves were shifted vertically to avoid overlapping.

The DSC curves of the second set of PUs are shown in Figure 5.14. All three samples show similar T_g 's around -56°C . The presence of low molecular weight polyols, especially in the castor oil/5K sample, did not seem to increase the T_g of resultant PU, which is consistent with the results seen in 1K and castor oil PUs, where high molecular weight fraction of the polyol seems to have a greater impact on the T_g of sample. The heat capacity change (ΔC_p) at T_g , on the other hand, was altered as molecular weight distribution changed. In 3K PU, the ΔC_p at T_g is the most visible. As the molecular weight distribution increased, the ΔC_p decreased slightly in 2K/4K sample scaling to 95 % of the 3K ΔC_p . Recall in

Table 5.1, the ΔC_p values are close among the model polyols. As the molecular weight distribution broadened even further, as in castor oil/5K sample, the ΔC_p scaled to 50% of the 3K, showing a significant change in the fraction of polyol chains that are mobile at T_g .

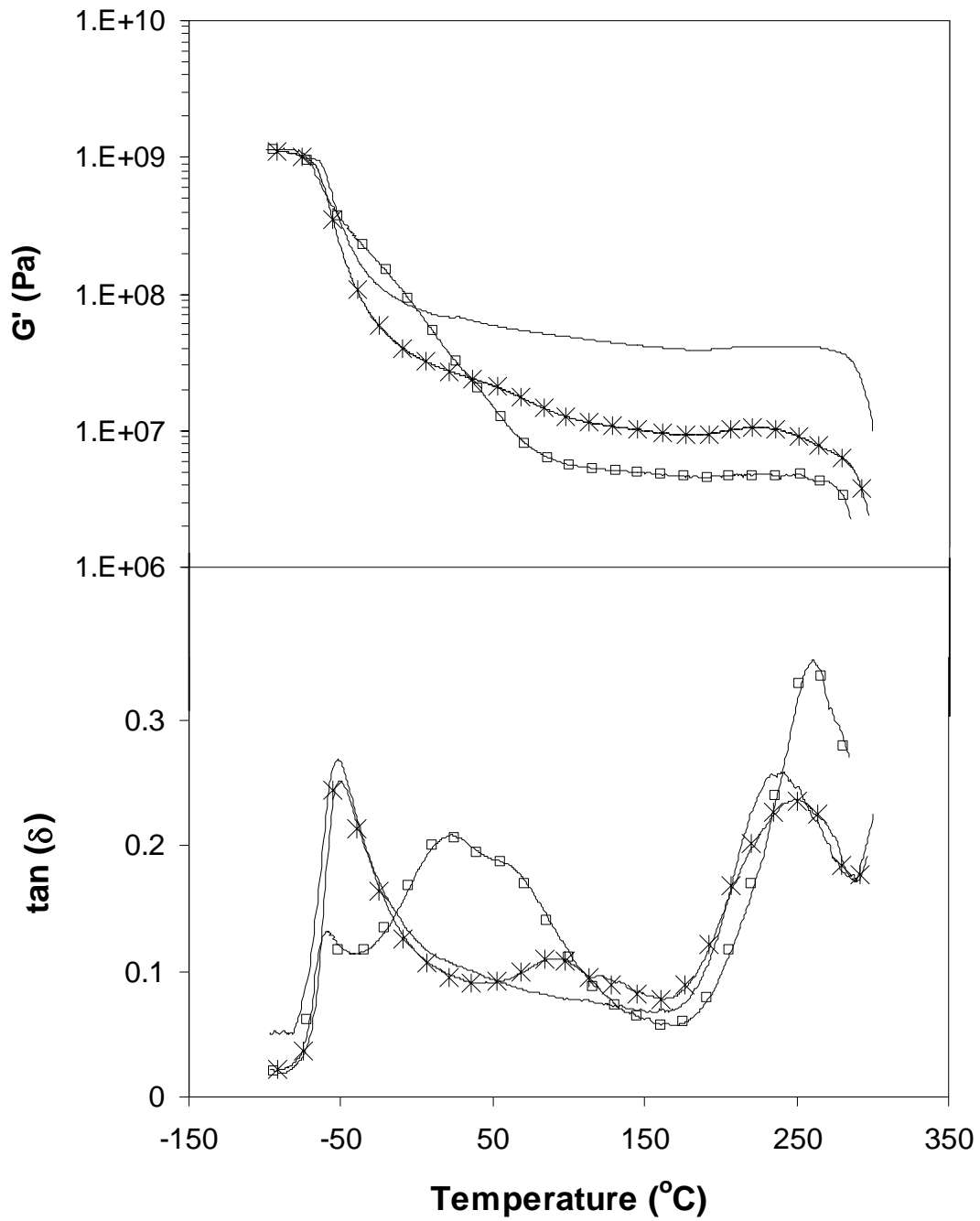


Figure 5.15: DMA and $\tan(\delta)$ curves of collapsed foams: 3K, 2K/4K (*), and castor oil/5K (\square).

The DMA results, in Figure 5.15, vary substantially among the three PU samples. The relative low PDI polyol-derived sample, 3K, shows a drop in the G' value at approximately $-55\text{ }^{\circ}\text{C}$ and quickly reaches a plateau at $T = 0\text{ }^{\circ}\text{C}$. As PDI of the polyol increased slightly from 1.30 in 3K polyol to 1.40 in 2K/4K (50/50 wt) polyol, the sample shows a similar drop in G' value at about $-55\text{ }^{\circ}\text{C}$ and the decay in G' value has a similar rate to that in 3K. However, two features in 2K/4K sample differentiate this sample from 3K PU. First, the sample does not reach its plateau region until a much higher temperature of $100\text{ }^{\circ}\text{C}$. Second, the G' plateau region modulus of 2K/4K sample is nearly one-fourth of the 3K PU. For the highest PDI polyol-derived sample, castor oil/5K, the G' curve shows a drop in value at slightly lower temperature of approximately $-57\text{ }^{\circ}\text{C}$ and decays at a visibly slower rate than the other two samples. The castor oil/5K sample reaches its plateau region at $T = 100\text{ }^{\circ}\text{C}$ and has the lowest plateau modulus of all samples, which is nearly one-tenth of the 3K sample. By broadening the molecular weight distribution, the G' decay rate is reduced and plateau region modulus is lowered, which is also seen in the previous set of PUs, 1K and castor oil.

Aside from the G' curves, $\tan(\delta)$ curves of the samples also show large variation. In the 3K PU, a single peak is observed indicating T_g of a 3K polyol-based soft domains. The 2K/4K sample, not only shows the T_g at approximately $-52\text{ }^{\circ}\text{C}$, which is the same as 3K, but also shows a second peak in its $\tan(\delta)$ curve with corresponding temperature of $80\text{ }^{\circ}\text{C}$. From Figure 5.8, a pure 2K model polyol based PU has a T_g of $-52\text{ }^{\circ}\text{C}$, significantly lower than the observed $80\text{ }^{\circ}\text{C}$. This high T_g phase, which is different from either 2K or 4K-rich soft domains or even hard domains, could be caused by the low molecular weight fraction of the polyols. As seen in Figure 5.2, the low molecular weight fraction of the polyol has a molecular weight below 600 g/mol , and soft domain resulted

from such could be the reason a second high temperature T_g , at 80 °C, is observed. Alternative phase mixing between the hard and soft segments may also raise the T_g . Similar observation is made in castor oil/5K sample, where a second even a third peak in $\tan(\delta)$ curve is seen. In Figure 5.8, castor oil-based PU has a T_g around 25 °C making the second peak in $\tan(\delta)$ curve in Figure 5.15 a possible indication of castor oil-rich soft domains. However, the third peak in $\tan(\delta)$ curve, which corresponds to a T_g of 65 °C, is unlikely the T_g of 5K or castor oil-based soft domains. Similar to the 2K/4K sample, the high T_g of 65 °C in castor oil/5K could be either phase mixing or low molecular weight polyol-based soft domains. However, if it were a low molecular weight polyol component effect that caused the high T_g , one would not expect changes in plateau modulus, which is an indication of loss in the volume fraction of hard domains. Therefore, the additional high T_g 's observed in both 2K/4K and castor oil/5K are potentially caused by phase mixing.

5.5 Conclusion

In this study, a series of model polyols with varying molecular weight were synthesized by polycondensation reaction using ricinoleic acid and trimethylolpropane. The goal is to investigate the effect of the number of covalent bonds between crosslinks on T_g of a PU. Thermal-mechanical study indicates that by increasing the number of covalent bonds between crosslinks, the T_g of a PU can be systematically lowered. However, the model polyol system differs from a petroleum polyol flexible foam system in two ways. First the polyol segments that participate in the formation of PU network were found to be "stiffer" than the petroleum polyol segments; second, the presence of dangling chains in natural oil polyol lower the T_g of a PU through plasticizing effect.

Molecular weight distribution effect was also studied using the model polyol systems. The results show that by increasing the PDI of a polyol, the sample modulus is lowered at high temperatures and was attributed to phase mixing between the soft and hard segments. The sample T_g was found to be determined largely by the high molecular weight fraction of the model polyols.

Chapter 6

Conclusion and Future Work

Contents

6.1	Conclusion	175
6.2	Future Work	178

6.1 Conclusion

In this work, we investigated natural oil polyols as a potential replacement to petroleum polyols and the goal of this work is to understand the potentials and the limitations of such polyols. In an early attempt, both an experimental polyol derived from soybean oil, SBOP, and a naturally occurring polyol, castor oil, were formulated as the sole polyol component in flexible foams. The samples produced were rigid and semi-flexible for SBOP and castor oil, respectively. Characterization results indicated that both SBOP and castor oil foams had phase mixed morphology and high T_g 's, which was believed to be the predominate factor giving rise to the rigidity in SBOP foam.

As neither SBOP nor castor oil is an appropriate candidate as sole polyol component in flexible foam, we took the approach of partially substitution. A series of flexible foams were synthesized by replacing part of a petroleum polyol with different substituent polyols including SBOP, copolymer-filled and crosslinker polyols. It was found that SBOP-containing foam has a high T_g second soft phase, which increased foam modulus giving rise to a high loadbearing sample. Characterization study found that by using SBOP a change in hard domain morphology also occurred, and the hard domains were smaller in size and broader in domain spacing distribution. The mechanism, through which the SBOP-containing foam achieved higher modulus, was shown to be different from either filler or crosslinker effect. A separate kinetic study was performed to examine the changes in foaming reactions as a petroleum polyol is substituted with natural oil polyols. The results showed that the use of substituent polyol, such as SBOP or castor oil, did not interfere with the reaction of water with isocyanate. However, the reaction of polyol with isocyanate was substantially altered. The initial rate of free urethane formation was increased in formulations containing natural oil polyols, and a second, lower, free urethane formation rate was observed. We attributed the increase in the initial free urethane formation rate to an increase in hydroxyl concentration and associated the second, lower, free urethane formation rate to the reaction of natural oil polyol with isocyanate. Morphology development comparison unveiled that the use of natural oil polyol delayed the onset of phase separation by approximately 15 seconds (~ 8% isocyanate conversion), which could result in delays in cell opening as thus leading to a higher content of closed cells. An important finding of the kinetics study is that although natural oil polyols are slow reacting, they are still involved in the formation of PU network.

Although partial substitution using natural oil polyols was proven successful, the amount of natural oil polyols can be added is limited. To increase the content of natural oil polyol in flexible foam formulations and ultimately achieving the goal of making flexible foam from entirely natural oil-based polyols, lowering the T_g of natural oil-based PU was determined to be the most important issue. We speculated in Chapter 2 that the reason high T_g 's were observed in castor oil and SBOP foams was the low number of covalent bonds between neighboring hydroxyls, which leads to high crosslinking density in these samples. Therefore, to lower T_g , we synthesized a series of natural oil-based model polyols with increasing number of covalent bonds between hydroxyls to examine its effect on T_g . Thermal-mechanical study on PU collapsed foams made from the model polyols showed that the sample T_g and the number of covalent bonds between crosslinks were inversely related. Compared to a number of crosslinked polymers, the model polyols was found to have a plasticizing effect and this effect was attributed to the presence of dangling chains. DMA experiments on model polyol systems as well as a 3000-molecular weight petroleum polyol sample suggested the plateau modulus was controlled mainly by the volume fraction of hard domains, and to a lesser extent by the crosslinking density. Molecular weight distribution in the model polyol systems was found to lower the plateau modulus through phase mixing, and the high molecular weight fraction of the polyol was found to control the T_g .

Through this work, natural oil polyols are shown to be potential replacements to petroleum polyols. In the case of low molecular weight natural oil polyols, such as SBOP, partial substitution is a viable route for implementing natural oil polyols into flexible foams. To increase the content of natural oil polyols in flexible foams, higher molecular weight polyols are required to achieve

desired T_g . Modulus tuning can be achieved by changing the molecular weight distribution of a natural oil polyol.

6.2 Future Work

Replacing petroleum feedstock with renewable resources in PU has benefits far beyond economic advantages and, over the last few years, has gained tremendous amount of attention from the industry [67, 68, 163, 164]. In this work, we explored the potentials and the limitations of natural oil polyols as either a substituent polyol or a sole polyol component in flexible foams. From the results, we concluded that by proper control of the polyol structural parameters flexible foam can be potentially synthesized using entirely natural oil polyols. Therefore, an immediate effort recommended to further this work is (1) optimization of additives, namely catalysts and surfactants. In addition, a number of other areas are also worthy of exploring: (2) compatibility/miscibility of polyols, (3) understanding the role of natural oil polyol in other PU applications, and (4) alternative synthesis route for natural oil polyols.

Additive optimization is of great importance for foaming natural oil polyols. As we demonstrated in Chapter 5, model polyols, 2K, 3K, and 4K, are potential candidates as sole polyol component in flexible foams, however, attempts made to foam either the 3K or the 4K model polyol were unsuccessful as cellular structure control proved challenging. Finding or developing the appropriate surfactants for natural oil polyol-based flexible foams can be a critical step towards commercial success of natural oil polyols. Catalyst optimization is another area needs attention. Since natural oil polyols are slower reacting than petroleum polyols, high loadings of gelling catalyst becomes inevitable. Both catalyst development and alternative polyol synthesis route could be considered to alter the gelling reaction rate.

The polyol compatibility/miscibility issue rose to attention as neither SBOP nor castor oil produced satisfactory flexible foams, and partial substitution approach requires a natural oil polyol be mixed with a petroleum polyol. In foams synthesized by partially replacing a petroleum base polyol with natural oil polyol, we found little evidence of incompatibility between SBOP and Hyperlite[®] E-848. However, the later kinetics study showed two distinct free urethane formation rates in both SBOP and castor oil-containing foams and led us to speculate potential polyol miscibility issues on the micro-scale level. A systematic study examining the miscibility between petroleum and natural oil polyols will shed light on this issue. Since polymer blend compatibility are determined by Gibbs free energy of mixing, the following equation applies:

$$\frac{\Delta G_m}{RT} = \phi_1 \phi_2 \chi + \frac{\phi_1}{N_1} \ln(\phi_1) + \frac{\phi_2}{N_2} \ln(\phi_2) \quad (6.1)$$

where ϕ and N are volume fraction and degree of polymerization of a polyol, χ is the polymer interaction parameter, ΔG_m is Gibbs free energy of mixing, T is the temperature, R is the gas constant and the subscripts are indicative of different polyols. For a natural oil polyol to be miscible with a petroleum polyol, the value of ΔG_m has to be less than "0". A number of parameters should be considered for studying the polyol miscibility. Molecular weight is the foremost parameter as it determines the value of N and influences the value of χ . Another parameter deserving the attention is the type of repeating unit that comprises the polyol. In the case of the model polyol system in Chapter 5, ricinoleic acid was used as the repeating unit, however, in most natural oils, ricinoleic acid is not present, oleic and linoleic acids are far more common. Natural oil made from either oleic or

linoleic acid repeating unit could be included for the study. Methods for examining miscibility could include FTIR and NMR, especially in mixtures containing close refractive indices polyols, where visual inspection will be insufficient.

The third area for future study is the use of natural oil polyols in applications other than flexible foams, such as rigid foams and elastomers. These areas are by no means new research frontiers, and there are a number of publications on natural oil polyol-based rigid foams and elastomers [47, 48, 56]. However, most of the studies have been focusing on thermal stability of natural oil polyol-derived PUs leaving the much desired information on thermal and mechanical properties largely un-examined [47-49, 56, 165, 166]. An in-depth study on thermal-mechanical properties of natural oil polyol-based rigid foams and elastomers is evidently needed.

The last area worthy exploring is alternative synthesis route for natural oil polyols. Among the five known methods, documented in Chapter 1, for deriving polyols from natural oils, only three are commercially viable. There is still room for alternative synthesis route. It would be desirable to selectively functionalize the terminal methyl groups of a triglyceride molecule and produce polyols with a higher number of covalent bonds between the crosslinks.

Appendix A

Polyol Structure Effect on PU

A.1 Introduction

Petroleum-based polyether polyols are synthesized from alkylene oxide monomers in the presence of active hydrogen-containing initiators. The most commonly used alkylene oxides are propylene oxide and ethylene oxide [1, 4]. The natural oil polyols appeared in recent years as potential replacements to petroleum polyols, are structurally different from the alkylene oxide polyols. One of the emerging questions is whether the hydrocarbon rich polyol chains found in natural oil polyols will result in PUs processing unique properties, different from petroleum polyol-based PUs.

To examine the effects of polyol structure on PUs, a series of tri-functional polyols with similar molecular weight but different repeating units were investigated.

A.2 Experimental

Materials

Three polyols were used in this study to examine the effects of polyol structures on PU. Two commercially available polyols, Jeffox[®] WL-440 (Huntsman Corporation., The Woodlands, TX) and Voranol[®] 270 (Dow Chemical Co., Midland, MI), were obtained from the manufacturers and used as received. A third polyol, which is an experimental polyol, was synthesized by Pittsburg State University (Pittsburg, KS), tri-nonoate glyceride polyol (TNG). Jeffox[®] WL-440, denoted as EO in this study, is a tri-functional polyol based on ethylene oxide only and the initiator used is glycerol. Voranol[®] 270, denoted as PO in this study, is a tri-functional polyol based on propylene oxide only and the initiator used is glycerol. Structures of the polyols are shown in Figure A-1.

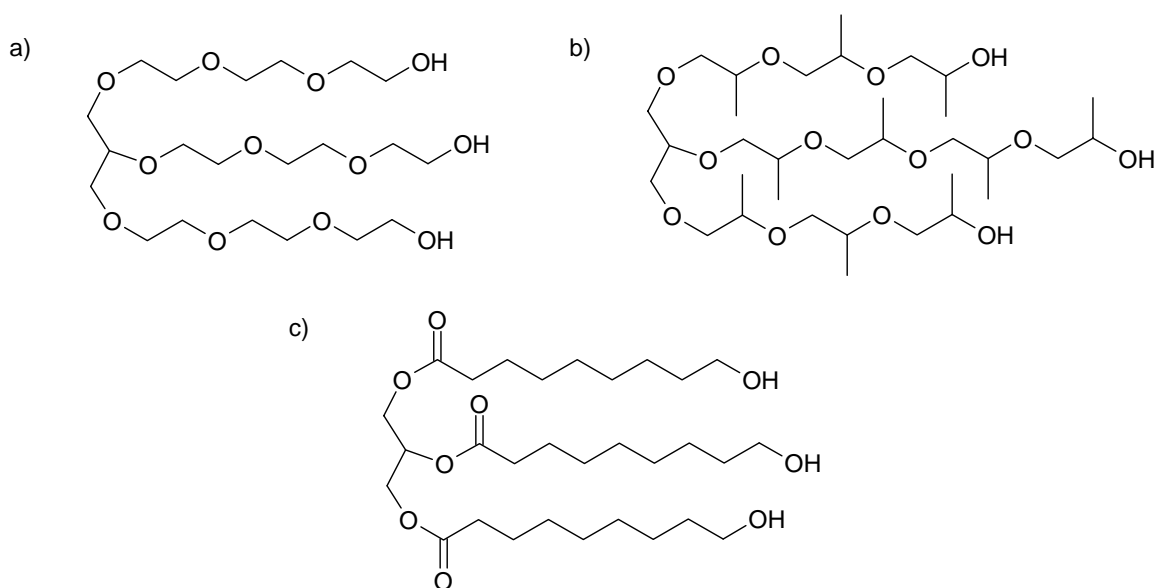


Figure A-1: Chemical structures of polyols. (a) Jeffox[®] WL-440, (b) Voranol[®] 270, and (c) TNG.

Sample preparation

All samples were made into collapsed foams following the formulations shown in Table A-1 and procedures documented in Chapter 5. The formulations were based on a total of 20 grams of materials and a 100-parts total of polyol. The functional groups were stoichiometrically balanced, namely the molar amounts of active hydrogen equal the molar amount of isocyanate.

Table A-1: Formulations used for sample synthesis.

	EO	PO	TNG
Jeffox [®] WL-440	100	--	--
Voranol [®] 270	--	100	--
TNG	--	--	100
Water, distilled	0.8	2.8	1.9
Dabco BL-11	0.08	0.08	0.08
Dabco 33-LV	0.1	0.1	0.1
TDI (g, index=100)	7.56	7.7	7.66
HS%	37.5	37.6	37.6

Characterization

Differential Scanning Calorimetry (DSC)

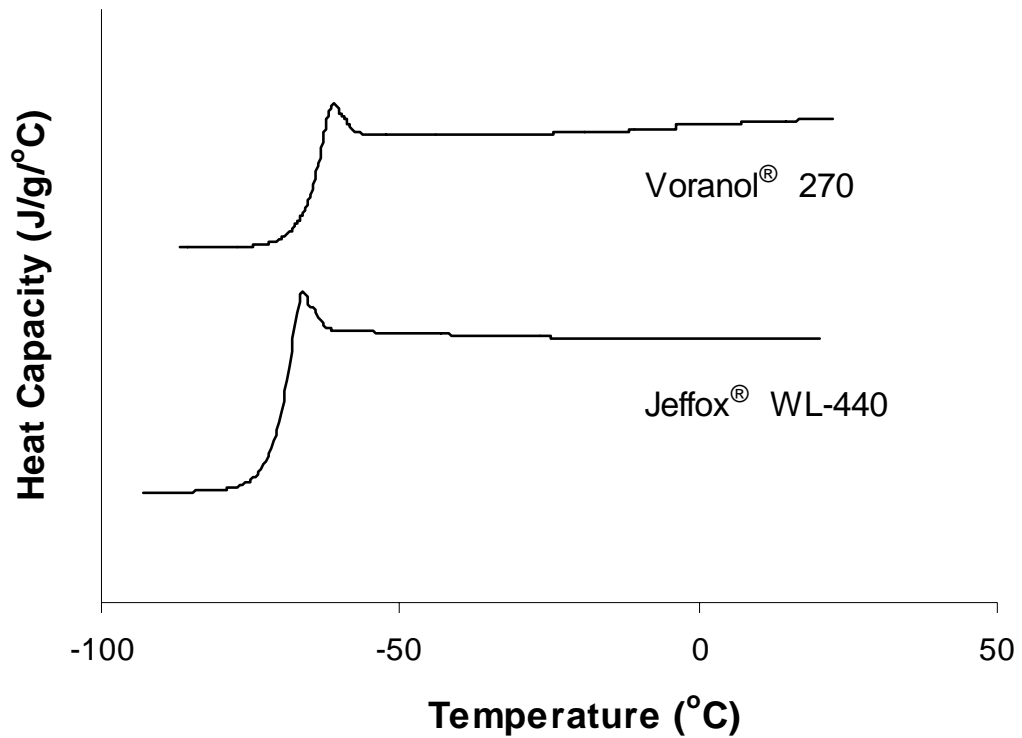
Same procedures were used as in Chapter 2.3.3.

Small Angle X-ray Scattering (SAXS)

Same procedures were used as in Chapter 2.3.3.

A.3 Results and Discussion

The thermal properties of pure polyols were measured using DSC and the results are shown in Figure A-2. Both petroleum derived polyols have low T_g 's. The EO



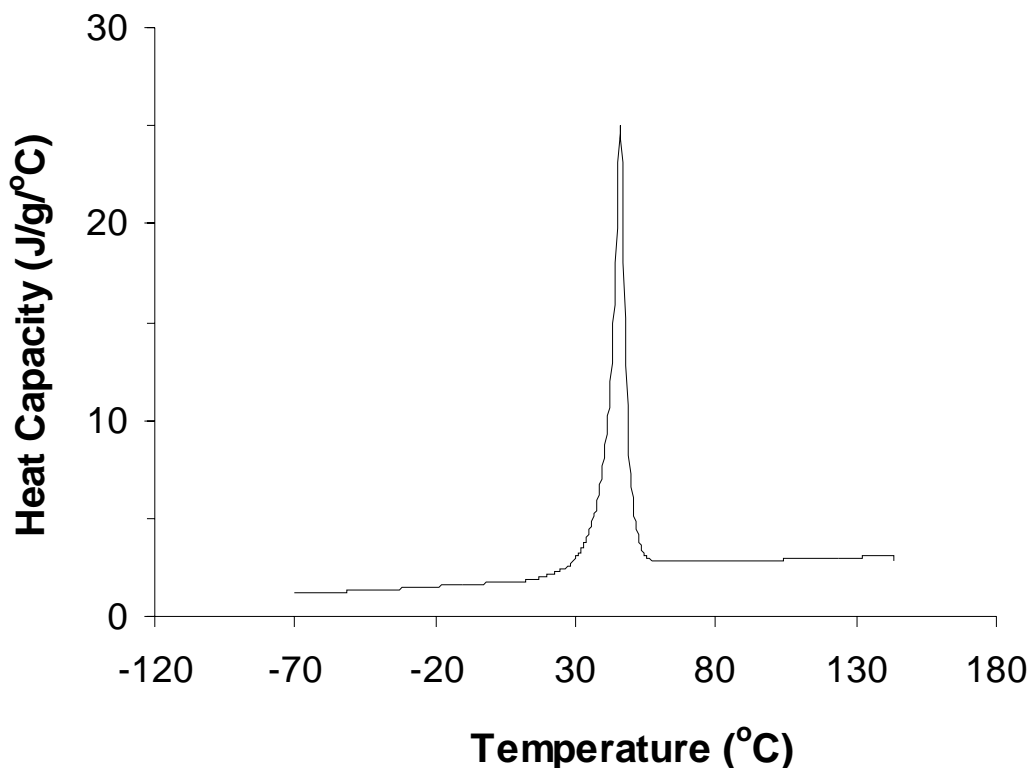
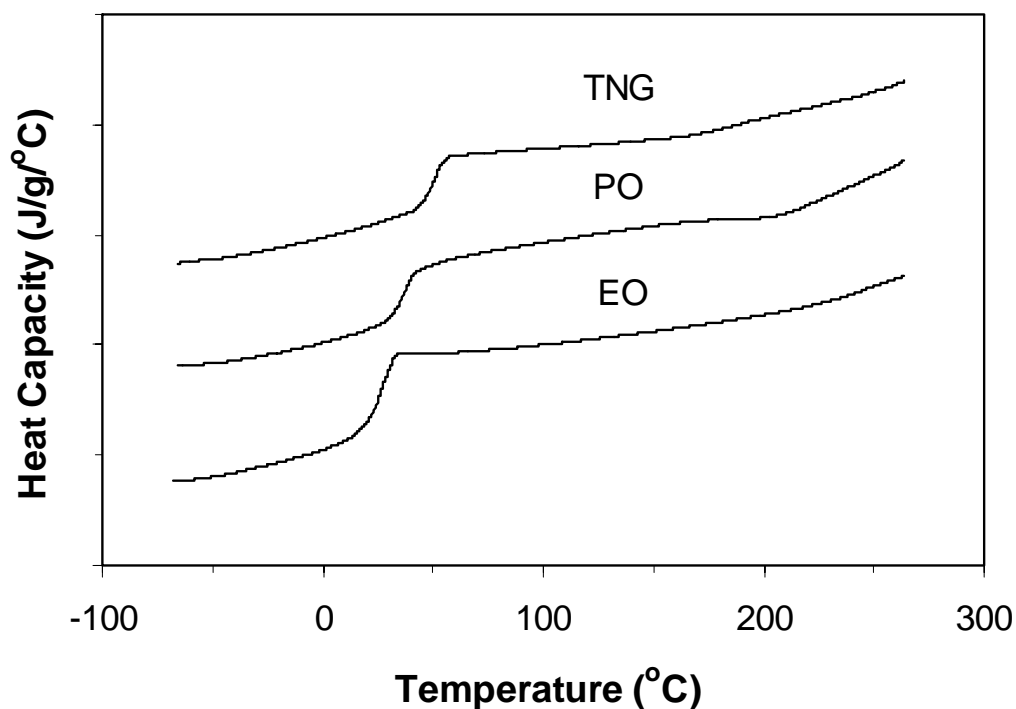


Figure A-2: DSC traces of polyols. Both traces of Jeffox[®] WL-440 and Voranol[®] 270 (first figure) have been shifted vertically to avoid overlapping. DSC trace of TNG is shown in the second figure.

Distinctively, both polyether polyols have low T_g 's: EO, -69 °C, and PO, -65 °C, while a T_g is absent in TNG polyol. Instead, a melting temperature of 46 °C is observed in TNG polyol. Collapsed foam samples synthesized from these three polyols were found to be relatively inflexible. As discussed in Chapter 2 and shown in Chapter 5 that molecular weight has a significant impact on PU properties, especially T_g . DSC traces of collapsed foams synthesized from the three polyols are shown in Figure A-3 and the glass transition temperatures of both polyol and collapsed foams are shown in Table A-2.

Table A-2: Transition temperatures of polyols and their corresponding PUs.

	Polyol	Collapsed Foam
EO	-69	29
PO	-64	37
TNG	($T_m = 46$)	51

**Figure A-3:** DSC traces of collapsed foam samples. The curves were shifted vertically to avoid overlapping.

Clearly EO sample has the lowest T_g following its lowest T_g of polyol shown in Figure A-2. PO, although has a T_g about 8 °C higher than EO collapsed foam, the 5 °C difference in the respective polyols made the 8-degree difference rather less significant. In the case of TNG, the crystallinity in the

polyol did not translate into crystallinity in its PU suggesting either the bulkiness of TDI unit or the irregularity of the hard segments have disrupted crystal structure formation. The T_g of PU derived from TNG is the highest of all samples.

Because all the polyols used here have a similar molecular weight, and thus similar crosslinking density, the difference in their T_g 's is likely a result of structural differences between these polyols.

Small angle X-ray scattering technique was applied to examine the degree of phase separation in the collapsed foam samples. Scattering profiles are shown in Figure A-4.

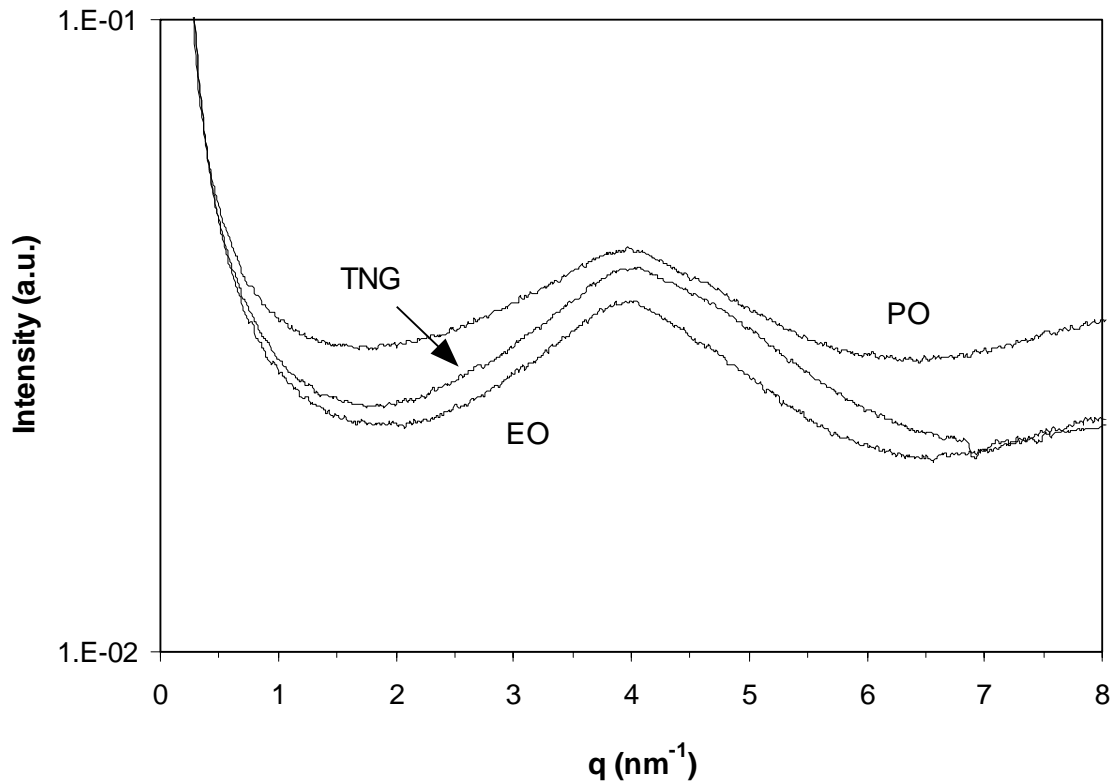


Figure A-4: Small angle X-ray scattering profiles of the samples.

Unlike the foam samples we have seen the previous chapters where the domains spacings are on the order of 10-nm range. The largest domain spacing we have observed in these low molecular weight polyol PUs is on the order of 1 nm. The scattering profiles themselves show very minor differences in the overall shape. Thus among the three PUs, the degrees of phase separation are rather similar, with EO-derived PU have the lowest degree in phase separation. This is expected, as EO is more compatible with polyurea-based hard segments than the other two polyols. The T_g difference observed in DSC results is less likely related to differences in degree of phase separations.

A.4 Conclusion

By examining a set of three polyols with similar molecular weight but different chemical structures, we found that hydrocarbon-based polyol chain have a profound effect on raising soft domain glass transition temperature. In the case of using either ethylene oxide or propylene oxide as repeating unit for polyol synthesis, the T_g of their resulting PUs is less influenced. X-ray scattering data showed that by decreasing the molecular weight of polyol, the spacing between hard domains is reduced, however little is changed in terms of the degree of phase separation among the three polyols used.

Appendix B

Model Polyol Viscosity

B.1 Introduction and Experimental details

The model polyols used in Chapter 5 were also tested for their viscosities as a function of temperature to gather more information on the physical properties of the materials. Viscosity testing was performed using ARES II (see Chapter 2.3.3 for details) under dynamic mode using two 25-mm parallel plates. Data were recorded at a frequency of 1 s^{-1} and the strain rate used was 0.1 s^{-1} .

The temperature dependency of viscosity is often described by Andrade-Eyring equation in the following form [167]:

$$\eta = Ae^{\frac{E}{RT}} \quad (\text{B-1})$$

where E is the activation energy, R is the gas constant, and T is temperature in Kelvin.

B.2 Results

Table B-1 tabulates the viscosity of polyols at 25 °C, and Figure B-1 details the viscosity-temperature relationship for the model polyols 1K through 4K (same as in Chapter 5) as well as castor oil.

Table B-1: Viscosity of polyols at 25 °C (unit:: Pa s).

	Castor oil	1K	2K	3K	4K
Viscosity (η)	0.525	1.119	1.516	2.695	2.188

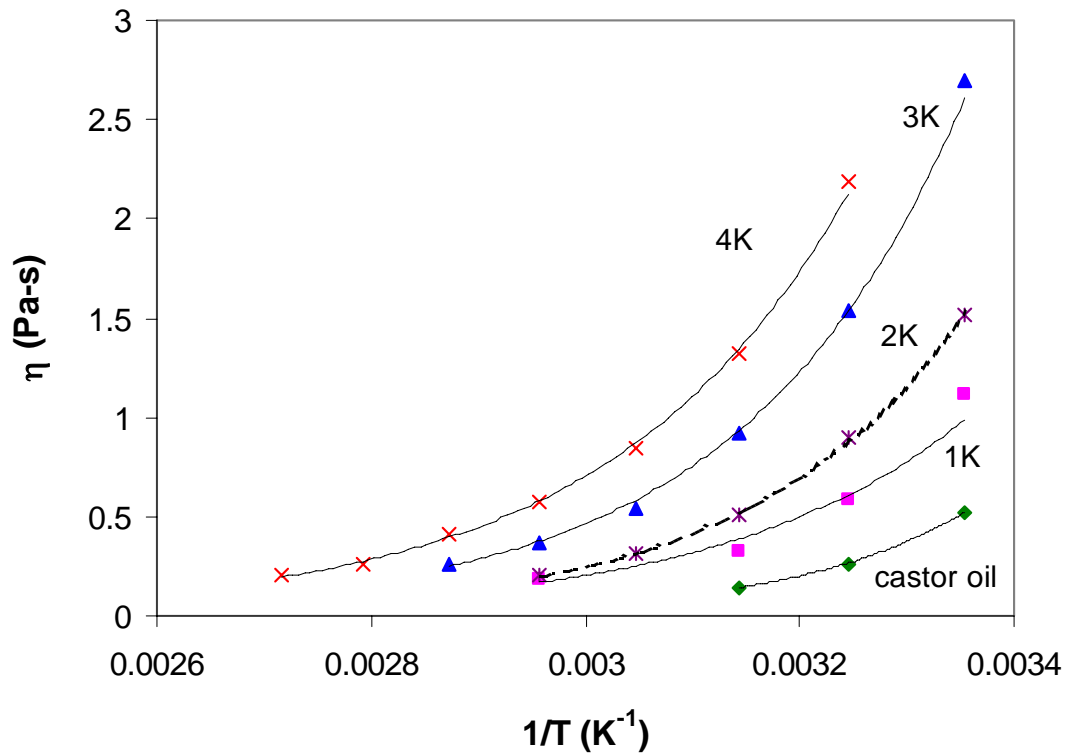


Figure B-1: Temperature dependence of polyol viscosity.

From Table B-1, the viscosity is lowest for castor oil and increases as molecular weight of the polyol increases. To put these values into perspective, the petroleum polyol used in this study have viscosity values of 1.10 Pa s for Hyperlite[®] E-848 and 0.48 Pa s for Arcol[®] F3022, at 25 °C.

Figure B-1 plots the temperature effect on viscosity and shows that high molecular weight model polyols are more susceptible to temperature change, which could provide latitude for processing. The synthetic polyols, 1K through 4K samples, consistently have higher viscosity than the naturally occurring polyol, castor oil, even in the case of 1K polyol, which has a similar molecular weight with castor oil. Table B-2 tabulates the viscosity-temperature relationship and the activation energy extrapolated from data fitting.

Table B-2: Temperature-viscosity relationship equations

Sample	Temperature-viscosity Equation	E (kJ/mol)
Castor oil	$\eta = 4.72 \times 10^{-10} e^{\frac{6.21 \times 10^3}{T}}$	51.63
1K	$\eta = 2.05 \times 10^{-7} e^{\frac{4.88 \times 10^3}{T}}$	40.57
2K	$\eta = 5.46 \times 10^{-8} e^{\frac{5.11 \times 10^3}{T}}$	42.48
3K	$\eta = 3.26 \times 10^{-7} e^{\frac{4.45 \times 10^3}{T}}$	37.00
4K	$\eta = 9.32 \times 10^{-7} e^{\frac{4.51 \times 10^3}{T}}$	37.50

References

- [1] Randall D, Lee S, editors. The Polyurethanes Book, John Wiley & Sons, Ltd., 2002.
- [2] McNulty M. Rubber & Plastics News Oct. 20, 2003;33(6):11-11.
- [3] Adhesives & Sealants Industry Dec/Jan, 2004;10(10):16-18.
- [4] Herrington R, Hock K, editors. Flexible Polyurethane Foams, 2nd ed. Midland: Dow Chemical Co., 1997.
- [5] Burkhart G, Kollmeier HJ, Schloens HH. J Cell Plast 1984;20:37-41.
- [6] Listemann ML, Wressell AL, Lassila KR, Klotz HC, Johnson GL, Savoca AC. Proceedings of Polyurethane World Congress, 1993: 595-608.
- [7] Derderian EJ, El Ghobary H, Esposito G, Muller LJ-M. Proceedings of SPI Polyurethanes Conference, 1994: 274-279.
- [8] Dupont. British Patent 731071; 1951.
- [9] Oertel G, editors. Polyurethane Handbook, Munich Vienna New York: Hanser Publishers, 1985.
- [10] Barrett KET. Dispersion Polymerization in Organic Media, London: John Wiley and Sons, 1975.
- [11] Bamford CH, Tipper CFH. Free Radical Polymerization, New York: Elsevier, 1976.

- [12] Spitler KG, Lindsey JJ. *J Cell Plast* 1981;17:43-50.
- [13] Kuryla WC, Critchfield FE, Platt LW, Stamberger P. *J Cell Plast* 1966;2:84-96.
- [14] Ramlow GG, Pizzini LC, Patton Jr. JT, Murphy JR. US Patent 4,014,846; 1977.
- [15] Van Cleve R, Armstrong GH, Simroth DW. US Patent 4,242,249; 1980.
- [16] Gibson LJ, Ashby MF. *Cellular Solids: Structure & Properties*, Elmsford, New York: Pergamon Press Inc., 1988.
- [17] Zhang J, Ashby MF. *J Mat Sci* 1994;29:157-163.
- [18] Saha MC, Mahfuz H, Chakravarty UK, Uddin M, Kabir ME, Jeelani S. *Mat Sci & Eng: A* 2005;406:328-336.
- [19] Gent AN, Thomas AG. *Rubber Chem Technol* 1963;36:597.
- [20] Whittaker RE. *J Appl Polym Sci* 1971;15:1205-1218.
- [21] Herrington R. In: Klempner D, Sendjarevic V, editors. *Polymeric Foams and Foam Technology*. 2nd ed, Munich: Hanser, 2004.
- [22] Bicerano J, Daussin RD, Elwell MJ, van der Wal HR, Berthevas P, Brown M, Casati F, Farrissey W, Fosnaugh J, de Genova R, Herrington R, Hicks J, Hinze K, Hock K, Hunter D, Jeng L, Laycock D, Lidy WA, Misprouve H, Moore R, Nafziger L, Norton M, Parrish D, Priestler Jr. RD, Skaggs K, Stahler L, Sweet F, Thomas R, Turner RB, Wiltz G, Woods T, Christenson CP, Schrock AK. In: Lee ST, Ramesh NS, editors. *Polymeric Foams: Mechanisms and Materials*. 1st ed, Boca Raton: CRC Press, 2004.
- [23] Macosko CW. *RIM, Fundamentals of Reaction Injection Molding*, Munich; New York: Hanser Publishers, 1989.
- [24] Artavia LD, Macosko CW. *J Cell Plast* 1990;26:490-511.
- [25] Ryan AJ, Willkomm WR, Bergstrom TB, Macosko CW, Koberstein JT, Yu CC, Russell TP. *Macromolecules* 1991;24:2883-2889.

- [26] Elwell MJ, Ryan AJ, Grunbauer HJM, Van Lieshout HC. *Polymer* 1996;37:1353-1361.
- [27] Cooper SL, Tobolsky AV. *Journal of Applied Polymer Science* 1966;10:1837-1844.
- [28] Seymour RW, Estes GM, Cooper SL. *Macromolecules* 1970;3:579-583.
- [29] Paik-Sung CS, Schneider NS. *Macromolecules* 1975;8:68-73.
- [30] Coleman MM, Lee KH, Skrovanek DJ, Painter PC. *Macromolecules* 1986;19:2149-2157.
- [31] Energy Information Administration, World Crude Oil Prices: <http://tonto.eia.doe.gov/dnav/pet/hist/wtotusaw.htm>, accessed on: April 11th, 2008.
- [32] Brand T. *Chemical Market Reporter* June 30th, 1997;251(26):19-19.
- [33] *Chemical Week* Nov. 17th, 2004;166(38):26.
- [34] *ICIS Chemical Business Americas* Oct. 30th, 2006;270(16):43-43.
- [35] *chemical week* May 23rd, 2007;169(18):27-27.
- [36] *Asian Pacific Coatings Journal* 2007;20(5):10-10.
- [37] Lewis DL. *Michigan Jewish History* 1995;79(3):10-17.
- [38] Appelqvist LA. In: Robbenlen G, Downey RK, Ashri A, editors. *Oil crops of the world*. ed, New York: McGraw-Hill, 1989.
- [39] Carlson KD, Chaudhry A, Bagby MO. *J Am Oil Chem Soc* 1990;67:438-442.
- [40] Lysenko Z, Morrison DL, Babb DA, Bunning DL, Derstine CW, Gilchrist JH, Jouett RH, Kanel JS, Olson KD, Peng WJ, Phillips JD, Roesch BM, Sanders AW, Schrock AK, Thomas PJ. WO Patent 2004096744 A2; 2004.
- [41] Dow Chemical Company, <http://www.dow.com/polyurethane/na/product/>, accessed on: June, 10th, 2008.
- [42] Lysenko Z, Schrock AK, Babb DA, Sanders A, Tsavalas J, Jouett R, Chambers L, Keillor C, Gilchrist JH. WO Patent 096882; 2004.

- [43] Petrovic Z, Javni I, Guo A, Zhang W. US Patent 6,433,121; 2002.
- [44] Petrovic ZS, Zhang W, Javni I. *Biomacromolecules* 2005;6:713-719.
- [45] Hou CT. *Adv Appl Microbio* 1995;41:1-23.
- [46] Garrett TM, Du XX. US Patent Application 20080076901; 2008.
- [47] Javni I, Petrovic ZS, Guo A, Fuller R. *J Appl Polym Sci* 2000;77:1723-1734.
- [48] Petrovic ZS, Cevallos MJ, Javni I, Schaefer DW, Justice R. *J Appl Polym Sci: Part B: Polym Phys* 2005;43:3178-3190.
- [49] Kong X, Yue J, Narine SS. *Biomacromolecules* 2007;8:3584-3589.
- [50] Yeganeh H, Mehdizadeh MR. *Eur Polym J* 2004;40:1233-1238.
- [51] Zlatanovic A, Lava C, Zhang W, Petrovic ZS. *J Polym Sci B: Polym Phys* 2004;42:809-819.
- [52] Stubiger G, Pittenauer E, Allmaier G. *Phytochem Anal* 2003;14:337-346.
- [53] Ramos LCD, Tango JS, Savi A, Leal NR. *J Am Oil Chem Soc* 1984;61:1841-1843.
- [54] Petrovic ZS, Guo A, Javni I, Cvetkovic I, Hong D. *Polym Int* 2008;57:275-281.
- [55] Pechar TW, Sohn S, Wilkes GL, Ghosh S, Frazier CE, Fornof A, Long TE. *Journal of Applied Polymer Science* 2006;101:1432-1443.
- [56] Guo A, Javni I, Petrovic ZS. *J Appl Polym Sci* 2000;77:467-473.
- [57] Tu Y-C, Kiatsimkul P, Suppes GJ, Hsieh F-H. *J Appl Polym Sci* 2007;105:453-459.
- [58] Tu Y-C, Suppes GJ, Hsieh F-H. *J Appl Polym Sci* 2008;109:537-544.
- [59] Hu YH, Gao Y, Wang D-N, Hu CP, Zu S, Vanoverloop L. *J Appl Polym Sci* 2002;84:591-597.
- [60] John J, Bhattacharya M, Turner RB. *J Appl Polym Sci* 2002;86:3097-3107.
- [61] Herrington R, Malsam J. US Patent Application 0070620; 2005.

- [62] Babb D, Phillips J, Keillor C. Proceedings of Polyurethanes Technical Conference, Salt Lake City, UT, 2006: 189-193.
- [63] Zhang L, Jeon HK, Malsam J, Herrington R, Macosko CW. Polymer 2007;48:6656-6667.
- [64] Nozawa K, Sasaki M, Okubo K. Proceedings of Polyurethane Technical Conference and Trade Fair, Houston, TX, 2005: 50-56.
- [65] IAL-Consultants, Alliance for the Polyurethanes Industry. 2004 End-use Market Survey on the Polyurethane Industry: Oct. 2005.
- [66] Reed D. Urethane Tech 2001;18:30.
- [67] Reed D. Urethane Tech 2006;23:6-7.
- [68] White L. Urethane Tech 2006;23:9.
- [69] White L. Urethane Tech 2006;23:22-28.
- [70] Reed D. Urethane Tech 2007;24:26.
- [71] White L. Urethane Tech 2007;24:45-49.
- [72] White L. Urethane Tech 2007;24:2.
- [73] Bayer Material Science NAFTA,
<http://www.bayermaterialsciencenafta.com/products/>, accessed on:
August, 10th, 2008.
- [74] Elwell MJ, Ryan AJ, Grunbauer HJM, Van Lieshout HC. Macromolecules 1996;29:2960-2968.
- [75] Luo N, Wang DN, Ying SK. Macromolecules 1997;30:4405.
- [76] Yilgor E, Yilgor I, Yurtsever E. Polymer 2002;43:6551-6559.
- [77] Hager KF, Brandien JE. J Cell Plast 1968;4:298-303.
- [78] Vespoli NP, Alberino LM. Polym Proc Eng 1985;3:127-147.
- [79] Artavia LD. Ph.D. Thesis: A model for low-density foams, University of Minnesota, 1991.
- [80] de Haseth JA, Andrews JE, McClusky JV, Priester Jr. RD, Harthcock MA, Davis BL. Appl Spec 1993;47:173-179.

- [81] Fox TG, Loshaek S. *J Polym Sci* 1955;15:371-390.
- [82] Bicerano J. *Prediction of polymer properties*, 3rd. New York, NY: Marcel Dekker, Inc., 2002.
- [83] Wang CB, Cooper SL. *Macromolecules* 1983;16:775-786.
- [84] Ramis X, Cadenato A, Morancho JM, Salla JM. *Polymer* 2001;42:9469-9479.
- [85] Aneja A, Wilkes GL. *Polymer* 2002;43:5551-5561.
- [86] O'Sickey MJ, Lawrey BD, Wilkes GL. *Polymer* 2002;43:7399-7408.
- [87] Wlodarczyk D. *J Appl Polym Sci* 1988;36:377-386.
- [88] Gaboriaud F, Vantelon JP. *J Polym Sci A: Polym Chem* 1982;20:2063-2071.
- [89] Zhang XD, Giles DW, Barocas VH, Yasunaga K, Macosko CW. *Journal of Rheology* 1998;42:871-889.
- [90] Szycher M. *Szycher's Handbook of Polyurethanes*, Boca Raton: CRC, 1999.
- [91] Agricultural Marketing Service, U. S. Dept. of Agriculture. *Monthly Feedstuff Prices and Peanut Report: Feb. 2007* Feb. 2007.
- [92] Schaefer BF. *Science* 2005;308:1267.
- [93] Lysenko Z, Babb DA, Stutts KJ, Robbyn P, Zhang M, Schrock AK. *WO Patent* 2006118995 A1; 2006.
- [94] Rhodes MB, Khaykin B. *Langmuir* 1986;2:643-649.
- [95] Han X, Zeng C, Lee JL, Koelling KW, Tomasko DL. *Polym Eng Sci* 2003;43:1261-1275.
- [96] Corbett GE, Wadie BJ. *J Elastom Plast* 1973;5:180-195.
- [97] Kaushiva BD, Dounis DV, Wilkes GL. *J Appl Polym Sci* 2000;78:766.
- [98] Shrinivas CS. *US Patent Application* 0025492; 2006.
- [99] Guo R, Lu X, Hua M, Fang D, Yao K. *Polymer International* 2001;50:1379-1383.

- [100] Gibson LJ, Ashby MF. Proc R Soc Lond A 1982;382:43.
- [101] Shutov FA. In: Klempner D, Frisch KC, editors. Polymeric Foams. ed, Munich: Hanser, 1991.
- [102] Blair EA. ASTM Special Publ 1967;414:84.
- [103] Shutov FA. Advances in Polymer Science 1983;51:155-218.
- [104] Rhodes MB. In: Cunningham A, editors. Low Density Cellular Plastics. 1st ed, New York: Chapman & Hall, 1994.
- [105] Rusch KS. Journal of Applied Polymer Science 1969;13:2297-2311.
- [106] Noshay A, McGrath JE. Block Copolymers, Overview and Critical Survey, New York, San Francisco, London: Academic Press, 1977.
- [107] Dlubek G, Pionteck J, Kilburn D. Macromol Chem Phys 2004;205:500-511.
- [108] Gier DR, O'Neill RE, Adams MR, Priester RDJ, Lidy WA, Barnes CG, Rightor EG, Davis BL. Proceedings of Polyurethanes Expo, Dallas, TX, 1998: 227-237.
- [109] Stout GH, Jensen LH. X-ray Structure Determination, New York: The Macmillan Company, 1968.
- [110] Velankar S, Cooper SL. macromolecules 1998;31:9181-9192.
- [111] Kaushiva BD, Wilkes GL. Journal of Applied Polymer Science 2000;77:202-216.
- [112] Kaushiva BD, Wilkes GL. Polymer 2000;41:6981-6986.
- [113] Li W, Ryan AJ, Meier IK. Macromolecules 2002;35:6306-6312.
- [114] McLean RS, Sauer BB. Macromolecules 1997;30:8314-8317.
- [115] Garrett JT, Runt J, Lin JS. Macromolecules 2000;33:6353-6359.
- [116] Kaushiva BD, Wilkes GL. Polymer 2000;41:6987-6991.
- [117] Garrett JT, Xu R, Cho J, Runt J. Polymer 2003;44:2711-2719.
- [118] Rossmly GR, Kollmeier HJ, Lidy WA, Schator H, Wiemann M. J Cell Plast 1977;13:26-35.

- [119] Rossmly GR, Kollmeier HJ, Lidy WA, Schator H, Wiemann M. *J Cell Plast* 1981;17:319-327.
- [120] Ryan AJ. *Polymer* 1990;31:707-712.
- [121] Rightor EG, Urquhart SG, Hitchcock AP, Ade H, Smith AP, Mitchell GE, Priester Jr. RD, Aneja A, Appel G, Wilkes GL, Lidy WE. *Macromolecules* 2002;35:5873-5882.
- [122] Li W, Ryan AJ, Meier IK. *Macromolecules* 2002;35:5034-5042.
- [123] lee HS, Hsu SL. *Macromolecules* 1989;22:1100-1105.
- [124] Heintz AM, Duffy DJ, Nelson CM, Hua Y, Hsu SL, Suen W, Paul CW. *Macromolecules* 2005;38:9192-9199.
- [125] Baker JW, Holdsworth JB. *J Chem Soc* 1947;713-726.
- [126] Hager W, Ueberreiter K. *Makromol Chem* 1979;180:939-948.
- [127] Iwakura Y, Okada H, Yamashiro S. *Makromol Chem* 1962;237-241.
- [128] Bailey ME, Kirss V, Spaunburgh RG. *Ind Eng Chem* 1956;48:794-797.
- [129] Brock FH. *J Org Chem* 1959;180:1802-1804.
- [130] Iwakura Y, Uno K, Kobayashi N. *J Polym Sci A: Polym Chem* 1968;6:1087-1096.
- [131] Davis TL, Farnum JM. *J Am Chem Soc* 1934;56:883-885.
- [132] Ephraim S, Woodward AE, Mesrobian RB. *J Am Chem Soc* 1958;80:1326-1328.
- [133] Dyer E, Taylor HA, Mason SJ, Samson J. *J Am Chem Soc* 1949;71:4106-4109.
- [134] Oberth AE, Bruenner RS. *Journal of Physical Chemistry* 1968;72:845-855.
- [135] Chang MC, Chen SA. *J Polym Sci A: Polym Chem* 1987;25:2543-2559.
- [136] Frisch KC, Reegen SL, Floutz WV. *J Polym Sci A: Polym Chem* 1967;5:35-42.
- [137] McGinn CE, Spaunburgh RG. *Proceedings of Symposium on Isocyanate Polymers, Atlantic City, NJ, 1956:*

- [138] Aranguren MI, Williams RJJ. *Polymer* 1986;27:425-430.
- [139] Kothanadaraman H, Sultan Nasar A. *J Macromol Sci, Part A* 1994;31:339-350.
- [140] McClusky JV, Priester Jr. RD, O'Neill RE, Willkomm WR, Heaney MD, Capel MA. *J Cell Plast* 1994;30:338-360.
- [141] Elwell MJ, Mortimer S, Ryan AJ. *Macromolecules* 1994;27:5428-5439.
- [142] Zhang XD, Davis HT, Macosko CW. *J Cell Plast* 1999;35:458-476.
- [143] Kanig G. *J Polym Sci* 1967;16:1957-1966.
- [144] Uberreiter K, Kanig G. *J Chem Phys* 1950;18:399-412.
- [145] Ray NH. *J Polym Sci A: Polym Chem* 1973;11:2169-2173.
- [146] DiBenedetto AT. "unpublished results", as cited by Nielsen, LE in *J Macromol Sci, Rev Macromol Chem* 1969;C3 (1):69-75.
- [147] Stutz H, Illers KH, Mertes J. *J Polym Sci B: Polym Phys* 1990;28:1483-1498.
- [148] Hale A, Macosko CW, Bair HE. *Macromolecules* 1991;24:2610-2621.
- [149] Shefer A, Gottlieb M. *Macromolecules* 1992;25:4036-4042.
- [150] Bicerano J, Sammler RL, Carriere CJ, Seitz JT. *J Polym Sci B: Polym Phys* 1996;34:2247-2259.
- [151] Petrovic ZS, Cvetkovic I, Hong D, Wan X, Zhang W, Abraham T, Malsam J. *J Appl Polym Sci* 2008;108:1184-1190.
- [152] Kulkarni MG, Sawant SB. *Eur J Lipid Sci Technol* 2003;105:214-218.
- [153] Cvengros J, Paligova J, Cvengrosova Z. *Eur J Lipid Sci Technol* 2006;108:629-635.
- [154] Markley KS. *Chemical and Physical Properties of the Fatty Acids*, New York: Wiley Interscience Publishers, 1947.
- [155] Doss MP. *Properties of the Principle Fats, Fatty Oils, Waxes, Fatty Acids, and Their Salts*, New York: The Texas Company, 1952.
- [156] Brown JB, Green ND. *J Am Chem Soc* 1940;62:738-740.

- [157] Morimoto S, Ito Y, Hamaguchi T. JP Patent 2004244443; 2004.
- [158] Loshak S. J Polym Sci 1955;15:391.
- [159] Marks MJ, Sekinger JK. Macromolecules 1994;27:4106-4113.
- [160] Martin GC, Shen M. ACS Polym Preprints 1979;20:786-796.
- [161] Zlatanic A, Petrovic ZS, Dusek K. Biomacromolecules 2002;3:1048-1056.
- [162] Bailey FE. In: Klemperer D, Frisch KC, editors, editors. Polymeric Foams. ed, Munich: Hanser, 1991.
- [163] Toloken S. Urethane Tech 2001;18:18.
- [164] Reed D. Urethane Tech 2007;24:8.
- [165] Chian KS, Gan LH. J Appl Polym Sci 1998;68:509-515.
- [166] Badri KH, Othman Z, Ahmad SH. Journal of Materials Science (Letters) 2004;39:5541-5542.
- [167] Bird RB, Stewart WE, Lightfoot EN. Transport Phenomena, New York: Wiley, 1960.